INVESTIGATION OF THE NATURAL HISTORY OF EQUINE ENCEPHALITIS VIRUSES WITH RADIOFREQUENCY TELEMETRY FOR DETECTION OF SUBCLINICAL DISEASE PATTERNS

by

Henry Ma

BS Biomedical Engineering and Public Health Studies, Johns Hopkins University, 2012

MSE Bioengineering, University of Pennsylvania, 2014

Submitted to the Graduate Faculty of

the Department of Infectious Diseases and Microbiology

Graduate School of Public Health in partial fulfillment

of the requirements for the degree of

Master of Public Health

University of Pittsburgh

2017

UNIVERSITY OF PITTSBURGH

GRADUATE SCHOOL OF PUBLIC HEALTH

This thesis was presented

by

Henry Ma

It was defended on

April 10, 2017

and approved by

Amy L. Hartman, PhD
Assistant Professor
Infectious Diseases and Microbiology
Graduate School of Public Health
University of Pittsburgh

Jeremy J. Martinson, DPhil
Assistant Professor
Infectious Diseases and Microbiology
Graduate School of Public Health
University of Pittsburgh

William B. Klimstra, PhD
Associate Professor
Department of Immunology
School of Medicine
University of Pittsburgh

Thesis Director: Douglas S. Reed, PhD
Associate Professor
Department of Immunology
School of Medicine
University of Pittsburgh

Douglas S. Reed, PhD

INVESTIGATION OF THE NATURAL HISTORY OF EQUINE ENCEPHALITIS VIRUSES WITH RADIOFREQENCY TELEMETRY FOR DETECTION OF SUBCLINICAL DISEASE PATTERNS

Henry Ma, MPH

University of Pittsburgh, 2017

ABSTRACT

Neither licensed vaccines nor antiviral therapeutics with proven efficacy exist to protect against the equine encephalitis viruses (EEVs), specifically Eastern, Western, and Venezuelan Equine Encephalitis Viruses (EEEV, WEEV, and VEEV, respectively). Due to rigorous ethical, regulatory, and scientific considerations, animal models that can faithfully demonstrate aspects of clinical disease must be established for testing of countermeasure candidates. Such models must satisfy the Animal Rule promulgated and enforced by the United States Food and Drug Administration and capture key aspects of equine encephalitis virus presentation in humans, especially with respect to encephalitic disease, whose manifestations include fever and neurological signs.

This study seeks to establish and study a model of human equine encephalitis virus infection via the aerosol route in the nonhuman primate, the cynomolgus macaque (*Macaca fascicularis*) with a focus on the natural history of disease through examination of radiofrequency electrocardiography data, and evaluates the feasibility of the use of such data to prognosticate severe disease courses which include encephalitis. Twelve nonhuman primate subjects, grouped

four per type of equine encephalitis virus, were challenged with aerosol exposures of the alphaviruses in various doses.

The following electrocardiography metrics compose a core set of variables suited to the characterization of disease rendered by EEVs: HR, PCt, P-Width, PR-I, QRS, QRSA, QT-I, R-H, and RR-I. Frequency spectrum analysis conducted on these metrics can be used to distinguish different periods of disease, if not distinguish between diseases, and Poincare plots of heart rate variability data can be used to track the progression of illness.

The public health significance of this work rests in its contributions to disease detection to aid in vaccine and therapeutic development for both the prevention of infectious disease and the mitigation of risk posed by potential biological weapons attacks. Finally, improved clinical disease detection through RF telemetry and other markers will abet the surveillance function of public health.

TABLE OF CONTENTS

LIST OF TABLES

LIST OF FIGURES

PREFACE

Foremost, I would like to thank Dr. Douglas Reed for mentoring me during my MPH year. Without his input, guidance, and patience, this work would not have been possible. Moreover, this thesis would not have been possible without the close collaboration between the Reed, Hartman, and Klimstra labs, as all members of the NHP alphavirus project were crucial to the continuation of the project. The Klimstra Lab deserves particular thanks for the growth and culture of the viruses used in this study, and thanks to Christina Gardner for looking over my thesis in part. I would also like to thank the staff and technicians at DLAR, for their daily custodianship of the animals when Reed, Hartman, and Klimstra Lab members were not available.

I would not have progressed as I had without the other excellent members of the lab, whose friendship and support helped sustain me through days in which I felt like I had accomplished nothing despite poring through reams of data and tens of thousands of lines of code. I'd like to thank Katie Willett for being a great team member in the NHP alphavirus project, as well as for being a great teacher, friend, and confidant. I am also fortunate to have made the acquaintance of Jennifer Bowling, a knowledgeable resource regarding aerobiology and supportive friend without whom this thesis would have been completed at least a month ago or more (I kid). Thanks to Morgan Midgett for her company and commiseration on late-night thesis work. Also, special, special thanks to Alan Watson for letting me hold his loaned hard drive hostage, on which I stored the vast majority of my thesis work.

Finally, I would like to thank the members of my committee, Drs. Hartman, Klimstra, Martinson, and Reed, for their time and consideration of my work, and Dr. Norman C. Wang, for his generous consultation regarding electrocardiography.

At the time of this writing, I have yet to learn whether or not I will remain in the lab to pursue a PhD. Completing the MPH within the span of a single year was a difficult undertaking, and I wish to post my most sincere thanks to the fellow travelers I've met along the way. I greatly appreciated the opportunity to put my background and skillsets acquired as a student of engineering, public health, and medicine to the test. Regardless of whether or not I remain with or depart from the lab to continue my medical education, I am richer for this years' experience.

1.0 INTRODUCTION

1.1 THE NATURAL HISTORY OF EQUINE ENCEPHALITIS VIRUSES

In the world of arthropod-borne viruses (arboviruses), equine encephalitis viruses (EEVs) compose a distinct portion of the alphavirus genera of the *Togaviridae* family of viruses. Alphaviruses, as detailed in Figure 1, consist of lipid-enveloped core icosahedral nucleocapsids enclosing ~10^1kb bicistronic nonsegmented, capped, and polyadenylated (+)ssRNA genomes with viral particles ranging from 60-70nm in diameter [1-3]. The alphavirus genome encodes four nonstructural proteins and five structural proteins, three of which, the capsid (C), and envelope proteins (E1, E2) have well-characterized functions [3, 4]. Subsequent to viral entry by receptor-mediated endocytosis, translation of nonstructural proteins begins immediately after the

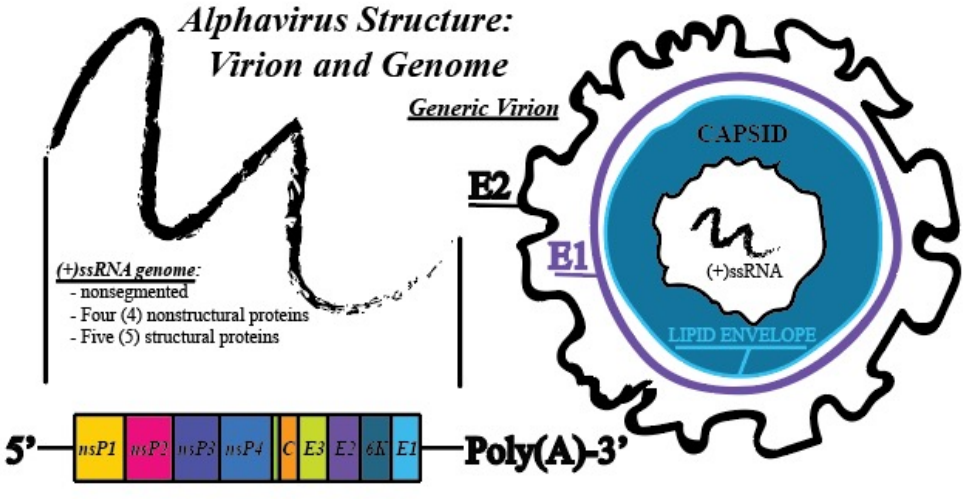

Figure 1. Alphavirus Structure.

unpacking of the virion; these nonstructural proteins, encoded by genes near the 5' end of the genome, generate a complementary (-)ssRNA transcript, from which novel (+)ssRNA progeny genomes are generated [5]. Concurrently, the nonstructural proteins also generate a subgenomic RNA which is translated to yield the structural proteins; all structural gene products, following necessary posttranslational modification, are then packaged into progeny.

Alphaviruses can be further subdivided into New World and Old World groups. Eastern Equine Encephalitis Virus (EEEV), Venezuelan Equine Encephalitis Virus (VEEV), and Western Equine Encephalitis Virus (WEEV) form three viral complexes of most interest in the New World group of viruses and constitute the focus of this project, as detailed in Figure 2 [2, 3, 6, 7]. These equine encephalitis viruses were the first alphaviruses to be isolated through the 1930s, and remain medically important pathogens unto the present day [5, 8-11].

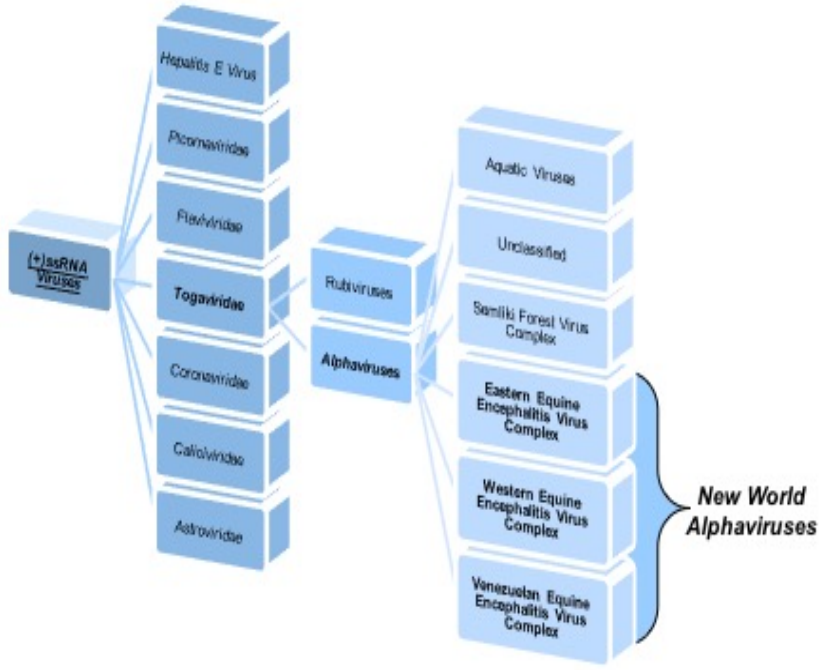

Figure 2. Equine Encephalitis Viruses.

Encephalitis here defines an infection of or inflammation of the brain parenchyma made manifest to observers by abrupt or subtle changes in brain structure or function [12]. Although humans inoculated with EEVs through mosquito bites may remain asymptomatic such that encephalitis is an uncommon finding, all three types of equine encephalitis virus can manifest with a febrile course (the length of which is dependent upon the virus), the eponymous encephalitis, and a variety of neurologic presentations including but not limited to photophobia, confusion, and seizures [1, 2, 12]. Survivors of virulent infections often develop lasting neurologic sequelae [1]. Symptoms range from nonspecific nausea, vomiting, diarrhea, and fever, to focal neurological signs or deficits, or altered mental status [1, 2]. The appearance of behavioral anomalies such as anorexia or depression is not uncommon [13]. More severe cases present with seizures, loss of consciousness, and coma [1, 2, 14]. Unlike the classical Wernicke's Triad for bacterial meningitis which consists of fever, nuchal rigidity, and altered mental status, encephalitis of a viral origin rarely if ever presents with such a neatly-bundled profile of signs pointing to a viral cause of illness [12].

Though post-mortem pathology can often render a definitive diagnosis of encephalitic etiology by examination of inclusion bodies, lymphocytic infiltrates, and staining, such methods cannot be used during the therapeutic window [15]. Although the most common cause of fatal nonepidemic encephalitis in the US remains herpes simplex virus I and II (HSV-1/2) encephalitis, enteroviruses are fast on the rise in terms of incidence in recent years [6, 12, 16]. Globally, other viruses, such as Japanese Encephalitis and West Nile Virus, are more commonly encountered than EEVs [1, 2, 5, 6, 13, 14, 17]. Differentiation of infection by EEVs requires a clear patient history, isolation of IgM or evidence of its conversion to IgG in cerebrospinal fluid, or confirmation by nucleotide amplification assay (reverse transcription PCR) in either blood, available tissues (in a

limited time frame), or CSF [13, 14, 18]. Radiological findings in the thalamus and/or basal ganglia can also confirm the presence of an EEV infection [14]. A summary table of the equine encephalitides discussed in this work is shown in Table 1.

Table 1. Equine Encephalitis Viruses and Encephalitides.

Virus	***Discoverer(s)***	***Year of Discovery***	***Disease and Encephalitis***
EEEV	Meyer, Haring, & Howitt [9]	1931	Presentation with sudden onset of fever and myalgia; seizures and coma occur with severe cases. In fatal cases, vascular damage observed in end-organs, including brain parenchyma. 4-10d latency via mosquito bite, 3-4d latency via aerosol [19, 20]. CFR 50-70% [1, 2].
WEEV	Broeck & Merrill [8]	1933	Presentation with sudden onset of fever, headache, anorexia, malaise, and altered mental status. Encephalitis characterized by vasculitis and focal hemorrhages in basal ganglia and thalamus. Often lasting neurological deficits. Variable profile of apparent disease according to age. 2-7d latency via mosquito bite [19]. CFR 3-4%.
VEEV	Beck & Wyckoff [11]	1938	Most commonly reported EEV in humans. Severe encephalitis less common than in EEEV or WEEV. Often asymptomatic, or presents as mild flu-like illness. Neurological disease or encephalitis detected in ~14% of infected individuals with a predilection for children and infants. 5-7d latency following mosquito bite [19]. 2-3d latency via aerosol; highly infectious via aerosol route. CFR<1% [19].

1.1.1 Eastern Equine Encephalitis Virus

Eastern Equine Encephalitis is primarily borne by the *Culiseta melanura* mosquito vector, and covers the eastern United States as well as parts of South America [2, 21]. Other species of mosquitoes of the *Aedes, Coqueillettidia,* and *Culex* genera can also carry the virus, though with

decreased frequency [21, 22]. Areas particularly high in virus burden include freshwater swamps/estuaries, and tree farms [1]. Four subtypes of EEEV exist: I-IV; type I is the most lethal, and circulates mainly in North America, while types II-IV predominate in South America and present significantly fewer concerns for virulent human disease [20, 23]. Natural infections typically occur in the summertime, and are relatively infrequent, although a notable increase in cases and vector range over the past decade have variously been attributed to climate change and increased virus viability through the winter in avian enzootic hosts[6, 24].

EEEV is notable for its high case fatality rate, which ranges from 30-70% in human hosts [25, 26]. Clinically, the incubation period is 4-10 days, sometimes with a prodrome of nausea, vomiting, fever, and headache[14, 17, 19, 25]. Across all subtypes, only 2% of adults and 6% of children progress to encephalitis, the onset of neurological symptoms heralds rapid deterioration, and the patient can become comatose. Other neurological signs include seizures and focal cranial nerve involvement. In the cerebrospinal fluid, a marked pleocytosis is observed, with a granulocytic (neutrophilic) predominance and elevated protein [13, 14]. One case series suggests that hyponatremia and pleocytosis in CSF lead to poor outcomes and a single case study points to viral myocarditis as a manifestation of EEEV infection [17]. Notably, treatment in humans with anticonvulsants and corticosteroids can result in worse outcomes [1, 2]. EEEV also presents a great risk of infection in aerosol form as well; a previous study in cynomolgous macaques demonstrated a dose-response relationship to the severity of aerosol-induced disease, and that at high doses, symptoms began to manifest within 72-96 hours of infection, with 100% lethality [20]. In examination of pathology in fatal human cases, lesions appear in the basal ganglia and thalami, suggestive of edema, ischemia, and/or hypoperfusion [14].

1.1.2 Western Equine Encephalitis Virus

Western Equine Encephalitis exists throughout the two American continents (in North America, mostly west of the Mississippi River); unlike the other two EEVs discussed, WEEV has not created the same number of case reports over the past decade, suggesting decreased virulence in humans or improved control though recent evidence suggests the latter through climate trends and agricultural industrialization practices [27]. Carried in North America by *Culex tarsalis*, WEEV is also significantly less virulent than EEEV, carrying a case fatality rate of 3-4%; however, documented reports of laboratory incidents with probable aerosol routes of infection portend a mortality rate of 40% [1, 2, 13, 28].

In a reversal of observations from the other two EEVs, the encephalitic presentation is more severe in older adults, though infants and children are more prone to permanent neurological damage [13]. The prodrome lasts for 1-4 days, and signs and symptoms that arise can fit a profile similar to that seen in EEEV. Encephalitis and neurological deficits become apparent with confusion or altered mental status, tonic-clonic seizures, and coma [19]. Progression to encephalitis results in focal neurologic deficits similar to, but reduced in severity compared to those seen in EEEV, and blood work demonstrates a rise in granulocytes [1, 2, 28]. Another similarity between EEEV and WEEV exists in that WEEV appears to damage the basal ganglia and the thalamic nuclei as well, with characteristic vasculitides and focal hemorrhages in the gray and white matter that may be confused for cerebral infarcts [19].

1.1.3 Venezuelan Equine Encephalitis Virus

Venezuelan Equine Encephalitis is the most well-researched EEV to date, and is known for its high infectivity via aerosol [29]. The enzootic ID, IE, and II subtypes present the most concern for human disease [1, 2, 19]. In contrast to EEEV, VEEV is not as lethal, and with respect to transmission dynamics, equines serve as amplification hosts, while a large number of probable mosquito vectors exist, such as *Culex, Aedes,* and *Mansonia, spp* [1, 2]. VEEV preferentially prefers lymphoid tissues for replication, and seeds the peripheral CNS through the olfactory system, regardless of whether the virus was delivered subcutaneously or by aerosol [30, 31].

The literature highlights pathologic changes in humans such as loss of neurons to apoptosis, neutrophilic penetration into the CNS, as in EEEV, and vasculitides in the CNS[13]. Presentation typically includes, apart from a nonspecific flu-like myalgia, a state of confusion or stupor, aphasia or mutism, muscular abnormalities such as involuntary movements and myoclonus, as well as ataxia [32]. Cranial nerve dysfunction can arise in the form of facial weakness, ocular palsies, photophobia, and nystagmus [32]. VEEV infection can manifest clinically as a febrile illness after a latent period ranging from a day to a week, and can be found early on by throat swabs, although the same diagnostic procedures and criteria as mentioned for the other two EEVs should be followed [5, 13, 28]. Mortality in humans from infection by VEEV is rare; however, for the 1% of adults and 4% of children who progress to encephalitis, associated events such as nuchal rigidity, ataxia, and convulsions may occur [1, 2, 28, 30]. A macular rash or arthritis can be seen in some cases, particularly around the distal extremities of the affected individuals [6, 13, 33]. Acute symptoms typically subside after four to six days, with complete resolution of the disease seen within one to two weeks, though neurological sequelae can persist [1, 2, 13].

1.1.4 Disease Pathogenesis by Aerosol Route

The pathogeneses of the equine encephalitis viruses share much in common. As with all alphaviruses, during the natural course of infection by the mosquito vector, the pathogen enters the human host subcutaneously and invades cells via heterodimeric trimers of glycoprotein in the lipid envelope termed E1 and E2 that initiate receptor-mediated endocytosis [1, 2, 33]. In the skin, the viruses display a particular affinity for Langerhans dendritic cell receptors DC-SIGN and L-SIGN [1]. The viral genome is released into the cytoplasm and viral reproduction occurs as discussed previously. Systemically, in a dead-end vertebrate host, virus inhibits the JAK/STAT pathway, allowing for evasion of the innate immune response, buying time for it to replicate and penetrate into the bloodstream to culminate in a detectable viremia [1, 4].

A growing body of research continues to support and expands upon the notion that the route of exposure influences not only disease presentation but specifically viral pathogenesis [31, 34, 35]. Although dissemination of the virus throughout the body by means of the viremia discussed above, the time at which this occurs is chiefly determined by the route of exposure, with the notable exception of VEEV [30]. Neuroinvasion by EEVs may occur before or after the establishment of viremia, and this can impact the severity of disease, especially in terms of the manifestation of encephalitic disease.

All three equine encephalitis viruses eventually establish a bloodborne viremia; in this mode of infection, entry into the brain parenchyma, if not initiated by trafficking through the olfactory bulb, is thought to occur by the dissemination of the virus into the choroid plexuses or through the infection of the aforementioned astrocytes that compose the blood-brain barrier [15, 36]. The end-organ damage and vasculitides described above suggest viral deposition by way of disruption of the integrity of the vasculature; the respiratory tract presents a large surface area for

infection to occur, with ready access to the vasculature through the mechanism of vertebrate gas exchange [34, 37-39].

A hypothesis expanded upon over the past few decades suggests that with respect to inhalational or aerosol exposure to viruses or other pathogens or toxins, the infection of the CNS and the induction of encephalitis can occur via trafficking of the agents through the neurons and support cells of the olfactory bulb, cranial nerve I (CNI) [26, 31, 34, 35, 40]. This hypothesis, hereafter referred to as the olfactory bulb hypothesis, proposes that the EEVs can access the olfactory sensory neurons embedded in nasal airway neuroepithelium; this concept is illustrated in a simian cross-section in Figure 3 [26]. The neural projections contained in the neuroepithelium connect the oronasal cavity in primates directly to the central nervous system;

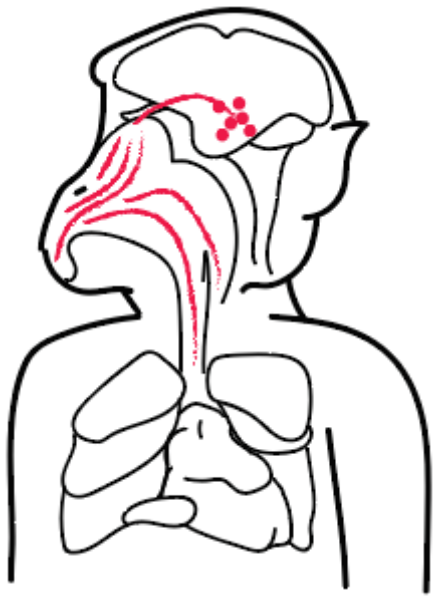

Figure 3. Olfactory Hypothesis.

A primate model. Inhalational infection of nasal neuroepithelium facilitates the seeding of the CNS with infectious particles through cranial nerve projections. The red lines represent the flow of infectious particles.

when this tissue encounters viral particles, olfactory receptor neurons and sensory neurons from the trigeminal nerve (cranial nerve V, CNV) are susceptible to viral entry [26, 41, 42]. Virions can also infect the lamina propria of this layer of tissue, accessing blood vessels and lymphatic tissue. The projections transit through the base of the cranial vault and into the brain proper by way of the cribriform plate in the ethmoid bone; cell-to-cell transmission in the CNS can then take place, between various cell types such as neurons, oligodendrocytes, and astrocytes, the last of which are notable for their role in the blood-brain barrier [41, 42].

1.1.5 Treatment and Prevention of Equine Encephalitis Viruses

Therapies for EEV currently consist of supportive treatment, and the use of human monoclonal antibodies; however, no licensed treatments exist [43]. With respect to prevention, while veterinary vaccines exist for equines, and prophylactic application in horses in the United States is highly recommended (though not strictly required), no licensed vaccines currently exist for broad use in humans [1, 2]. The exception to this lies in the availability of EEV vaccines for laboratory workers at increased risk of exposure to these pathogens; one of the fruits of the US biological weapons program lay in the development of two VEEV vaccines: TC-83 (for Tissue Culture, 83 passages), an attenuated strain of VEEV, and C-84 formalin-inactivated vaccine for VEEV [44]. Neither vaccine is licensed, and are both administered only under investigational new drug (IND) rules, but the vaccines have been proven to confer time-limited protection against VEEV, and may require booster doses for prolonged efficacy. Though formalin-inactivated vaccines also exist for WEEV and EEEV, no vaccine has achieved proven efficacy against WEEV or EEEV. These latter vaccines are also administered as INDs, and neutralizing antibody titer is used to determine immunity.

1.2 A NONHUMAN PRIMATE MODEL OF EQUINE ENCEPHALITIS VIRUS AEROSOL INFECTION

1.2.1 A Cynomolgus Macaque (*Macaca fascicularis*) Model of Aerosolized EEV Infection

1.2.1.1 FDA Animal Rule

The risks posed by EEVs both from seasonal/incidental infections by a bridge or epizootic vector and from the intentional use of aerosolized EEVs as biological weapons make the case for further study of these diseases. The mouse model falls short not only in the approximation of human anatomy, but also presents challenges with generalizability of findings to humans in comparison to the phylogenetically closer nonhuman primates. In light of the contextual risks, and due to the fact that no extant non-animal model exists which can replicate to a high degree of fidelity and robustness of a respiratory and systemic biological response to an aerosolized alphavirus infection, an inhalational nonhuman primate model for EEV infection represents a highly desirable goal for the continued study of EEV-type alphaviruses.

1.2.1.2 Nonhuman Primate Encephalitis Model Motivation and Rationale

The lasting neurological sequelae from survivors of symptomatic EEV disease are poorly characterized; their profiles are defined by aggregate case series and case reports collected incidentally following isolated outbreaks rather than by systematic reviews of the literature, and no definitive doctrine governs the management of the diseases or the aforementioned sequelae, though proof-of-principle treatments both specific and nonspecific, as well as some prophylactic interventions exist [43, 44].

To date, human infections with aerosolized EEVs remain relatively uncommon, unreported, or unrecognized. Of the known human cases, most have arisen in accidental exposures of laboratory workers and personnel [44]. Currently, diagnosis relies upon a high index of clinical suspicion given a patient's geographic location and/or travel history; in the case of attack by a biological weapon, these methods may prove insufficient to capture diagnoses in a timely manner. EEV encephalitis remains nonspecific for the diagnosis of any particular EEV, not least because its presentation shares a similar profile with that of other diseases, such as West Nile Virus, St. Louis Encephalitis, and other flaviviruses. Perhaps the most reliable indicator of an active or previous infection lies in serological testing for either EEVs themselves through reverse transcriptase PCR (RTPCR) or through detection of virus-specific antibody through enzyme-linked immunosorbent assays (ELISA) [18]. Similarly, detection of either sufficient virus or antibody in the CSF is diagnostic.

Animal models of disease for the advancement of knowledge have been in use since the days of Aristotle; in the case of simulating the encephalitis in humans wrought by the various equine encephalitis viruses, much work has been performed in the murine model [45]. Although mice retain many similarities with humans, infection with EEV aerosols tends to produce much more virulent disease in mice, particularly for VEEV, blunting the usefulness of the murine model for direct analogy to human disease [27, 31, 34, 36, 46, 47].

Certain species of nonhuman primates, such as rhesus (*M. mulatta*) and cynomolgus macaques (*M. fascicularis*), have been well-characterized with respect to anatomy and physiology, as well as to immune responses in the contexts of diseases caused by a multitude of infectious pathogens [20, 28]. Studies with EEVs in rhesus and cynomolgus macaques date back to the 1930s; these studies demonstrated that intranasal inoculation with EEEV and WEEV could cause fatal

encephalitis. The cynomolgus macaque as a model organism provides a distinct advantage due to its pattern of susceptibility to EEVs and the structural similarity and tissue composition of the nasal epithelium in macaques to that of humans [20, 28, 38, 41, 42]. A body of work has demonstrated that infection of macaques by various means including but not limited to subcutaneous and aerosol routes of infection can reproduce lesions in the brain that recapitulate those produced during the course of an infection by an equine encephalitis virus in human cases [20, 28, 30, 48]. Since each of the EEVs pose potential threats as weaponized agents, the goal of reproduction of encephalitic disease by the respiratory route remains paramount. Not only will the faithful recapitulation of clinical markers and histopathology of encephalitic disease advance the body of knowledge regarding the clinical course in species substantially phylogenetically closer to humans, it will also provide for a testbed suitable for the study of vaccines and therapeutic agents due to its ascendant relevance to human disease.

1.2.2 Radiofrequency Telemetry – Electrocardiography

Radiofrequency telemetry serves as a method of monitoring for encephalitic disease in animal models and has been successfully implemented in previous work [20, 34, 49]. The EEVs, upon induction of encephalitic disease, will generate clinical signs that can be monitored by direct observation, and can manifest a febrile illness, which may be monitored remotely by a discrete or continuous stream of data. A wealth of other physiological parameters, such as electroencephalography (EEG) and electrocardiography (ECG) can be used to track the course of disease as well.

The ability to complement observations of the test subjects with a sustained feed of electrophysiological data provides an improved ability to monitor the model organisms.

Radiofrequency telemetry can enhance the clinical relevance of data, and can perhaps provide prognostication of whether or not an animal will manifest with signs of encephalitic disease. Indeed, in the encephalitic disease state, though temperature remains the foremost method of tracking fever, it is too nonspecific a measure to exclusively implicate encephalitis. Replication of virus in the periphery can also present with fever; other measures, such as those provided by analysis of ECG data, have not yet been explored for the purposes of tracking encephalitis. Although a fair degree of correlation exists between an increased core temperature and other physiological parameters, the examination of those other previously unexamined parameters can add multiple dimensions to the knowledge of encephalitic disease.

Regardless of the mechanism by which EEVs access the central nervous system, the brain is undoubtedly affected, with specific attention paid to the basal ganglia and the thalamus, as previously described. Infection of the brain through the hypothesized olfactory bulb route provides a route for penetration into the hypothalamus, which receives olfactory cues, among other inputs [31, 36, 39, 41, 42, 50, 51]. The hypothalamus plays an integrative role in maintaining homeostasis in almost all aspects of vertebrate physiology, and is fairly robust in handling perturbations to the system in a healthy animal; it is further subdivided into a number of nuclei responsible for specific functions such as those governing wakefulness and appetite [50, 51]. At a more tangible level, the hypothalamus controls the autonomic nervous system by regulating sympathetic and parasympathetic output, to regulate global parameters in the body, including vasoconstriction, secretion from glands, and heart rate [50, 51]. Although the heart retains its own local, specialized pacemakers in the form of the sinoatrial (SA) and atrioventricular nodes (AV), normal physiological function relies on a delicate balance of sympathetic and parasympathetic output regulated by the hypothalamus; encephalitic disease that penetrates into the CNS will most

certainly directly or indirectly induce hypothalamic dysregulation [5, 26, 33, 50, 51]. This proposed mechanism underlines the value of monitoring electrocardiographic data as a surrogate, sentinel, or prognosticator of encephalitic disease, notwithstanding the manifestation of electrocardiographically detectable events suggestive of direct end-organ damage by the EEVs.

1.2.2.1 Principles of Electrocardiography

The mammalian heart is composed of a unique type of muscle, cardiac myocytes. Cardiac myocytes are conductive, and form a cardiac syncytium linked by gap junctions in a spatially oriented manner, such that electrical impulses from action potentials result in coordinated contraction of muscle. Cardiac anatomy separates the circulation into two parallel circuits of blood flow: deoxygenated blood travels from the heart to the lungs and back, and oxygenated blood travels from the heart to supply all tissues.

William Einthoven in the early 1900s devised a method of monitoring heartbeat through the directional detection of electrical impulses over the surface of the skin, and perfected the method through the century [52]. Consider the ECG diagrams in Figure 4. At its core, the electrocardiogram generated by a single heartbeat provides the PQRST (defined below) profile of an atrial and ventricular contraction and repolarization. From this signal, different segments of the waveform may be used to compute several key measures that provide insight into various aspects of cardiac physiology. The P wave corresponds to the depolarization of the atria, the QRS complex corresponds to both ventricular depolarization and atrial repolarization, and the T wave represents ventricular repolarization. The entire complex represents one heartbeat. Voltage-gated, inactivating sodium channels prevent backward flow of electrical current. Gross abnormalities in electrical conduction due to abnormal tissue growth or scarring become evident when viewed on

an electrocardiogram, and the rate and rhythm can raise red flags for other cardiac pathologies, as well.

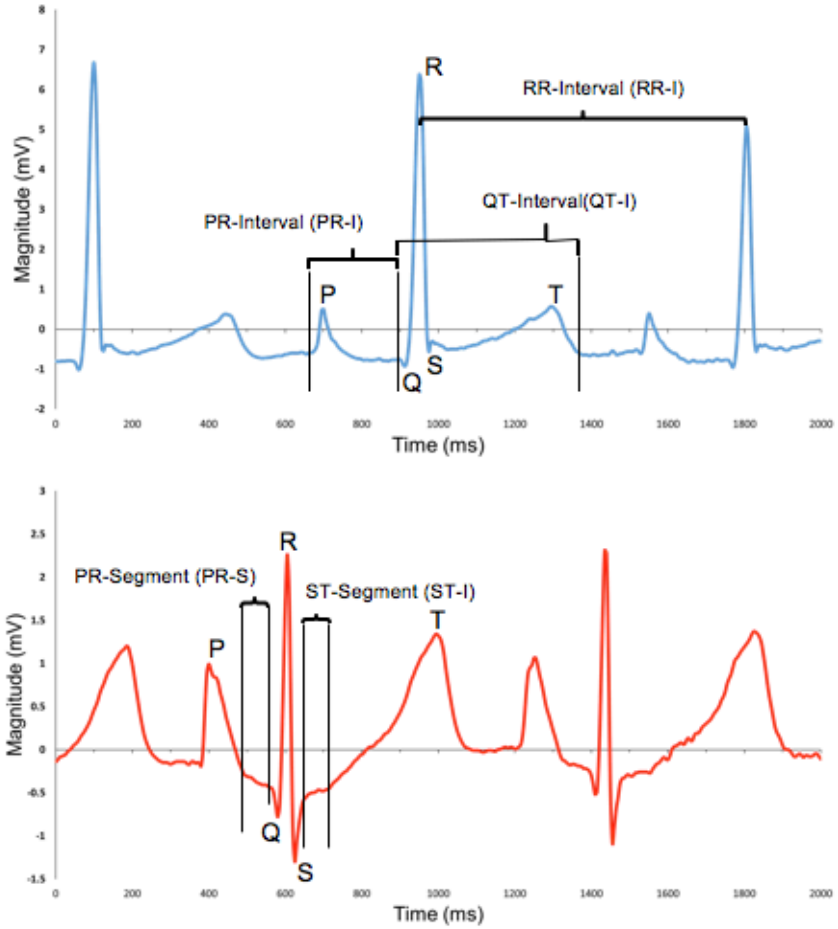

Figure 4. ECG Waveforms from *M. fascicularis* with Relevant Physiological Parameters.

Data from a study performed in the 1980s provide the most complete set of information regarding the characteristics of ECG waveforms in *M. fascicularis;* however, as the authors used traditional 12-lead ECG to conduct these studies, the macaques required sedation, which may have masked the true baseline values [53]. Perhaps the most basic consideration is the heart rate (HR); in the various literature reviewed, the resting HR of cynomolgus macaques in laboratory conditions appears to range from 150-250 beats per minute, roughly twice that of human adults, but relatively

normal for human infants [53, 54]. Heart rate is constructed from the RR-interval (RR-I), defined as the interval of time between two beats of the heart, which is calculated continuously. In conjunction with other biological information, ECG can help construct clinically relevant conclusions regarding such matters as the hydration status of the animal and the state of the subject's autonomic function [51]. Furthermore, the information used to calculate heart rate can also be used to monitor heart rate variability (HRV). HRV represents the variation in the time interval between heartbeats, expressed in units of interbeat interval (ms) [55]. Diminished HRV is associated with such pathology as DM neuropathy, heart failure, and generalized stress. Again, this provides insight into the hypothalamic regulation of heart rate during the sleep-wake cycle.

Other measures of interest include the QT-interval (QT-I); it documents the time elapsed between the Q wave of the ECG trace and the end of the T wave. QT-I can further be subdivided into the QRS complex and the ST interval/segment (ST-I). Elevation of the magnitude of the signal over the ST segment (ST-E) has traditionally been used to detect myocardial infarctions in clinical settings. The PR-interval (PR-I) can provide insight into the integrity of the electrical conductivity of the atrial myocardium, informing on conditions such as atrial-ventricular conduction block. Notably, the PR-I was found to vary with HR in *M. fascicularis*, which differs from conventional doctrine regarding PR-I in humans; however, given the typical short length of the PR-I in the animal model, 80ms, such variation may not hold any implications for statistical significance [53]. For ventricular contraction, the QRS complex (QRS) can denote whether or not pathology is disrupting the speed with which ventricular contraction occurs. The T-Wave has many metrics associated with it, such as the time between the peak and end of the T-wave (T-Pe), which examine the repolarization of the ventricles of the heart, and can identify problems affecting the speed of repolarization, such as ischemia in the various layers of myocardium.

1.2.2.2 Other Telemetric Monitoring of Clinical Course

Intuitively, continuous monitoring of temperature in a macaque serving as a model for a febrile illness presents a highly desirable modality, such that a profile of the fever itself may be generated and analyzed. Several articles have documented that in the case of EEEV, VEEV, and WEEV infections, marked temperature elevations occur, ranging from 0.5-2.0^{o}C depending upon the virus and the dose given [1, 20, 25, 28]. Moreover, temperature can provide insight into whether or not subjects have entered a state of terminal decline, as hypothermia may afflict moribund individuals. The prime importance of temperature lies in its ease of observation, status as a cardinal clinical vital sign, and its ability to define the period of frank illness in the NHP model.

The temperature, as discussed previously, can also vary collinearly with electrocardiographic signals. A manuscript in preparation at the time of this writing by Reed suggests that in disease states induced by infectious disease (*B. anthracis*, *Y. pestis*, EEEV, WEEV), HRV becomes decoupled from temperature. Published work by Reed, et al. broached the use of telemetry by taking measurements of temperature every 15 minutes to record subjects' body temperature over the disease course [20].

2.0 SPECIFIC AIMS

The work precipitating this project lies in the characterization and establishment of a primate model of EEV-attributable disease, to investigate the pathogenesis and course of aerosol-induced encephalitic EEV illness, and to use the information obtained towards the development and testing of safe and efficacious treatments or vaccines. Goals primary to the completion of the project include investigation of dose-response relationship between clinical and telemetric signs observed and dose of virus administered, and to evaluate the utility of electrocardiographic surveillance of the disease course as indicators of encephalitis and disease outcome. The leading goals of this work revolve around the study of the characterization of the natural history of disease through electrocardiographic monitoring following the aerosol exposure of nonhuman primates to EEVs. Pursuant to the continued development of the cynomolgus macaque as a model for aerosolized alphavirus infection, this thesis will consist of analyses and investigation in concordance with a pair of multi-part specific aims.

2.1 SPECIFIC AIM 1: TO ESTABLISH A SET OF TELEMETRIC PARAMETERS THAT ACCOMPANY THE COURSE OF ILLNESS

The scope of this project lies in the investigation of the natural history of disease through the monitoring of electrocardiography. Thus, the establishment of a core set of telemetric parameters that can aid in the determination of the course of illness for each type of equine encephalitis virus comprises a primary aim of this work. Therefore, subparts of this aim include:

a. Determine which electrocardiographic parameters are relevant to or reflect the progression of disease.

b. Establish a basis of analytical comparison of telemetry parameters to distinguish between sick and well states.

2.2 SPECIFIC AIM 2: TO ASSESS DISTINGUISHING FEATURES OF EQUINE ENCEPHALITIS VIRUSES WITH RESPECT TO TELEMETRY SIGNATURES

Similarly, pursuant to the development of the cynomolgus macaque as a model for aerosolized infection of equine encephalitis viruses, drawing comparisons between differing disease courses through analysis of the telemetry data remains fertile ground for investigation. Therefore, subparts of this aim require the:

a. Establishment of a basis of comparison of telemetry parameters to characterize EEEV, WEEV, and VEEV courses of illness.

b. Determination of whether telemetry metrics prognosticate or correspond to subclinical physiological or behavioral responses with onset and severity of encephalitis.

3.0 MATERIALS AND METHODS

This investigation occupies a niche of a larger project: "*Improved nonhuman primate models of inhalational alphavirus infections for use in preclinical evaluation of novel therapeutics,*" IACUC protocol 16026773, funded by Department of Defense (DOD) – Army grant number/project ID W911QY-15-1-0019. This study was fully approved by the University of Pittsburgh IACUC, and research is fully compliant with rules, regulations, and recommendations stipulated by the Animal Welfare Act and the Guide for the Care and Use of Laboratory Animals. The University of Pittsburgh, which includes the regional biocontainment laboratory (RBL), is fully accredited by AAALAC International.

3.1 GENERAL BIOSAFETY AND SELECT AGENT HANDLING

Biological safety is key to handling any pathogen. Virus culture was performed under BSL-3 conditions for Eastern, Western, and Venezuelan Equine Encephalitis Viruses in Class II biosafety cabinets with appropriate use of a 1:128 phenol-based Vesphene IIse (Steris Corporation, *Catalog No. 646101*) to water dilution for disinfection. Aerosol procedures were performed in a Class III biosafety cabinet modified with apparatus appropriate for transport and containment of animal subjects, within the Aerobiology Suite in the University of Pittsburgh Regional Biocontainment Laboratory (RBL). In animal suites within the RBL, wherein both animal subjects and telemetric monitoring equipment were housed, powered air-purifying respirators (PAPRs) were worn in

addition to Tyvek® high-density polyethylene (HDPE) hooded coveralls, rubberized boots, and double layers of nitrile gloves as personal protective equipment.

Due to the classification of EEEV and VEEV as select agents as outlined by the United States Select Agent List, laboratory work with these pathogens must be conducted within the BSL-3 laboratory of a facility registered with the Centers for Disease Control's Division of Select Agents & Toxins (DSAT).

3.2 VIRUS CULTURE AND CHARACTERIZATION

The selection of virus strains in these studies was made by the Department of Defense in conjunction with the Food & Drug Administration. For FDA Animal Rule studies, human isolates of virulent pathogens are preferred. The EEEV used in this study was the V105 strain of Eastern Equine Encephalitis Virus; WEEV used in this study was the Fleming strain; and the VEEV used in this study was the INH-9813 strain on the IC epizootic subtype. All alphavirus stocks were generated through construction of cDNA clones by Dr. William Klimstra's laboratory; capped, infectious viral RNAs were generated by *in vitro* RNA synthesis from linearized cDNA plasmid template genomes that were electroporated into baby hamster kidney (BHK-21, ATCC) cells. The supernatant was clarified by centrifugation between 18-24 hours post-electroporation, and single-use aliquots were stored at -80^{o}C to create zero-passage (p0) stocks. These p0 stocks were titered by standard plaque assays on BHK-21 cells. The p0 stocks were then used to infect roller bottles containing kidney cells from African Green Monkey (VERO cells, ATCC CCL-81) at a multiplicity of infection of 10. At 18-24 hours post-infection, the supernatant was clarified by centrifugation and then subjected to sucrose purification. Supernatant was carefully layered over

a 20/60% sucrose cushion and subjected to ultracentrifugation. The interface between the 20/60% sucrose cushion was collected and then diluted in 10mM Tris, 1mM EDTA, 100mM NaCl - STE 10X NaCl (TNE) buffer. The interface was then layered over 20% sucrose and again subjected to ultracentrifugation to pellet the virus. The pelleted virus was then resuspended in Opti-MEM® Reduced Serum Medium (ThermoFisher, Cat. No. 31985-070) and single-use aliquots were stored at -80^{o}C. The virus stock was then tittered using standard plaque assays on BHK-21 cells and the LD_{50} was confirmed in mice by Dr. Klimstra's laboratory before being used for NHP studies.

3.3 AEROSOL CHALLENGE AND DOSE DETERMINATION

3.3.1 Aerosol Challenge

For each aerosol challenge, aerosol generation was performed in a modified Class III biosafety cabinet specially outfitted with apparatus for work in aerosol generation and aerobiology. The platform housed in the cabinet consists chiefly of the AeroMP aerosol management platform (Biaera Technologies, Hagerstown, MD). A robust, automated system, Aero MP creates a highly controlled environment for the administration of EEVs to the animal subjects by implementing computer control of cabinet barometric pressure, humidity, subject plethysmography/spirometry, and exposure duration to minimize differences in inhaled doses delivered to individual macaques.

In preparation for the aerosol, each subject received anesthesia consisting of 6 mg/kg Telazol® (Tiletamine HCl / Zolazepam HCl), and was weighed. Blood was drawn for analysis of clinical chemistry and complete blood count (CBC) with the Abaxis VetScan VS2 and HM2, respectively. Each subject was then transferred into the modified Class III biosafety cabinet.

Respiratory Inductive Plethysmography (RIP; Data Sciences International (DSI), St. Paul, MN) belts were attached to the macaque's chest and abdomen to record respiratory function via Ponemah software (DSI). Macaques were exposed for 10 minutes inside an acrylic head-only chamber to an aerosol of EEEV, WEEV, or VEEV, created with an Aeroneb vibrating mesh nebulizer (Aerogen, Chicago, IL) Aerosol exposures were controlled and monitored using the Aero3G exposure system (Biaera Technologies, Hagerstown, MD). Aerosol sampling to determine presented dose was done with an all-glass impinger (Ace Glass, Vineland, NJ). Each aerosol was followed by a 5-minute air wash. Throughout the aerosol challenge, each NHP received a continuous infusion of ketamine (at the rate of 10 mg/kg/hr) to maintain the anesthetic effect brought upon by the initial Telazol knockdown. The aerosol challenge apparatus as configured in the Class III biosafety cabinet is illustrated in Figure 5.

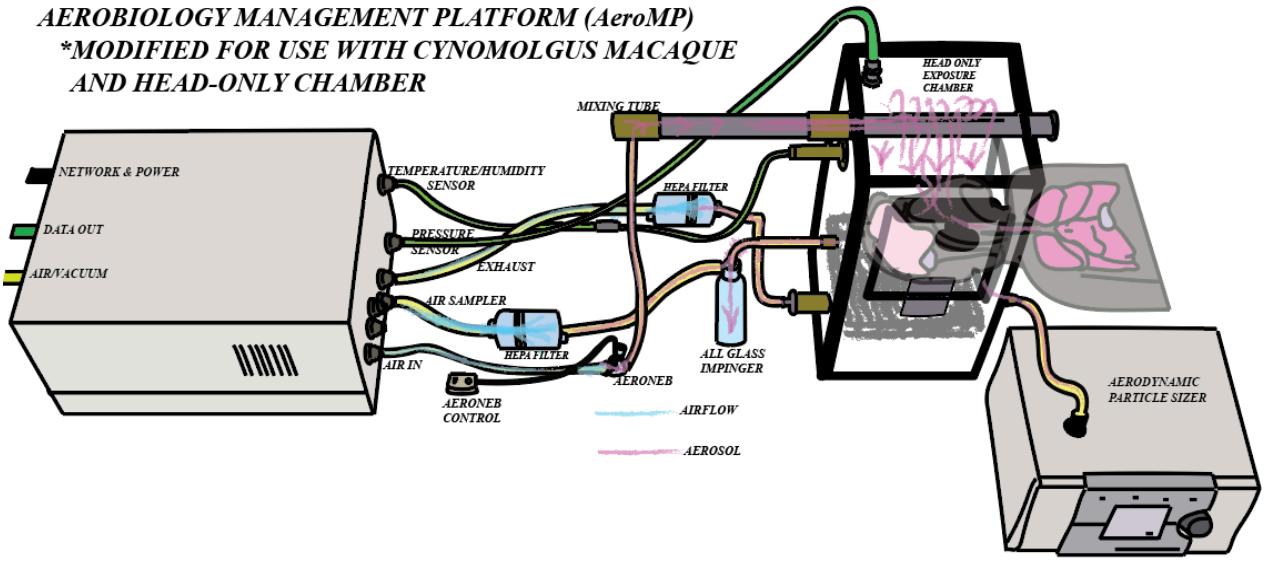

Figure 5. Schematic of AeroMP Aerosol Apparatus.

Modified from Lackemeyer, et al [56]. Vacuum pulls air through the HEPA-filtered apparatus in the biosafety cabinet. Virus is loaded into Aeroneb nebulizer, which is activated via external computer control. Vibrating mesh generates aerosol, which is pulled into mixing tube and into the head-only chamber wherein macaque awaits exposure.

3.3.2 Dose Determination

Plaque assays with BHK-21 cells were done on samples collected in an all-glass impinger (AGI; Ace Glass, Vineland, NJ) during the aerosol to determine the aerosol concentration and presented dose. Aerosol concentration was calculated as the product of the virus concentration in the AGI multiplied by the volume of liquid in the AGI divided by the product of the flow rate of the AGI (6 Lpm) and the duration of the exposure. Presented dose (i.e. inhaled dose) is calculated as the product of the aerosol concentration, the minute volume of the macaque and the duration of the exposure. All cells were grown at 37ºC with 5% CO_2. Calculated doses for aerosol challenges for EEEV, WEEV, and VEEV are listed in Table 2.

Table 2. Doses of Equine Encephalitis Viruses Given During Aerosol Challenges.

Nonhuman Primate	***Virus***	***Aerosol Date***	***Dose Received (PFU)***
M160-16 ♂ (1st Aerosol)	EEEV V105	08/26/2016	1.10×10^7
M160-16 ♂ (2nd Aerosol)	EEEV V105	10/06/2016	2.98×10^8
M161-16 ♂	EEEV V105	10/14/2016	1.60×10^8
M162-16 ♂	EEEV V105	10/28/2016	4.64×10^5
M163-16 ♂	EEEV V105	09/02/2016	3.39×10^7
M164-16 ♀	VEEV INH-9813	11/04/2016	1.27×10^8
M165-16 ♀	VEEV INH-9813	11/04/2016	7.88×10^6
M166-16 ♀	WEEV Fleming	01/30/2017	9.88×10^7
M167-16 ♀	WEEV Fleming	01/30/2017	2.89×10^8
M168-16 ♀	WEEV Fleming	02/13/2017	2.21×10^7
M169-16 ♀	WEEV Fleming	02/13/2017	3.76×10^7
M170-16 ♂	VEEV INH-9813	01/09/2017	2.22×10^6
M171-16 ♂	VEEV INH-9813	01/09/2017	1.02×10^6

3.4 RADIOFREQUENCY TELEMETRY AND DATA COLLECTION

3.4.1 Radiofrequency Electrocardiography

Telemetry data from twelve healthy, adult cynomolgous macaques (*Macaca fascicularis*) was collected continuously from DSI *PhysioTel Digital* radiofrequency transmitters (DSI Model No. M01) for a baseline period preceding aerosol challenge as well as for the days following the exposure to EEV. The transmitters were surgically implanted intra-abdominally in each animal at Covance Laboratories (Princeton, NJ) by a DSI veterinarian. ECG leads were sutured in place, one under the right pectoralis muscle and one parallel to the left inguinal area, approximating Lead II placement in a 12-lead ECG. The unit also contains a temperature sensor that samples core temperatures on a continuous basis, as well as an accelerometer designed to track the movement of the animal. The implanted unit itself is pictured in Figure 6.

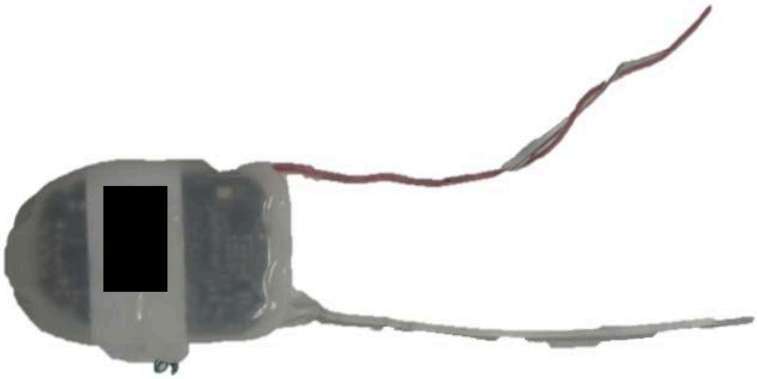

Figure 6. Radiofrequency Telemetry Electrocardiography Implant.

The collection apparatus, located inside the RBL, consisted of a designated telemetry computer outfitted with a communication link controller (CLC) supplied by DSI. The CLC was

optimized for collecting signals from transceivers mounted on caging containing singly-housed NHP subjects, with cameras positioned to record NHP behavior; the setup as described is detailed in Figure 7.

Figure 7. Radiofrequency Telemetry Setup *in toto*.

The Ponemah software package (v.5.2; Data Sciences International) provides a graphic user interface (GUI) that presents a unified, multichannel display of the data collected from the implant's sensors. For analysis, data can be either read in raw form (.RAW file extension) or reviewed in common spreadsheet, statistical analysis, and plotting programs. Body temperature

and electrocardiographic measures including heart rate are sampled at 10 Hz and recorded every 5 seconds [49]. Telemetric monitoring began for each NHP at least three days before exposure to the aerosol challenge to develop a baseline. For body temperature, recorded values outside two standard deviations of the mean were used to compute fever duration and cumulative fever-hours (cumulative total hours of significant temperature elevations). Because of the potential for a high degree of variation in physiology, baseline data of relevant biological metrics were compiled into a study-population specific database to establish the baseline for this specific study population, viewable in Appendix A. A brief summary of available metrics are exhibited in Table 3; standard deviations of these metrics were also measured and recorded at the same sampling frequencies.

Table 3. Electrocardiogram Metrics of Study.

Electrocardiography Metric	***Abbreviation***	***Significance***	***Units***
Arrhythmic Beat Detection	BAD	The number of arrhythmic beats detected during a logging period.	*Count*
Heart Rate	HR	Number of heartbeats per minute.	*bpm*
Heart Rate Variability	HRV	$RR\text{-}Interval_n$ matched with $RR\text{-}Interval_{n+1}$, plotted as an ordered pair.	*ms, Unitless*
Maximum Voltage Derivative of R-Wave	MxdV	Maximum rate of change of ECG trace at R-Wave.	*mV/ms*
Noise in ECG Trace	Noise	Approximation of noise level in ECG cycle; root-mean-square value of derivative in a single ECG cycle.	*Unitless*
P-Wave Count	PCt	Number of P-waves counted in one sample.	*Count*
P-Wave Height	P-H	Height of P-Wave from isoelectric level.	*mV*
PR-Interval	PR-I	Interval of time between beginning of P-Wave to the beginning of the R-Wave. Can detect atrial conduction block.	*ms*
P-Wave Width	P-Width	Interval of time from the P-Wave to the end of the P-Wave.	*ms*
QaT	QATN	Interval of time between the Q-Wave to the peak of the T-Wave.	*ms*
QR-Interval	QR-I	Interval of time between the Q-Wave to the peak of the R-Wave. Indicator of ventricular depolarization and/or contraction.	*ms*
QRS-Interval	QRS	Interval of time between the Q-Wave to the beginning of the S-Wave. Indicator	*ms*

Table 3 (cont'd)			
		of ventricular depolarization and/or contraction.	
QRS Amplitude	QRSA	Amplitude of QRS complex from the isoelectric level. Indicator of ventricular contraction.	*mV*
QT-Interval	QT-I	Interval of time between the Q-Wave to the end of the T-Wave. Indicator of electrolyte status as well as speed of total cardiac repolarization.	*ms*
R-Wave Height	R-H	Height of the R-Wave from the isoelectric level.	*mV*
RR-Interval	RR-I	Interval from one R-Wave peak to the next R-Wave peak.	*ms*
ST-Elevation	ST-E	Height of the T-Wave at algorithmically-determined point between S-Wave and T-Wave, to detect myocardial infarction.	*mV*
ST-Interval	ST-I	Interval of time between the S-Wave and the end of the T-Wave.	*ms*
T-Wave Height	T-H	Highest point between the end of the S-Wave and end of the T-Wave.	*mV*
T-Wave Trough	T-HN	Lowest point between the end of the S-Wave and end of the T-Wave.	*mV*
Peak of T-Wave	T-P	Peak of T-Wave relative to isoelectric level, between end of S-Wave and end of the T-Wave.	*mV*
T-Wave Peak-to-End	T-Pe	Time between the peak of the T-Wave to the end of the T-Wave; indicator of ventricular reperfusion.	*ms*

3.4.2 Clinical Scoring for Encephalitis.

To monitor signs of clinical encephalitis for nonhuman primates, animals were monitored at least twice daily following aerosol challenge. Generally, animals were monitored for stool and urine output and appropriate nonhuman primate behavior. Food consumption and water intake were closely monitored throughout the animals' stay at the RBL. All EEVs were expected to cause a period of illness ranging in severity within a week after aerosol challenge. In the most fulminant of cases of EEV encephalitis, death due to febrile/encephalitic disease was expected within 2-3 days of fever onset [20]. As mentioned previously, the clinical signs of illness, features of

EEEV/WEEV/VEEV, can include anorexia and dehydration with accompanying fever and/or encephalitis. Tremors, myoclonus, seizures, coma, nystagmus, photophobia, and many other clinical signs of note were flagged for observation, as well.

Macaque subjects were thus given a clinical score during each (twice-daily) post-aerosol observation composed of three individual rankings: temperature, activity, and neurological status scores. Temperature scores were given on an ordinal scale of 1-6: 1 denotes a temperature between 37-39^{o}C, 2 denotes a febrile temperature over 39^{o}C but below 40^{o}C, 3 for a temperature over 40^{o}C but below 41.5^{o}C, 4 for temperatures over 41.5^{o}C. As temperatures below 37^{o}C indicate slight or severe hypothermia, common in moribund animals, temperatures between 35-37^{o}C and temperatures below 35^{o}C rank a 5 and a 6, respectively. The neurological scores and activity scores were also ordinal scales of 1-6: a score of 1 constituted normal neurological function and activity; a score of 2 corresponded to occasional loss of balance, drooling, or muscle control, and/or photophobia, for neurological signs, and decreased body language interactions for the activity score. A score of 3 includes nystagmus, head pressing and tremors for neurological signs, and a sluggish response from the animal for the activity score. A score of 4 represents the presentation of occasional seizures for the neurological score, and an upright but otherwise completely unresponsive subject for the activity score. Frequent seizures warrant a neurological score of 5, while the same score for activity level is begotten by a recumbent or moribund animal; the latter triggers the humane endpoint for the study, discussed below. Finally, a comatose animal begets a neurological score of 6 and likewise prompts the humane endpoint for the study. These scores were formulated based off previous work in *M. fascicularis* subjects [20, 28, 57].

Animals that scored a 10 or higher warranted an observation schedule with an increased frequency of observation: once every eight hours. If an animal reached a score of 14 or higher, the

humane study endpoint was triggered following principal investigator and veterinarian approval, and the animal euthanized by complete exsanguination via transcardial perfusion with 12L of sterile 0.9% saline following administration of 10 mg/kg ketamine, intravenous sodium nitroprusside diluted in heparin solution for maximum vascular vasodilation, and a sublethal intravenous dose of 15 mg/kg sodium pentobarbital. Death was confirmed by observed cardiac arrest, cessation of respiration, and corneal areflexia.

3.5 ANALYSIS OF TELEMETRIC DATA

Statistical analysis was performed through the use of MATLAB (MathWorks) in addition to Excel (Microsoft). Repeated measures ANOVA, one-way ANOVA (Tukey's post-hoc correction) and pairwise t-tests were performed to compare each subject's post-aerosol challenge metrics with pre-challenge baseline metrics, daily and in aggregate, to compare metrics from the sick state from animals that became sick, to the well state, and to compare metrics from the febrile post-challenge period to the afebrile post-challenge period. To compare between different groups of subjects within one EEV subset, ANOVA was used to provide for more robust analysis of differences between discrete time periods (i.e. sick and well states) between animals challenged with the same EEV. Analyses of frequency-spectrum data were also performed to compare differences between different periods in relation to disease onset and pre-/post-aerosol samples. One-way ANOVA was used to assess differences in heart rate variability by day.

3.5.1 Data Processing

Electrocardiographic measures were sampled at a rate of 10 Hz, recorded at a minimum interval of 5s; the volume of raw data printed at this rate proved too much for the processing capabilities of all forms of analytical software employed to plot and analyze the data, with the sole exception of MATLAB. However, even with the latter software package, processing was difficult due to the volume of data, and a one-minute standard for interval data was chosen, as an aggregate of data recorded every five seconds. Although an arbitrary choice, this interval proved manageable for computation times while still presenting a respectable maximum of 1440 data points per day from 17280, an entire order of magnitude fewer.

Timescales were converted from dd:hh:mm:ss format to a scalar days-post-infection frame for all NHP subjects. This was not essential, but greatly aided the establishment of pre- and post-infection time frames. To do this, all time points were referenced to a canonical start time: the initialization of telemetry recording for M160-16 was considered the beginning of the study. This way, data could easily be converted from dd:hh:mm:ss from the initial start point into seconds, and from then, referenced to the time of the aerosol challenge to give days pre/post-infection, with the variable name “M1XX-16_DPI” for each NHP.

Raw data was imported into Excel and variable names made palatable for importation into MATLAB and subsequent data processing. To tailor processing and comparisons, each variable name contained the subject number, sex, live/dead status, and the variable of interest. The template thus described: “M1XX-16_(M/F)_(E/W/V)_(L/D)_Var,” with M/F representing the sex of the NHP subject, E/W/V representing the EEV administered, and L/D representing the survival status of the macaque “L” for survived, and “D” for NHPs that reached the humane study endpoint within the course of post-challenge observation. The data were then ported into MATLAB, whereupon

data processing censored data that was missing, and likewise censored unphysiological values. Plots of all measures were generated against the disease course as measured by temperature profiles (plot of mean temperature in addition to cumulative fever-hours) and clinical scores.

3.5.2 Establishment of Disease Courses

To determine the periods for comparison within each nonhuman primate subject, temperature and clinical score profiles were plotted such that the periods prior to aerosol and post aerosol were clearly delineated. Although each NHP in effect served as its own control due to the small quantity of NHPs in each alphavirus group, the disease profiles were similar enough across multiple NHPs in each group, as noted in preliminary examination of the data, to establish a consistent disease course that could be separated into distinct segments. Statistical analysis was carried out by comparing the statistics between baseline (pre-infection), incubation (post-infection, pre-disease-onset), febrile, and recovery periods.

3.5.3 Analysis of Variance

Analysis of variance was carried out to measure differences both within the same NHP as well as to determine differences between NHP subjects administered the same EEV but whose natural histories were differentiated by sick and well states. Repeated-measures ANOVA was run on each NHP subject, as data was collected continuously from each NHP. When analyzed at the standardized rate of one minute, the preponderance of samples from the data combined with the paucity of degrees of freedom between the days of the disease course resulted in ANOVA attaching significant differences in day-to-day variations in physiological measures at baseline when such

values were expected to lie within normal physiological parameters for a macaque. Therefore, a secondary standard rate of samples collected every 15 minutes was used for the repeated measures ANOVA. All significance levels utilized were $\alpha<0.05$.

3.5.4 Frequency Spectrum Analysis

To examine changes in the circadian rhythm captured by electrocardiographic data, frequency spectrum analysis was carried out by use of the fast Fourier transform (FFT). Any periodic signal or waveform can be composed of a linear combination of basic trigonometric functions such as sine waves or cosines. Consider a function f(t), an irregularly shaped time series, with or without some obvious pattern, such as that in the example illustrated by Figure 8. For simplicity, consider

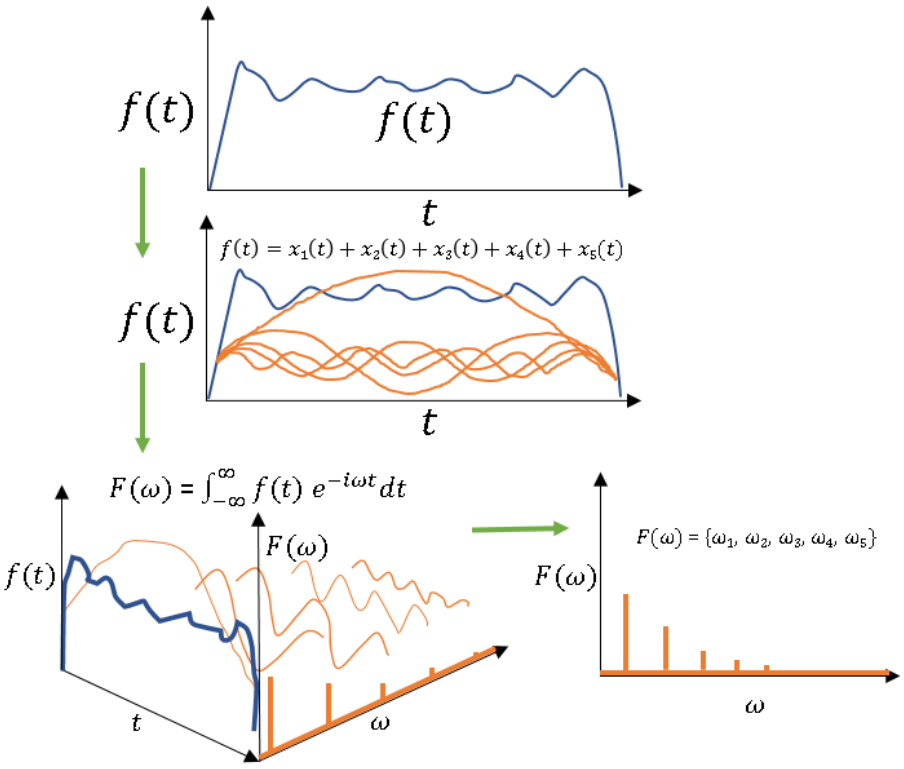

Figure 8. Frequency Spectrum Analysis.

a known quantity of 5 sines or cosines, all functions of time. The FFT is applied, through the convolution integral (illustrated), and a discrete spectrum is produced, with each frequency point representing a component frequency of its respective trigonometric function. The y-axis represents the magnitude of the trigonometric function it represents, or how much of a role it plays in defining the original time-domain function. In this manner, subtle changes in the number of cycles per day, or the subcomponents of the normal cyclic rates of physiological or electrocardiographic parameters can be visualized and correlated with disease processes. These procedures were carried out in MATLAB with the use of native frequency analysis algorithms, modified for use with incomplete time series. Differences in frequency spectra were characterized by the absence or presence of peaks at various periods; the fundamental frequency, or the first defining frequency peak in the frequency spectrum window (delineated by ω_1 in the example given above) was used pursuant to distinguishing the differences in pre-/post-infection, febrile, and recovery periods.

3.5.5 Heart Rate Variation

Due to the cardinal value of heart rate as a clinically relevant vital sign, variations in heart rate over days can point to shifts in physiological status. As stated previously, perturbations of HRV are associated with various pathological states. To characterize the heart rate variation, Poincare plots of daily HRV were generated by creating ordered pairs of a measured RR-Interval and the one immediately following it. The Poincare plots were then color-coded by pre-/post-infection, febrile, and recovery periods, and overlaid. This served to better visualize changes in HRV post-infection and at baseline; the RR interval histograms were also plotted and overlaid for each

Poincare plot, and were compared through ANOVA. The method of constructing the histograms is as detailed in Brennan et al, and is detailed on the next page in Figure 9 [59].

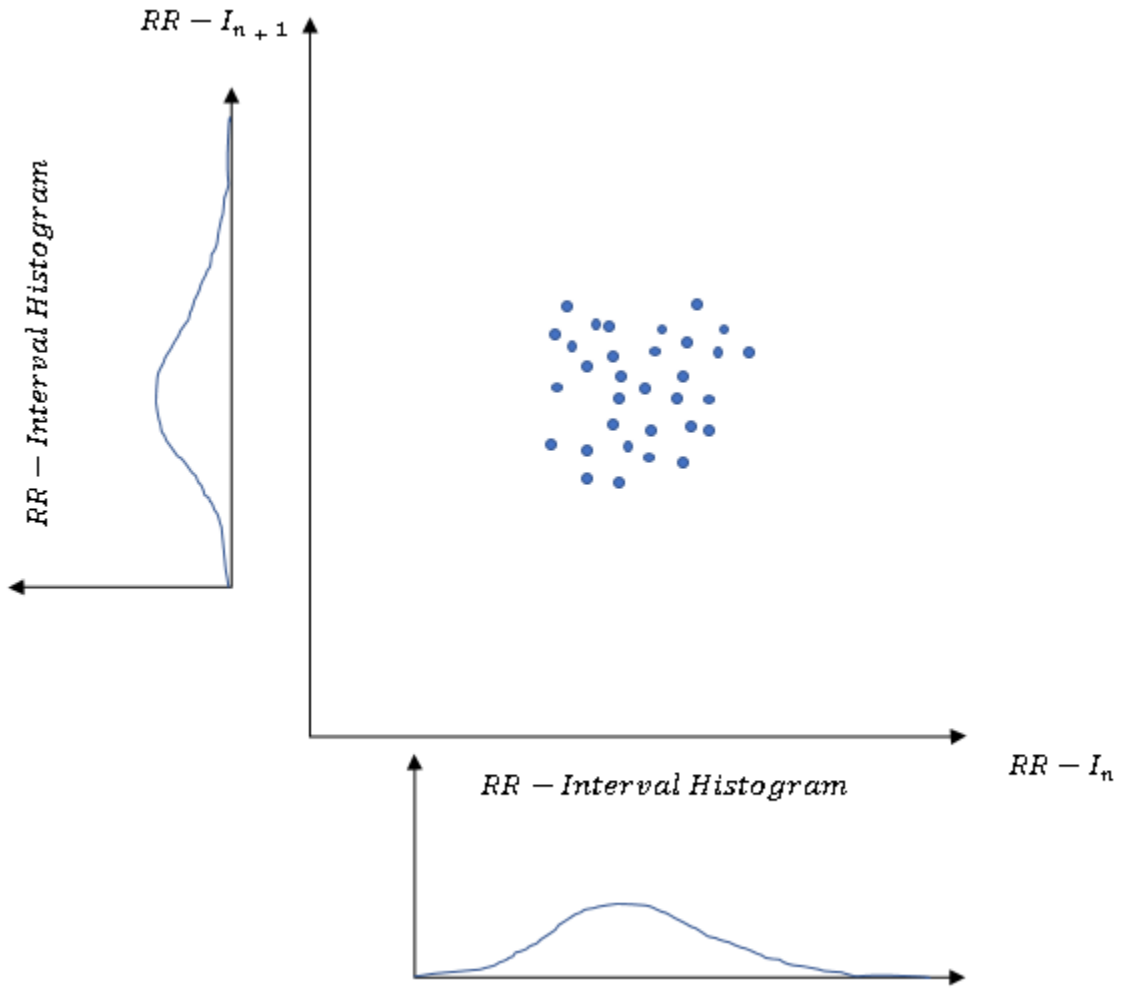

Figure 9. HRV Poincare Plot Analysis.

As mentioned previously, heart rate variability, as tracked by comparing an RR-interval measurement with its following RR-interval measurement, is prone to change as a function of autonomic homeostatic mechanisms and/or autonomic dysfunction.

4.0 RESULTS

The analyses described were performed in rough triplicate for the three types of equine encephalitis viruses. Comparisons were also made between the disease profiles of the various EEVs. As the sheer number of ANOVA results and figures generated for the analyses are too voluminous to be concisely displayed in the results, some results are displayed in the appendix for the sake of manuscript brevity.

4.1 ANALYSIS OF TELEMETRIC DATA

4.1.1 Eastern Equine Encephalitis Virus

4.1.1.1 Disease Course

As far as delineating the courses of disease, infection with EEEV produced frank signs of disease in the form of fever and activity/neurological signs. Animals that received more than $1.1*10^8$ PFU of EEEV died, whereas animals that received below this dose survived.

In the animals that succumbed to infection, the disease course was replicated with high fidelity between both animals that did so. Post-challenge, the animals became febrile shortly after the 3-day mark, culminating in a febrile plateau of 40-41^{o}C between days 4-5 post-infection. The fever plateau was followed by a decline in temperature at approximately 5.5 days post infection corresponding to a rapidly deteriorating state of health in the nonhuman primates as determined by both clinical score and the temperature profiles, the latter as detailed in Figure 10.

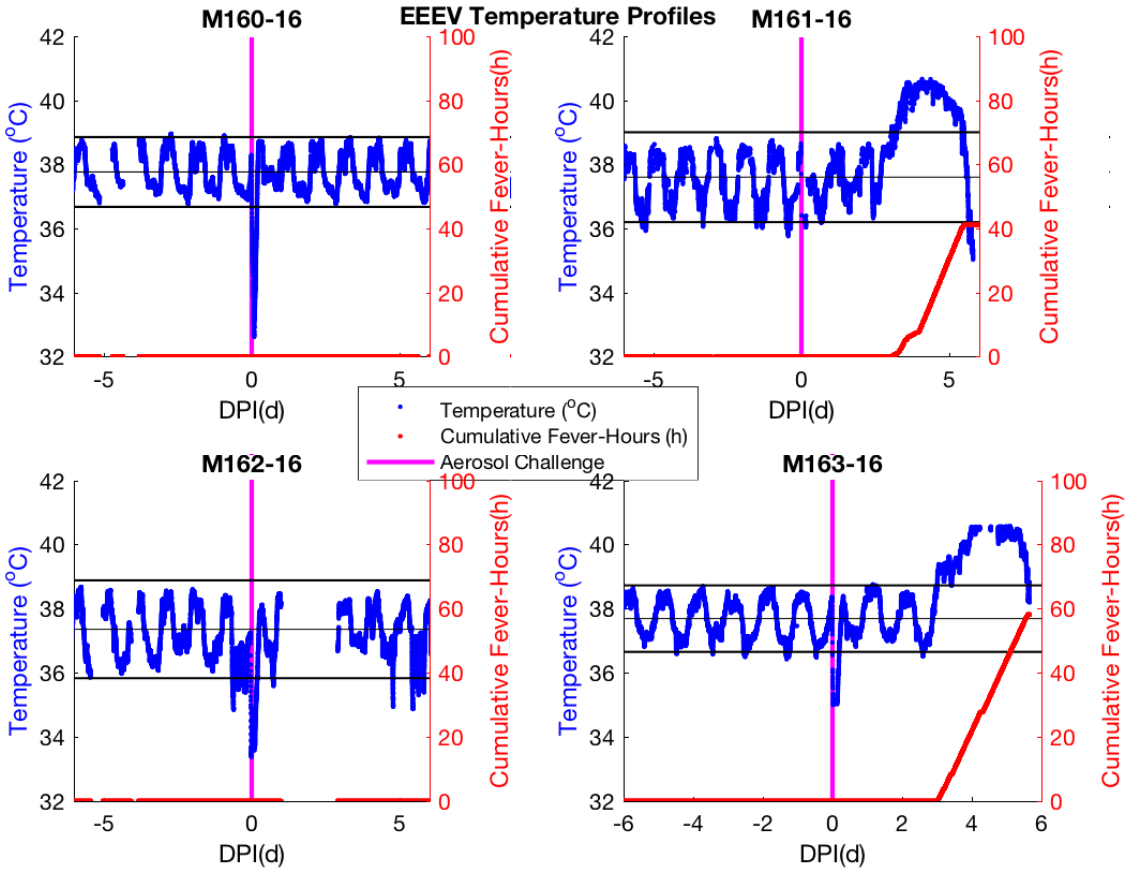

Figure 10. EEEV Disease Profiles.

M160-16 and M162-16 displayed no signs of disease, while M161-16 and M163-16 manifested febrile illnesses and were considered lethally infected animals.

In contrast, in the nonhuman primates that survived, M160-16 and M162-16, no manifestation of fever occurred, and no signs of encephalitides made themselves manifest in their behavior or activity. The animals appear to have emerged with no clinically apparent sequelae, either. Of note, one of the NHP subjects challenged with EEEV that survived the initial challenge was rechallenged, with the subsequent course illustrated in Figure 11, with the initial course plotted alongside for comparison. The results from the initial survey of the disease course

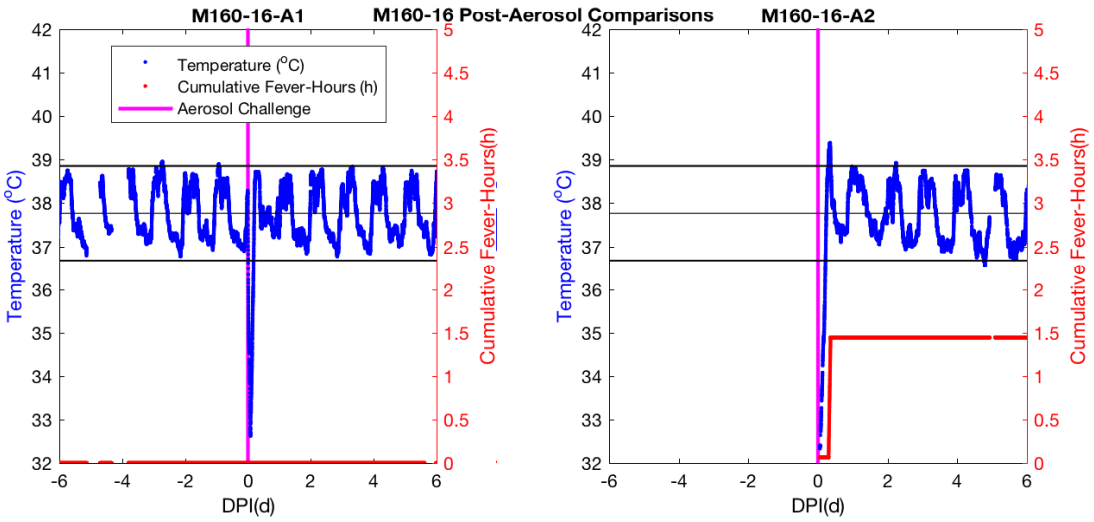

Figure 11. EEEV Post-Challenge Profiles of M160-16.

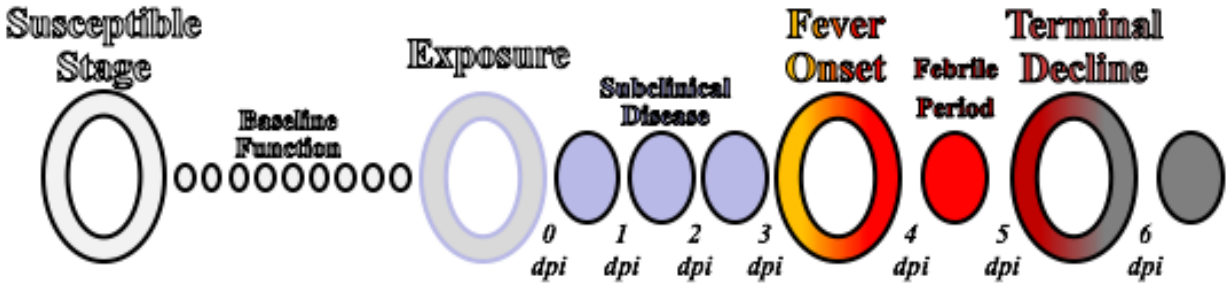

Figure 12. EEEV Disease Course.

This model holds for the NHPs sickened by EEEV; no signs of illness appear for up to three days; at three days, the onset of fever occurs and plateaus until the animal becomes moribund at ~5.5 days post infection.

allowed for the construction of a model disease course for NHPs that succumbed to EEEV detailed in Figure 12. As per this model, the pre-infection period was defined as the period before the aerosol challenge, whereas the post-infection period is defined as the period following infection. For NHPs that did not progress to febrile illness (who did not show any overt signs of infection for the duration of their time courses), this constitutes the remainder of their data. However, for

NHPs that manifested febrile illness and encephalitis, the febrile period was consistently seen after three days post-infection, such that the post-infection and febrile periods in these NHPs were defined as 0-3 days post aerosol challenge, noninclusive, and 3-days post aerosol challenge, respectively. As neither of the sickened NHPs recovered, a recovery period was not applicable for definition in the case of Eastern Equine Encephalitis.

4.1.1.2 Analysis of ECG Metrics

The ECG metrics and their standard deviations (considered as ECG metrics in their own right) for which significant differences were found are summarized in Appendix A.1.

ECG metrics were compared within each animal, due to the variability encountered in the baseline metrics collected for each NHP. Data obtained post-infection was compared to pre-infection data for subjects M160-16 and M162-16 by t-tests upon satisfaction of the assumption of equal variances between data collected post-infection and that collected pre-infection, and one-way ANOVAs were used to compare pre-infection, post-infection, and febrile period ECG data for NHPs M161-16 and M163-16. As M160-16 was challenged twice by aerosol, only data from the peri-challenge period of the first aerosol challenge was used. Repeated measures ANOVA tables can be found in the appendix. No significant differences were observed in any of the electrocardiography metrics for M160-16 and M162-16, the NHPs who survived the EEEV challenge by aerosol. Determination of infection status is subject to further analysis in pathology.

In NHPs challenged with EEEV, few to no arrhythmic beats (BAD) were detected throughout the recorded study, and no significant differences existed between the number of arrhythmic beats generated pre-/post-infection in any of the NHPs under study. The heart rate, however, exhibited differences between the NHPs that succumbed to infection versus those who did not; HR demonstrated a decrease in the post-infection period in M161-16 and peaked during

the febrile period, while the same metric demonstrated an increase in the post-infection period in M163-16 and also peaked during the febrile period. In both cases, the heart rate during the febrile period was increased by a factor of ~1.5x compared to baseline. The HR trends are illustrated *en bloc* in all NHPs in Figure 13, and a comparison between a nondiseased/diseased NHP by day is demonstrated in Figure 14.

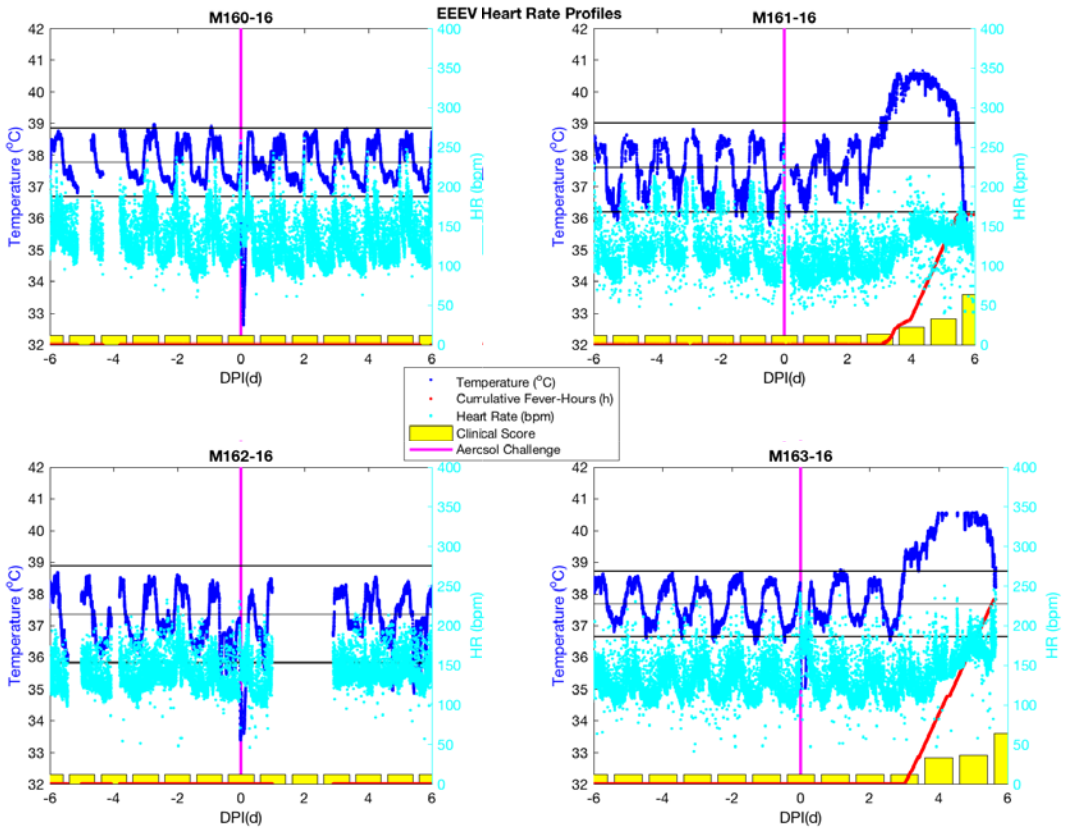

Figure 13. EEEV Heart Rate Profiles.

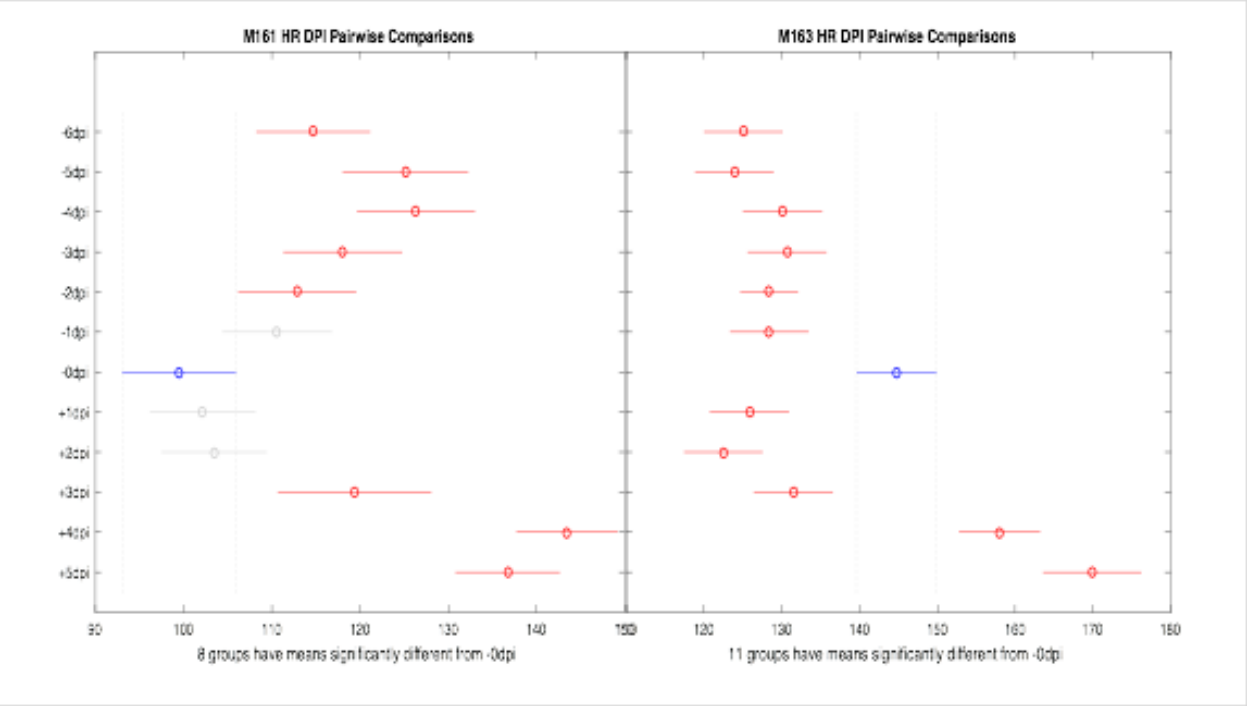

Figure 14. Heart Rate in EEEV-infected NHPs (daily).

Units in (bpm). Red indicates significant differences by day; the amount of daily variability in average HR is evident through this figure.

The PCt profiles of all 4 EEEV NHP subjects is displayed in Figure 15. The number of P-waves counted in each sampling period (PCt) changed as well, in subjects M161-16 and M163-16, as would be expected due to the increased heart rate. At a closer examination, however, this increase appears only to manifest at the end of the disease course, during the moribund stage of the febrile period. Though this difference distinguished the sickened NHPs from the NHPs that did not die from their illness, the number of P-waves documented in each sampling period demonstrated a persistent downward trend with a spike in P-wave count during terminal decline, when compared to M163-16, which demonstrated no change during the post-infection period but an increase during the fever, documented in Figure 16.

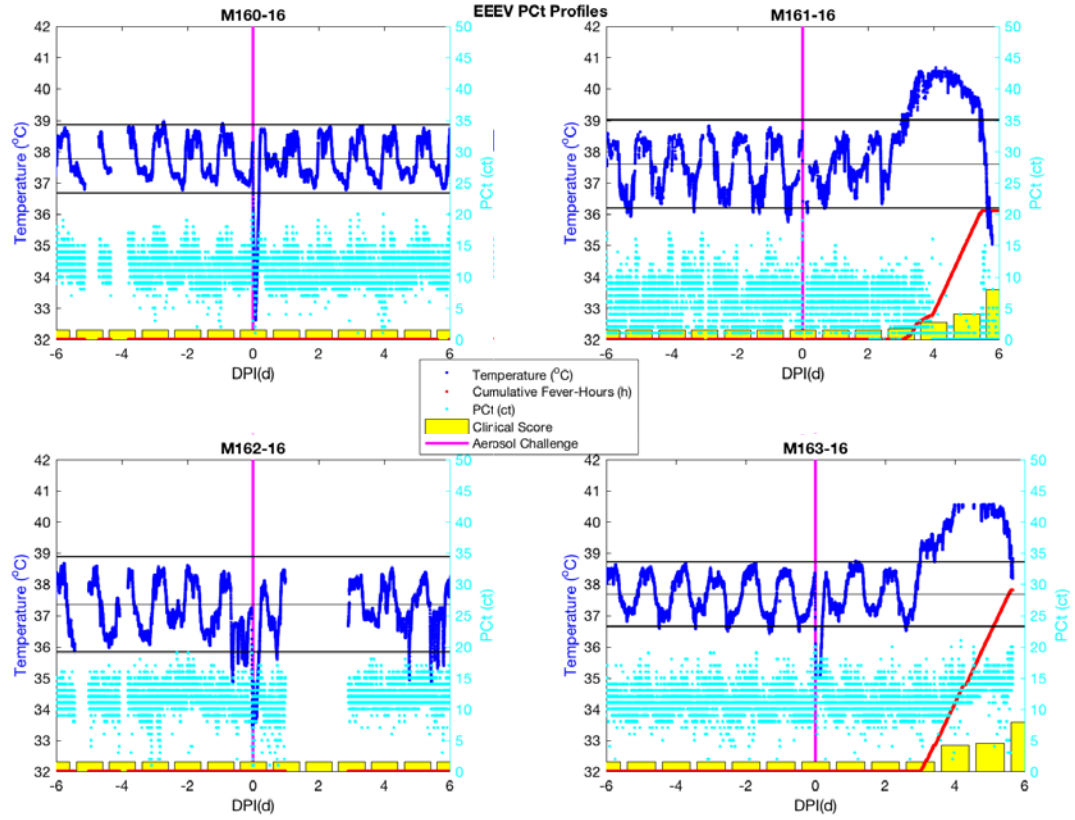

Figure 15. EEEV P-Wave Count Profiles.

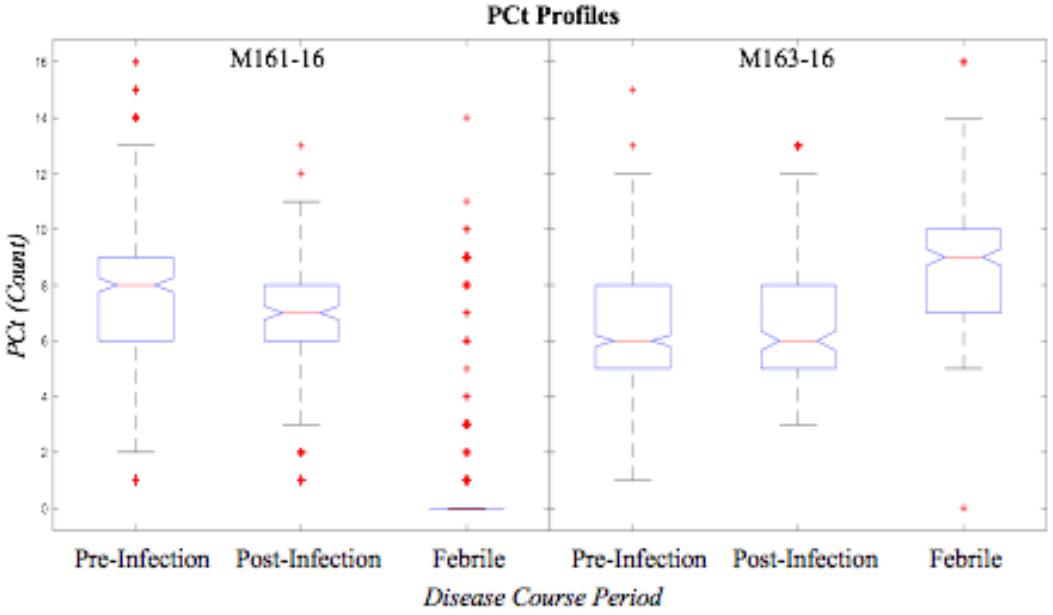

Figure 16. EEEV P-Wave Count by Disease Period in Sickened NHPs.

The PR-Interval appears to decrease following the onset of the febrile period in the sickened NHPs, as documented in Figure 17. However, between the sickened NHPs M161-16 and M163-16, it appears that the PR-I initially increased from baseline in the post-infection period, whereas a negligible effect occurred in the PR-I of M163-16 post-infection, only showing an overall decrease during the febrile period with a small spike in PR-I as the animal became moribund, illustrated in Figure 18. The PR-I metric exhibited the same paradoxical behavior between the sickened NHPs M161-16 and M163-16 as with the PCt metric.

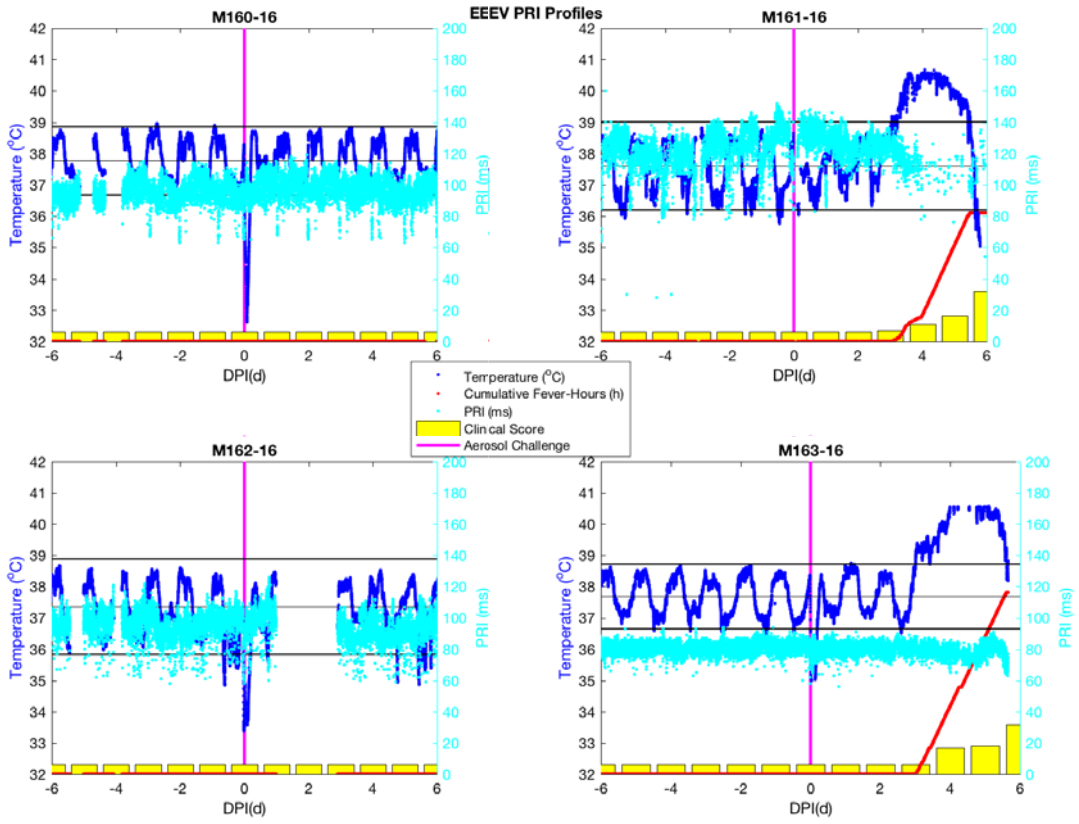

Figure 17. EEEV PR-Interval Profiles.

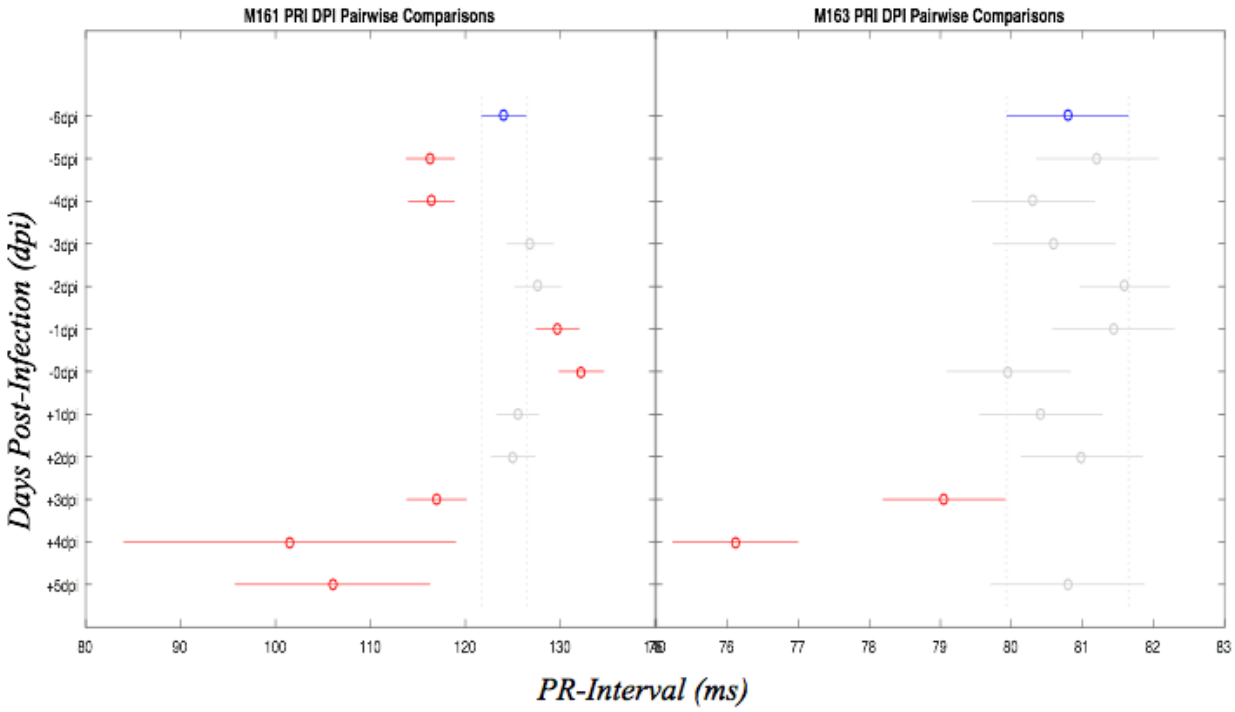

Figure 18. EEEV PR-Interval Changes in Sickened NHPs compared to baseline.

The width of the P-wave, P-Width, decreases during the febrile period in the sickened NHPs; profiles of P-Width are plotted in Figure 19. No changes were detected by period in the NHPs that did not become ill. The P-Width appears to have dampened in M161-16 post-infection, although the average P-Width increased in the post-infection period before decreasing in the febrile period, as demonstrated in Figure 20. In M163-16, no significant change appears to have taken place in the post-infection period, and the febrile period likewise saw a decrease in the P-wave width.

The next metric to reveal significance was the QRS-interval; in this case, as documented by Figure 21 and Figure 22, QRS in both EEEV-sickened NHPs exhibited a progressive increase in the days following infection, through the febrile period. However, while the mean QRS in M161-16 increased by a factor of 1.16x, the mean QRS in M163-16 only increased 1.03x.

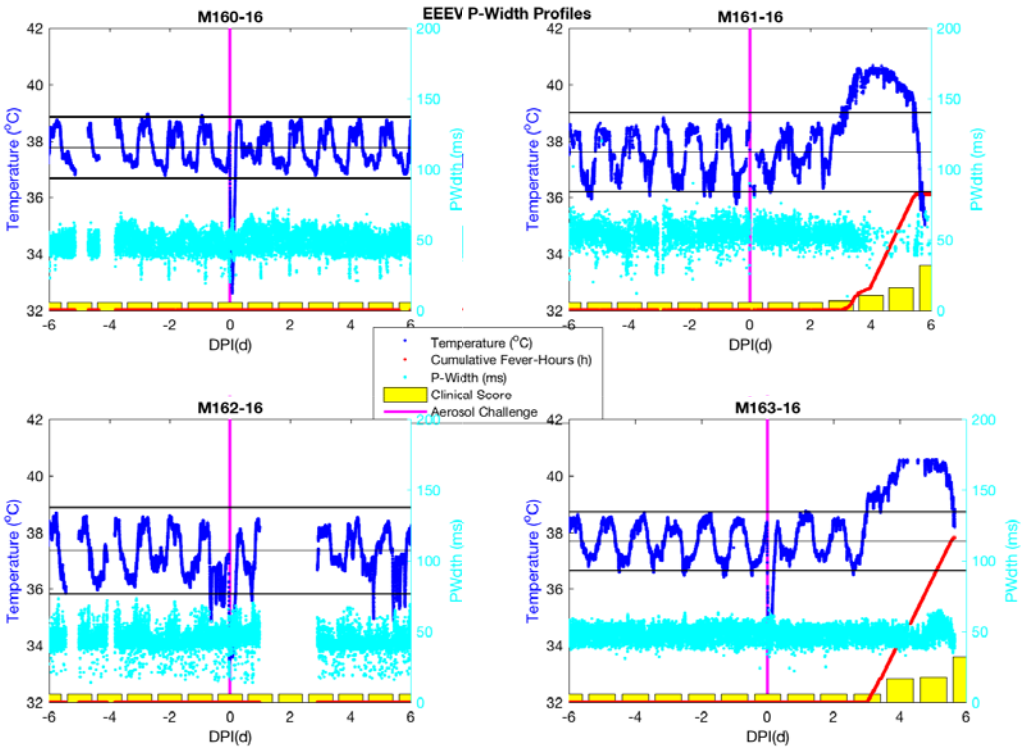

Figure 19. EEEV P-Width Profiles.

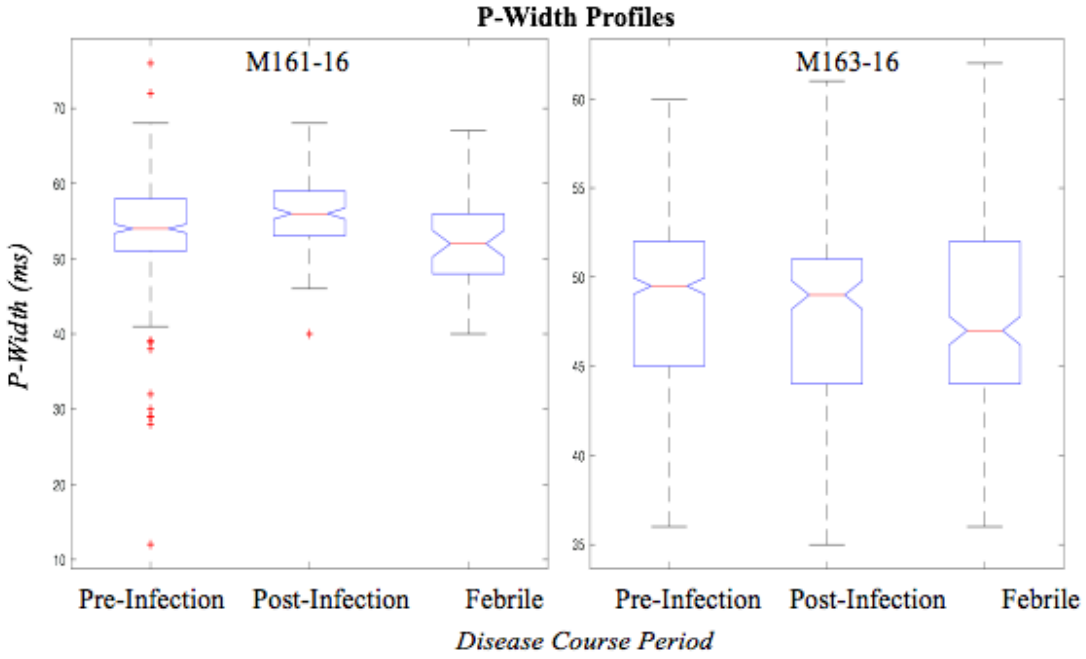

Figure 20. EEEV P-Width Changes in Sickened NHPs.

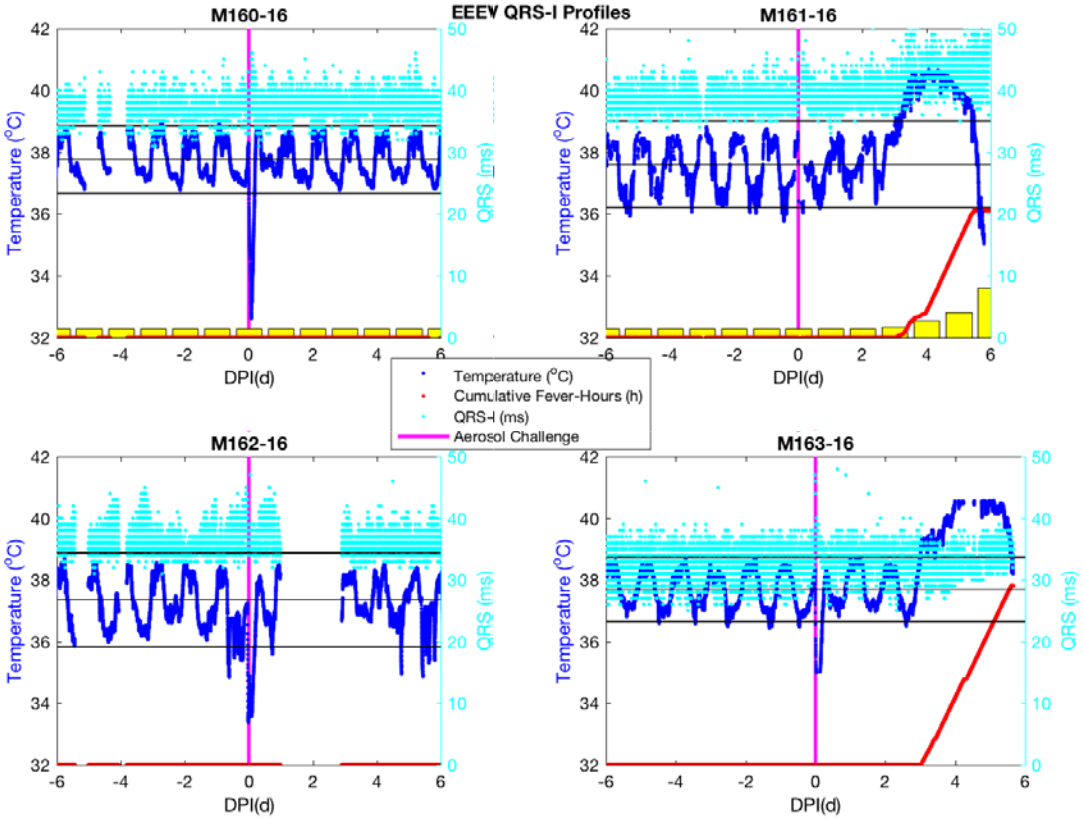

Figure 21. EEEV QRS Profiles.

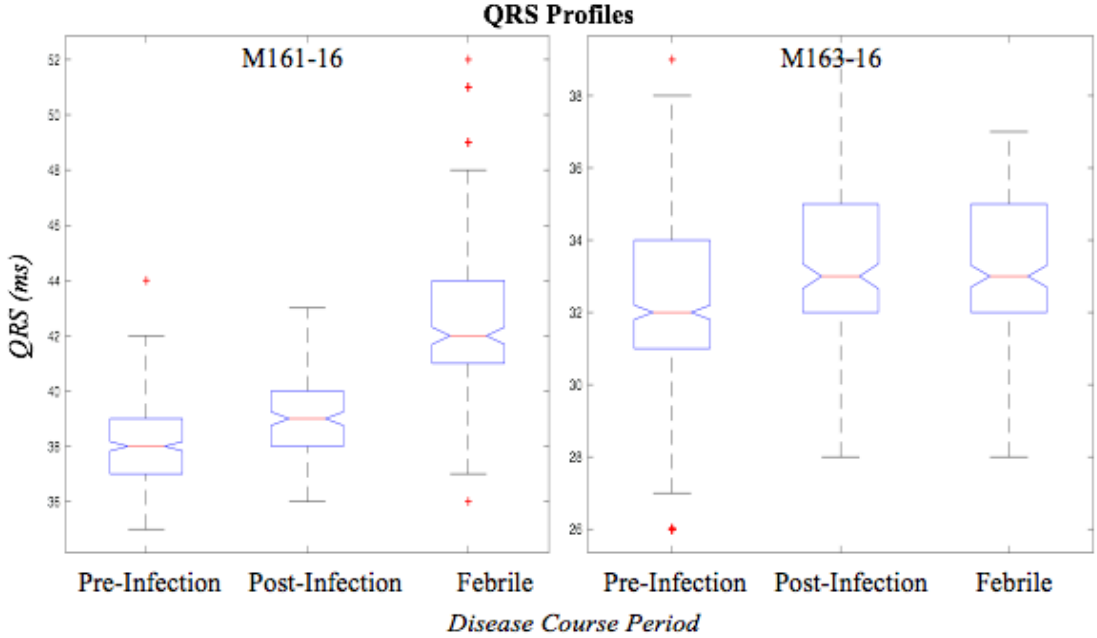

Figure 22. EEEV QRS Changes in Sickened NHPs.

The QT-interval data of the EEEV NHP subjects that succumbed to infection provided an interesting finding in that during the febrile period, the mean daily QT-I of both M161-16 and M163-16 decreased by factors of 1.25x and 1.24x, respectively, or to phrase it differently, reduced to 85% and 80% of their baseline values. No significant differences were detected in QT-I in the post-infection period, though for the following two days post-infection, there was an increase in the mean daily QT-I for both M161-16 and M163-16. Profiles of QT-I data against the disease course are demonstrated in Figure 23, while the mean daily QT-I profile is illustrated in Figure 24. M161-16 exhibited a great deal of noise in the QT-I signal, which required filtering, possibly leading to artifact generation, but the ANOVA data remains valid.

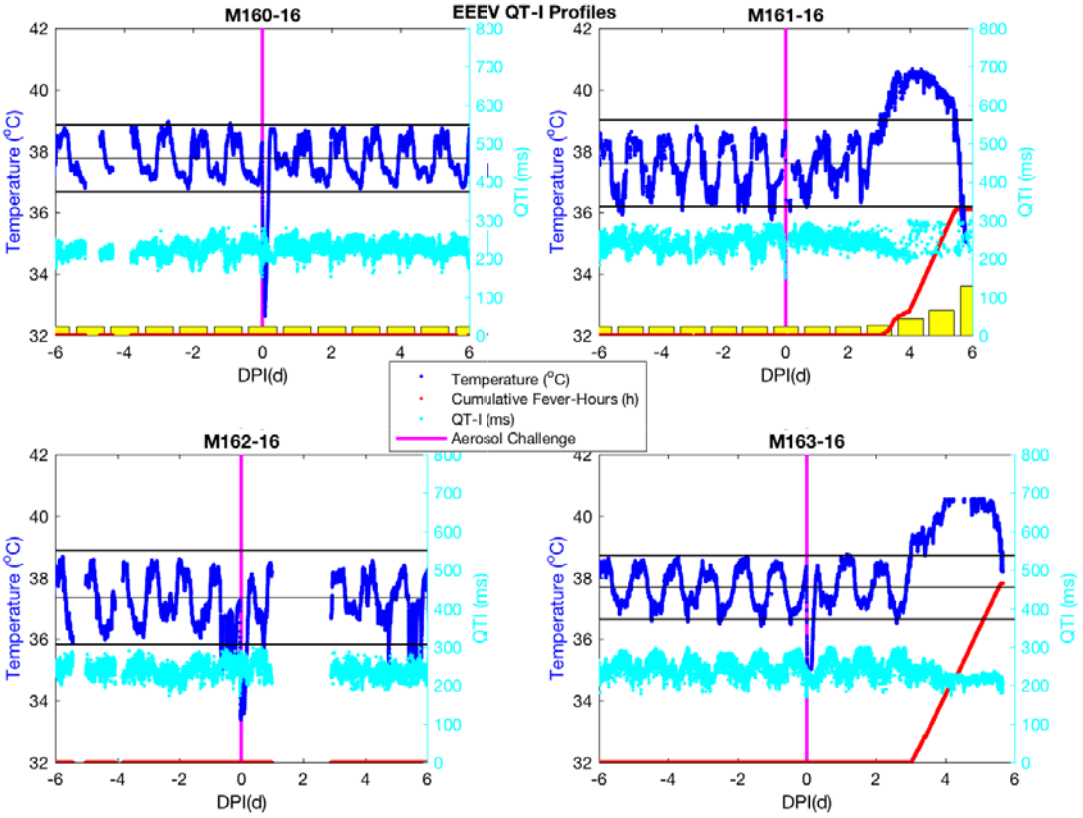

Figure 23. EEEV QT-I Profiles.

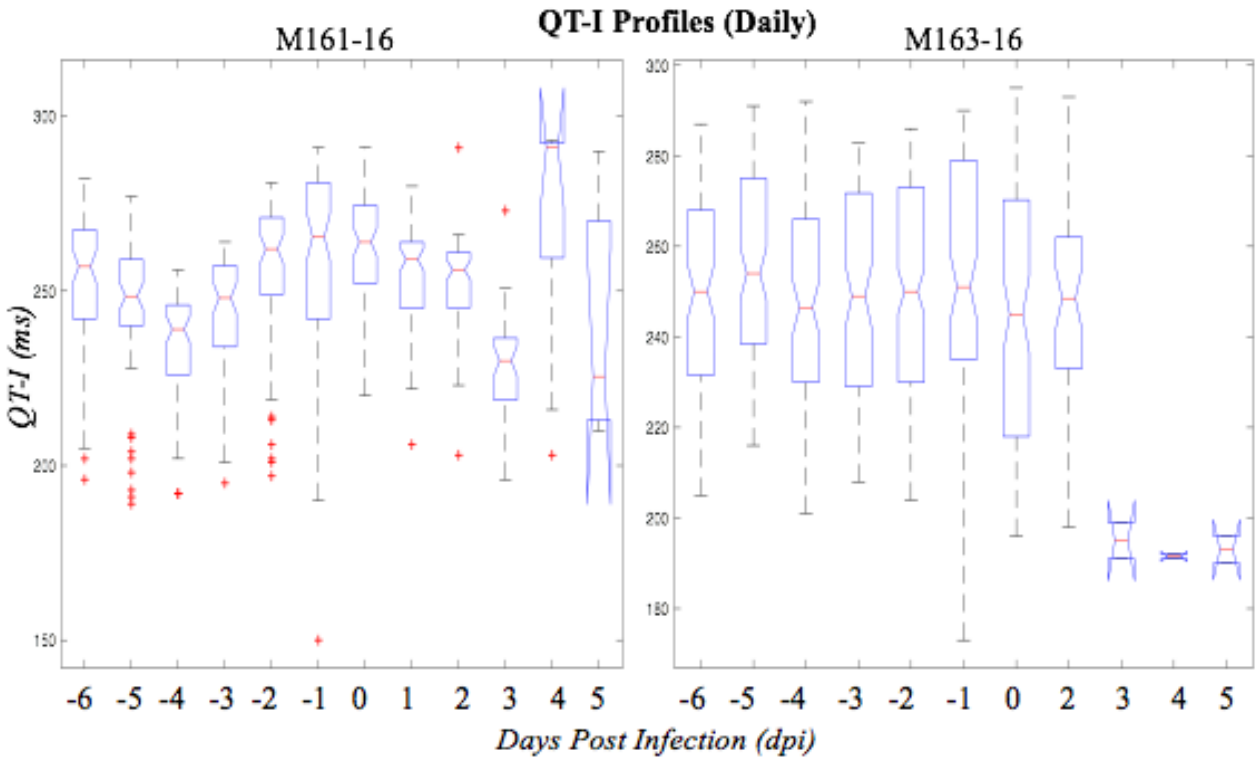

Figure 24. EEEV Mean Daily QT-I in Sickened NHPs.

Finally, the last metric for which significance was discovered was the RR-interval, which is reasonable given its collinearity with HR. The trend uncovered mirrored that of HR; RR-I in both M161-16 and M163-16 had decreased to 80% and 81% of baseline mean daily RR-I during the febrile period. RR-I profiles plotted against disease course are illustrated in Figure 25, and RR-I by period in the NHPs who succumbed to infection are displayed in Figure 26.

The heart rate increase in the NHPs that succumbed to EEEV aerosol infection was the most consistent metric that accompanied the disease course; it stands to reason that the heart rate would increase as the animal becomes febrile, since altered homeostasis following the infection preceding and during the febrile period create a physiological milieu that favors immune cell chemotaxis to infected areas [60, 61]. The other significant metrics examined here

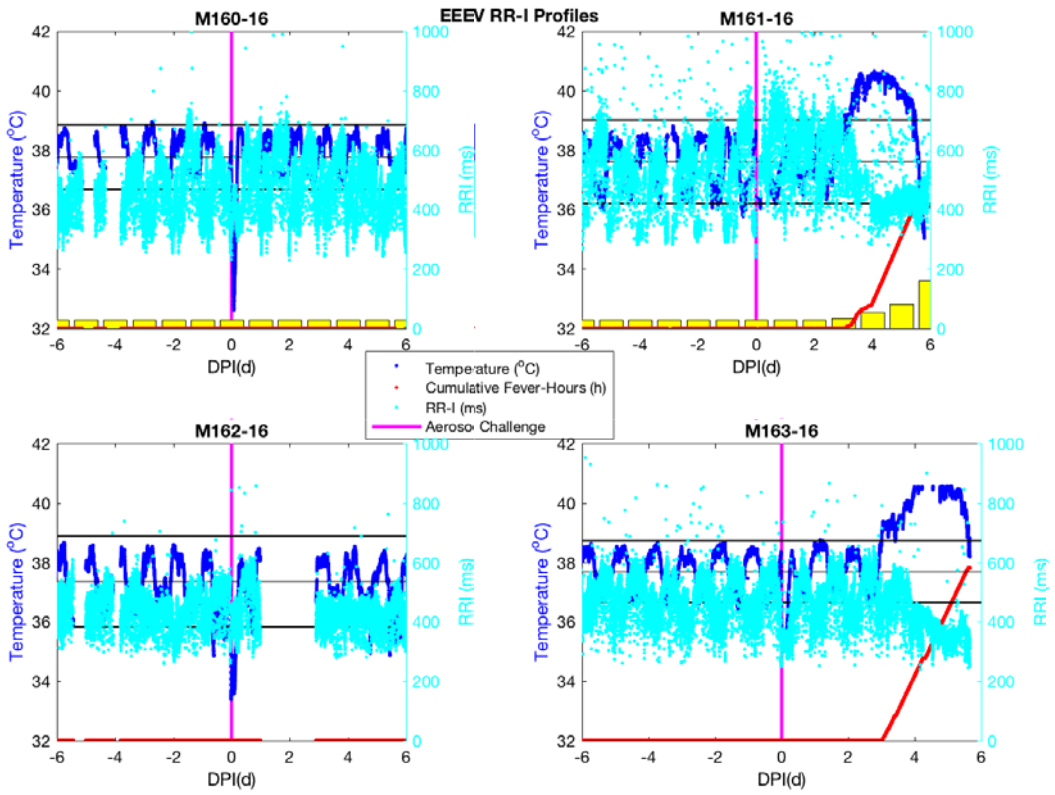

Figure 25. EEEV RR-I Profiles.

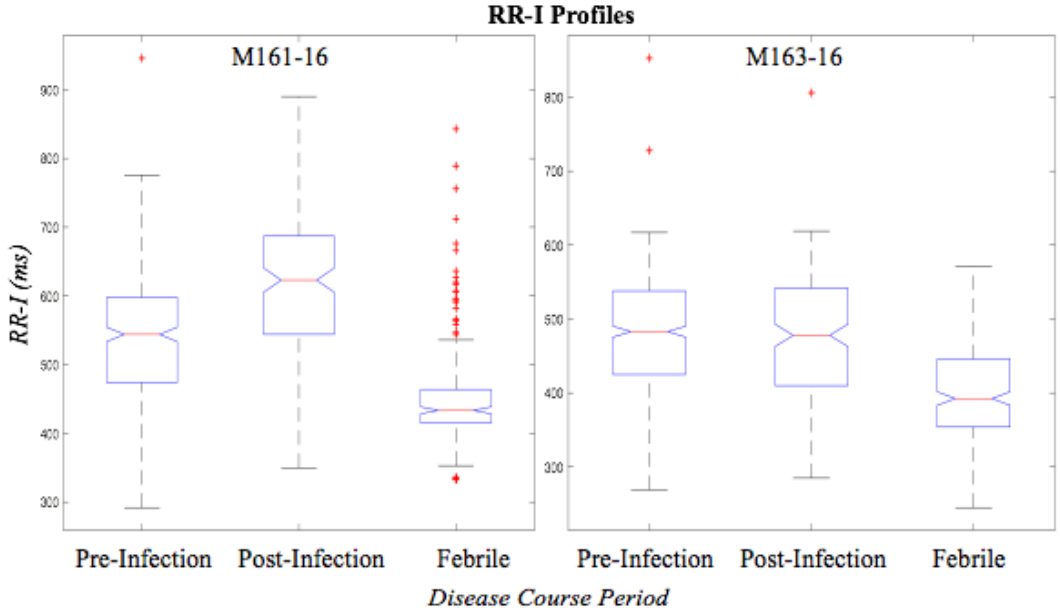

Figure 26. EEEV Mean Daily RR-I in Sickened NHPs.

will covary with heart rate, as the compression of the entire ECG cycle relies on the compression of some or all of its constituent parts. In light of this information, it is unsurprising that PCt, P-Width, and QT-I exhibit decreases by the end of the febrile period as well; what is surprising is the lengthening of the QRS interval during the febrile period. Examination of raw ECG trace obtained during the febrile period compared to the baseline ECG revealed no gross pathological signs, such as split or deformed QRS complexes (including R' wave formation), of direct cardiac pathology such as a conduction / bundle branch block. As the QRS interval corresponds to ventricular depolarization in the heart, a widened QRS interval could point to electrolyte imbalances such as hypokalemia; as clinical observations noted, both M161-16 and M163-16 exhibited decreased imbibition during their febrile periods, and also signs of dehydration. However, blood chemistry obtained at baseline, during aerosol, and at necropsy of M161-16 and M163-16 did not bear out this hypothesis, as potassium levels were within normal limits (3.5-5 mEq).

4.1.1.3 Frequency Spectrum Analyses

The frequency spectrum analysis of the NHP subjects in EEEV present several interesting findings, the most exciting one of which lies in the observation that when subjected to the Fourier transform, pre-/post-infection and febrile periods are distinguishable in the NHP subjects that became ill by examining the fundamental frequency of each metric. The frequency spectra appear to vary little between ECG metrics, especially those that covary; for instance, metrics associated with HR, as discussed above, by and large exhibit similar trends, with few exceptions. In Figure 27, the four plots demonstrate the time-domain data (left) and frequency-domain (right) spectra of the RR-Interval for M160-16, M161-16, M162-16, and M163-16. The amplitude of

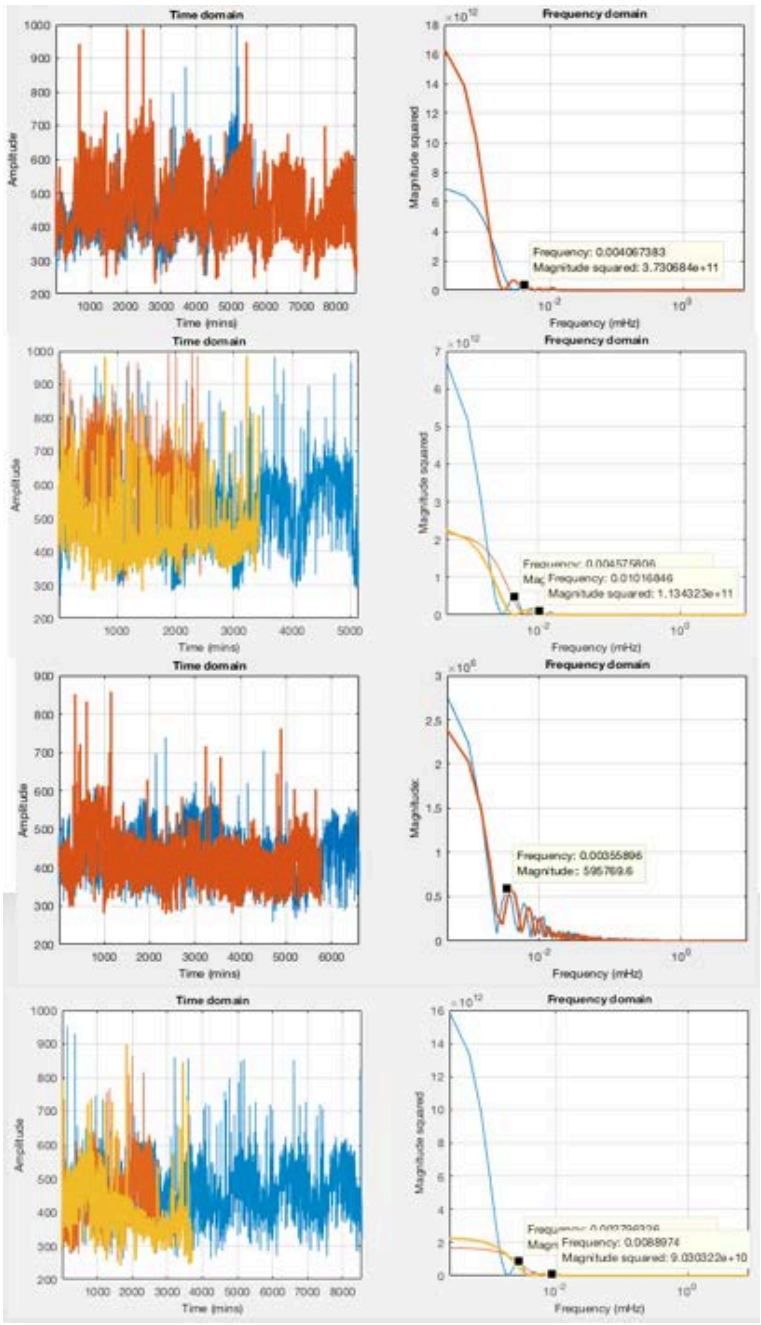

Figure 27. EEEV RR-I Frequency Spectra.

RR-Interval data plotted on the left, frequency spectra plotted on the right. From top to bottom: M160-16, M161-16, M162-16, M163-16. Blue for pre-infection, red for post-infection, and yellow for febrile period.

the frequency spectrum plots is not significant, as magnitude squared (ms^2 in this case) is determined by the number of points fed into the Fourier Transform and also the value of time-

domain function. The fundamental frequency, defined here as the first local maximum, represents the frequency with which the signal repeats, with all following peaks registering as harmonics, or echoes of the initial peak frequency. The trend seen in the EEEV NHPs that succumbed to infection was defined by an initial baseline frequency of 0.242 and 0.395 cycles per day (cpd) for M161-16 and M163-16, respectively. Post-infection, this jumped to 0.769 and 0.879 cpd, then decreased to 0.549 and 0.579 cpd for M161-16 and M163-16, respectively. NHPs thar emained healthy had small changes in RR-I frequency post-infection, but not to the same degree seen in sick NHPs. These data are summarized in Table 4.

Table 4. EEEV Frequency Analysis Results.

NHP	***Fundamental Frequency (cpd)***	***Post-Infection Frequency (cpd)***	***Febrile Period Frequency (cpd)***	***Differences (Pre-Post-Feb) (cpd)***
M160-16	0.351	0.242	N/A	(-0.109)
M161-16	0.395	0.879	0.571	(0.484, -0.308)
M162-16	0.307	0.351	N/A	(0.044)
M163-16	0.242	0.769	0.549	(0.527, -0.220)

4.1.1.4 Heart Rate Variability

Heart rate variability in NHPs exposed to EEEV was decreased during the febrile period in sickened NHPs relative to healthy NHPs, who manifested no such changes (Figure 28).

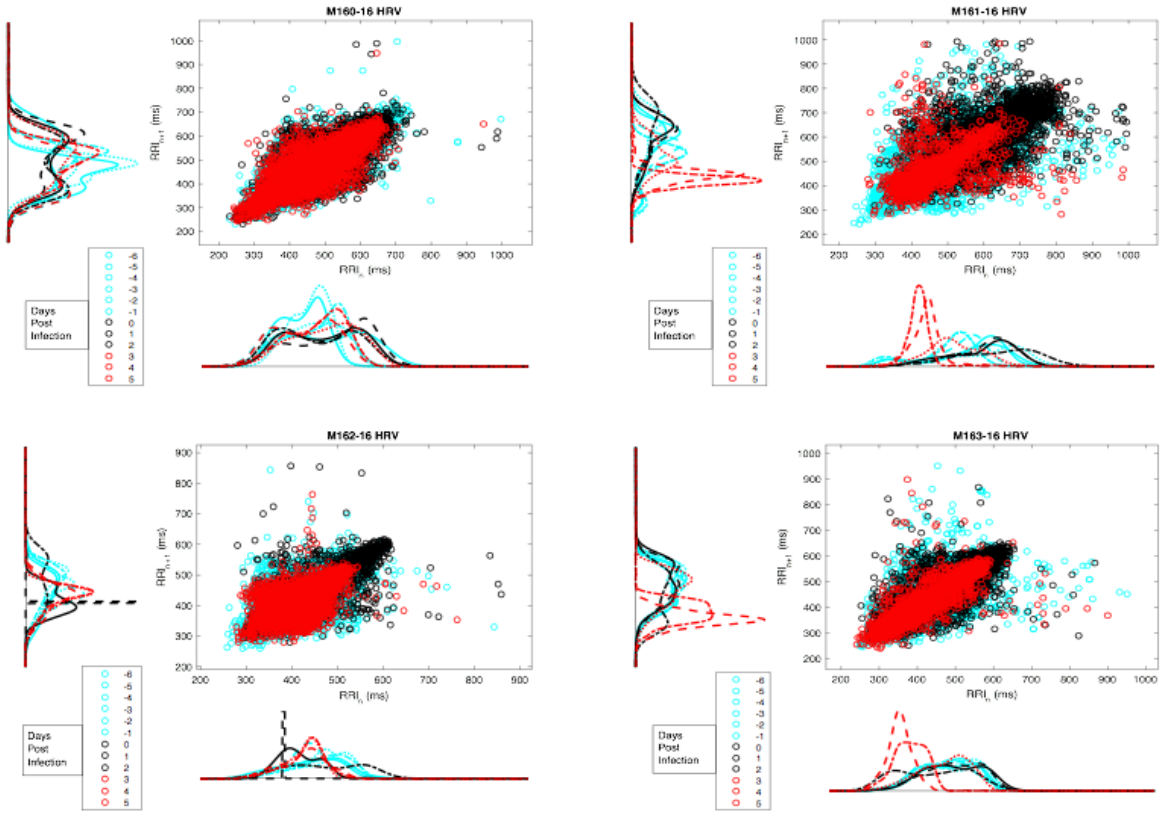

Figure 28. EEEV HRV Poincare Plot Overlays.

Poincare plots of HRV by day; cyan denotes the pre-infection period, black the post-infection period, and red the febrile period. Though trends are visible by inspection, these ultimately proved not to be significant.

One way ANOVA (Table 6), demonstrated that although significant differences exist between daily HRV plots, these differences are not meaningful when compared both within the same NHP subject and between sick and healthy subjects, as demonstrated by a comparison of the pairwise tests of the probability distributions.

Table 5. EEEV HRV Probability Density one-way ANOVA Results.

M160-16 HRV owANOVA

ANOVA Table

Source	SS	df	MS	F	Prob>F
Columns	0.00016	11	1.47168e-05	5.38	2.23766e-08
Error	0.00325	1188	2.73724e-06		
Total	0.00341	1199			

M161-16 HRV owANOVA

ANOVA Table

Source	SS	df	MS	F	Prob>F
Columns	0.00028	11	2.50146e-05	11.64	6.83532e-21
Error	0.00255	1188	2.14811e-06		
Total	0.00283	1199			

M162-16 HRV owANOVA

ANOVA Table

Source	SS	df	MS	F	Prob>F
Columns	0.00009	11	8.37622e-06	2.18	0.0133
Error	0.00456	1188	3.83453e-06		
Total	0.00465	1199			

M163-16 HRV owANOVA

ANOVA Table

Source	SS	df	MS	F	Prob>F
Columns	0.00007	11	6.69681e-06	12.1	8.42144e-22
Error	0.00066	1188	5.53537e-07		
Total	0.00073	1199			

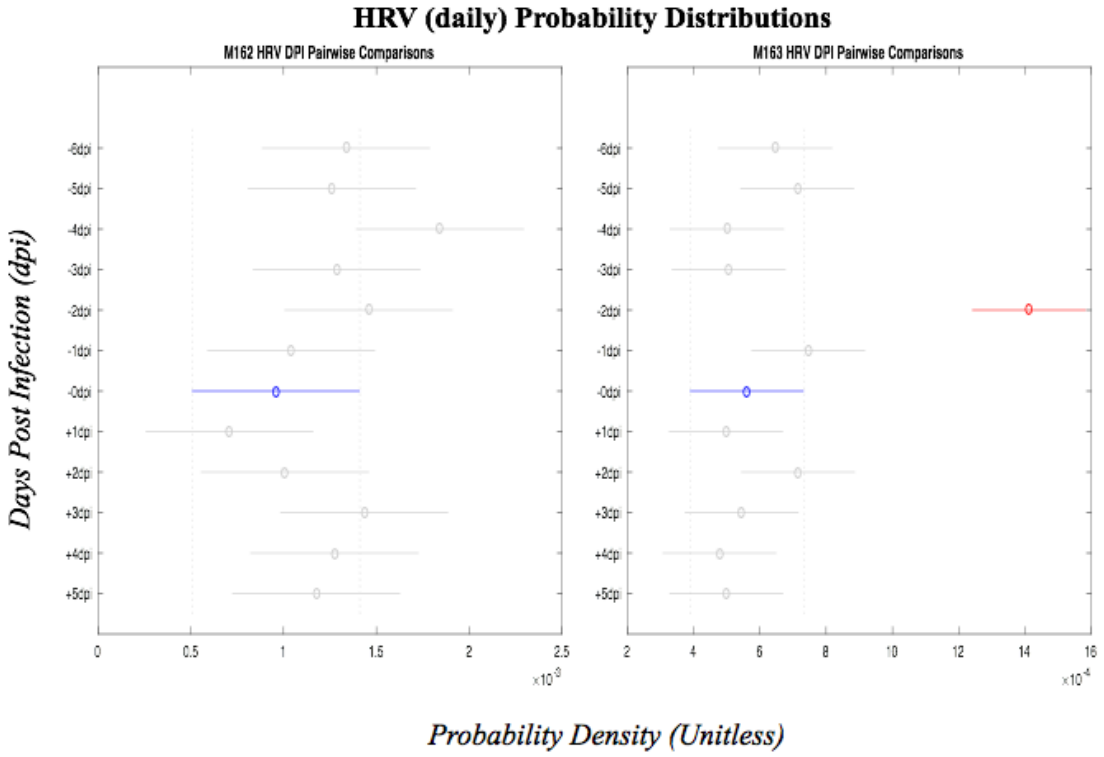

Figure 29. EEEV HRV pairwise comparisons of probability density in M162-16 and M163-16.

4.1.2 Western Equine Encephalitis Virus

4.1.2.1 Disease Course

Challenge of NHPs with Western Equine Encephalitis Virus produced few signs of disease in the majority (75%, n = 4) of NHPs challenged, within a week post-infection. All animals survived the aerosol challenge except for the NHP (M169-16).

The disease course of M169-16 serves as the only record with which to model the disease. M169-16 became febrile shortly after the 2-day mark, that slowly progressed to a febrile peak of 40.56°C at 4.5 days post-infection, which persisted for another 2.5 days before the combination of temperature, activity, and neurological scores invoked the humane endpoint. Febrile courses for NHPs M166-16, M167-16, M168-16, and M169-16 are plotted in Figure 30.

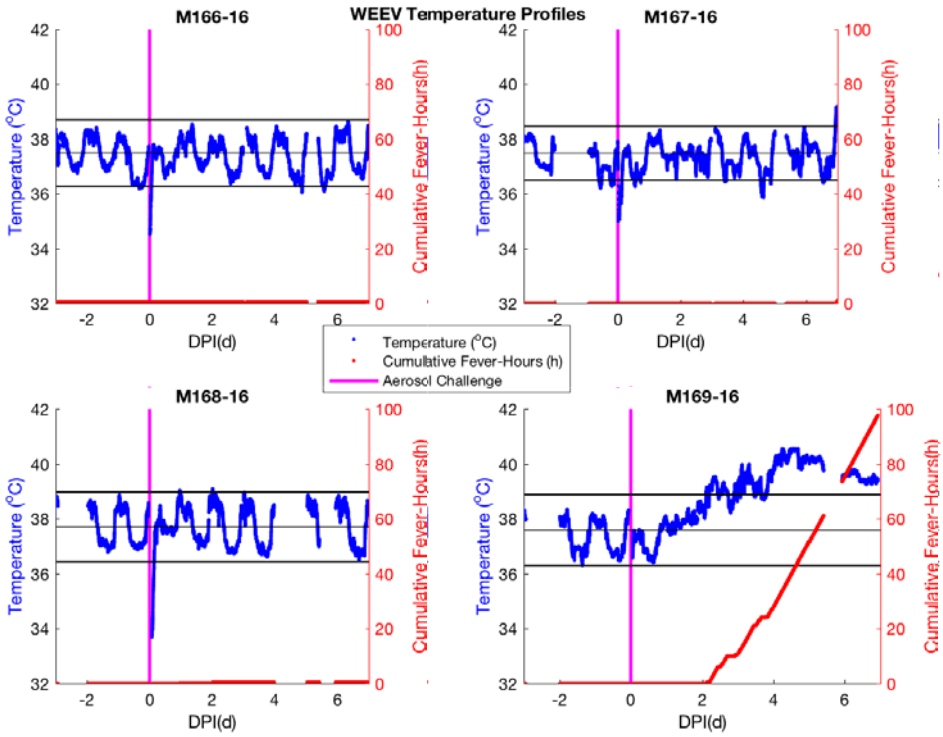

Figure 30. WEEV Disease Profiles.

By temperature profile and clinical scoring, NHP subjects M166-16, M167-16, and M168-17 remained healthy post-challenge, with no manifestation of fever, and few if any signs of encephalitis. M167-16 arrived at the RBL with a malfunctioning implant, such that most data required censoring due to the unreliable accuracy of the data gathered. As such, M169-16 provided the only template for the construction of a model disease course for fatal WEEV infection by aerosol route, with the model shown in Figure 32.

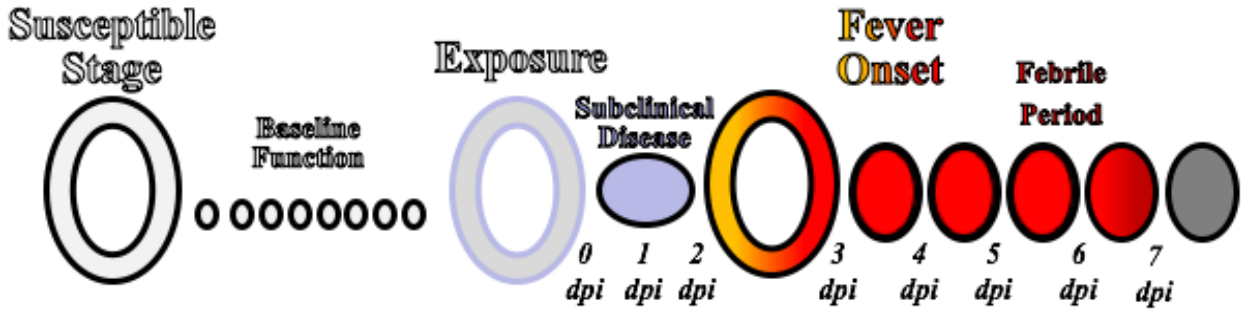

Figure 31. WEEV Disease Course.

As with the EEEV model, the pre-infection period for WEEV consists of the baseline period before the aerosol challenge. The post-infection period consists of the period of seven days following aerosol challenge for healthy NHPs, while the period between 0-2 dpi, noninclusive, is defined as the post-infection period in M169-16. The febrile period then, is defined as 2-7 days, inclusive. This model as of the time of this writing holds only for this one observed subject. As the sickened NHP did not recover, no recovery period could be defined for Western Equine Encephalitis Virus.

4.1.2.2 Analysis of ECG Metrics

The ECG metrics and their standard deviations (considered as ECG metrics in their own right) for which significant differences were found are summarized in Appendix A.1.

Repeated measures ANOVA tables can be found in the appendix. Increased variability was found in the ECG metrics for the WEEV-exposed NHPs; therefore, follow-up t-tests and one way ANOVAs by day were required to assess whether or not true differences existed between the NHPs' metrics. Due to the large number of significant variables, only the metrics in common with those significant in EEEV and VEEV NHPs will be discussed.

In NHPs challenged with WEEV, no significant differences developed in pre- and post-infection period HR in M166-16 and M168-16, the NHPs that did not develop a febrile illness. In contrast, in M169-16, the HR was not affected during the post-infection period, but increased by a factor of 1.5x its initial value during the febrile period. The HR profiles are documented against the disease profiles in Figure 32. Initially, repeated measures ANOVA had documented significant changes in the afebrile NHPs, but upon further analysis, it appears that baseline variability had triggered significance in the repeated measures analysis. The results of the change in HR for M169-16 are plotted in Figure 32.

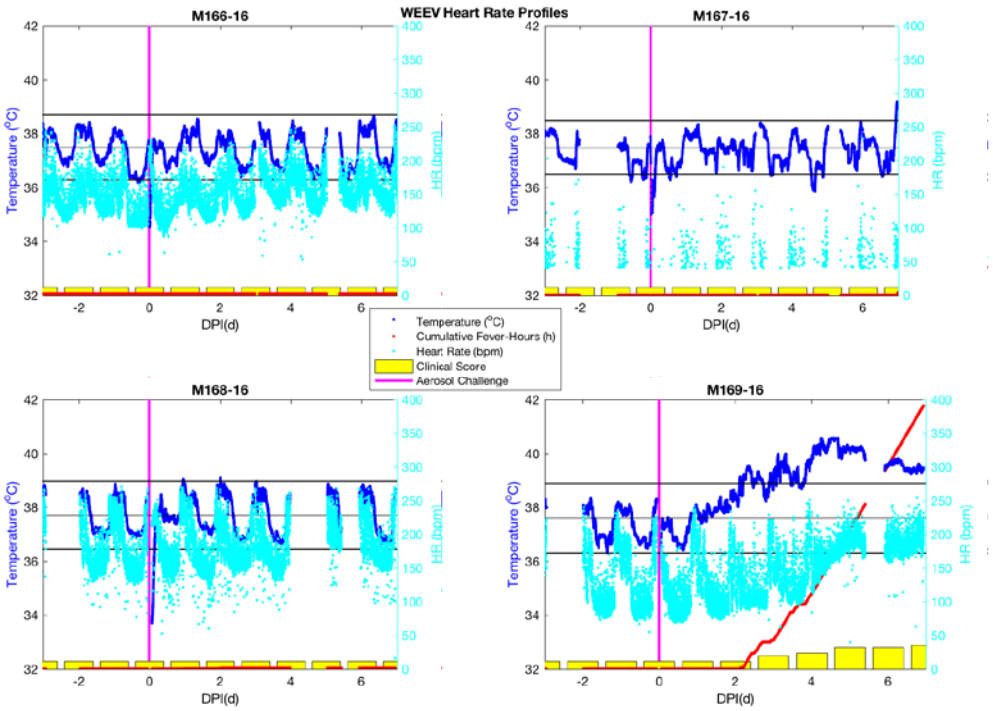

Figure 32. WEEV Heart Rate Profiles.

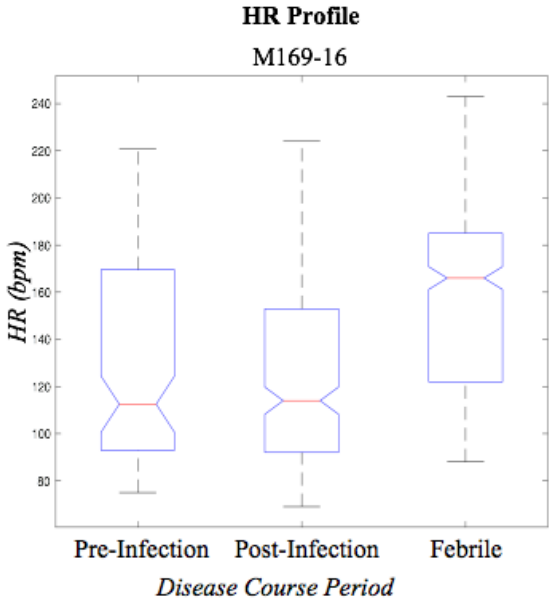

Figure 33. Heart Rate in WEEV-sickened NHP.

No significant differences were detected in PCt for M166-16 and M168-16; however, it appears that as M169-16 entered the febrile period, its PCt increased by a factor of 1.5x, as would be expected from the HR data. These results can be seen in Figure 34 and 35, respectively.

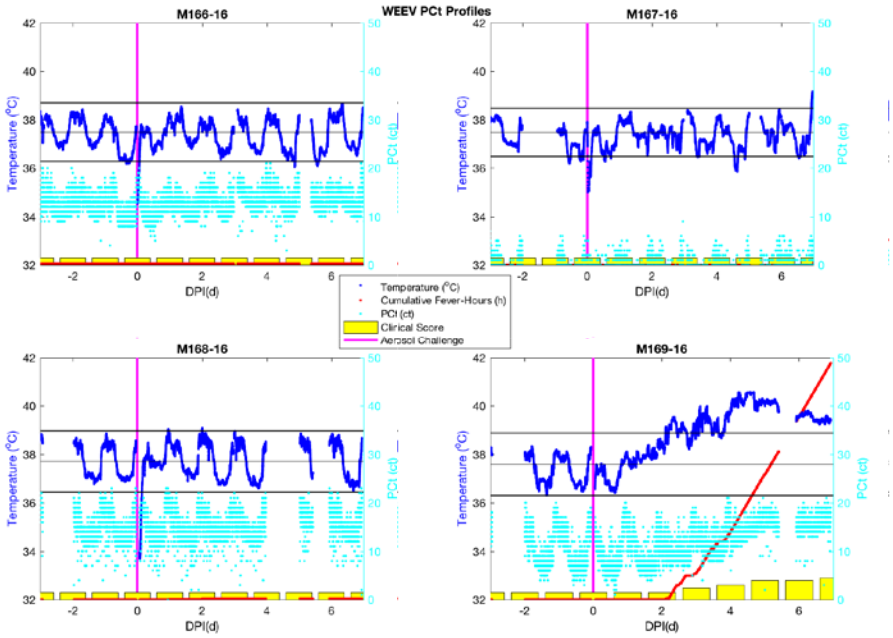

Figure 34. WEEV P-Wave Count Profiles.

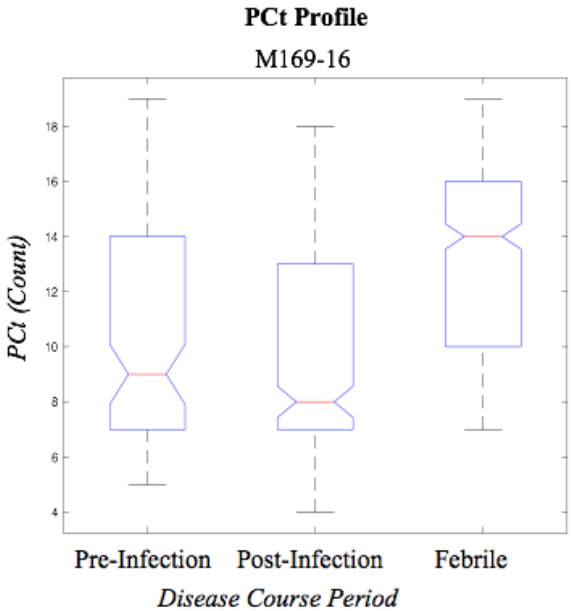

Figure 35. WEEV P-Wave Count by Disease Period in Sickened NHP.

The QRS data for WEEV are plotted against disease course in Figure 36. The QRS-interval in WEEV-infected NHPs exhibited a variety of behaviors; in M166-16 and M168-16, repeated measures ANOVA yielded significant results, which were then followed up by one way ANOVA of daily mean QRS-interval. The latter also yielded significant results, but post-hoc pairwise testing produced no significance. When compared by pre-infection and post-infection period, QRS in M166-16 decreases pre-infection to post-infection. In contrast, M168-16 exhibits an increase in QRS from pre-infection to post-infection. In M169-16, a much more marked effect was observed; on 2dpi, the QRS became reduced, eventually reaching 84% of its baseline value. To contrast the QRS profiles between fatal WEEV cases and afebrile cases,

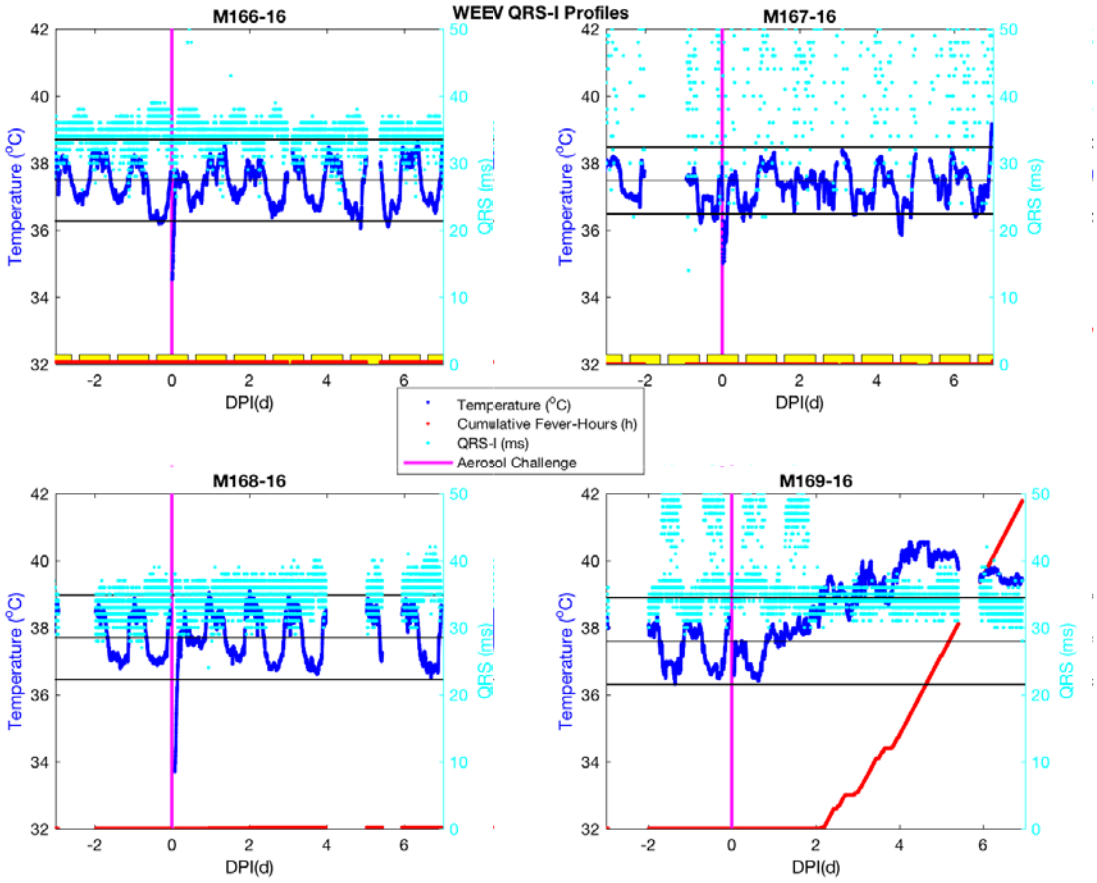

Figure 36. WEEV QRS Profiles.

Figure 37 demonstrates the relative lack of change in QRS in the afebrile NHPs as compared to M169-16, who succumbed to the infection.

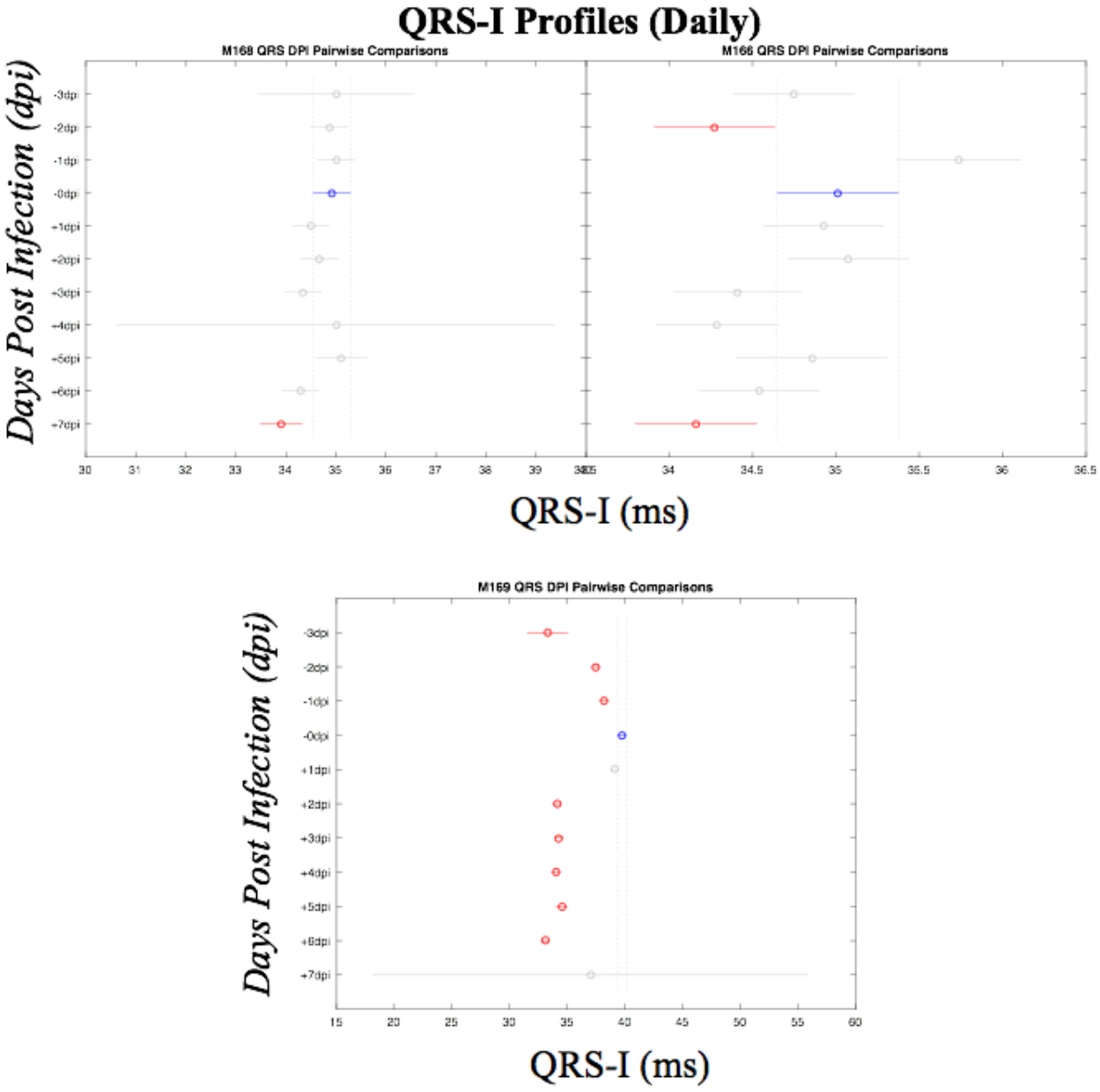

Figure 37. WEEV QRS Changes (Mean Daily QRS-I).

The QT-interval data of the WEEV NHP subjects recapitulates an interesting trend also visible in the QR-interval data (not significant); it demonstrates, in M169-16, the complete

suppression, or shortening of the QT-I during the febrile period, a characteristic not immediately visible in the afebrile NHPs M166-16 and M168-16. These data can be visualized in Figure 38. However, the repeated measures ANOVA and subsequent one way ANOVA also demonstrated significance for M166-16 and M168-16, similar to the QRS-I data. Again, pairwise comparisons of pre-infection vs. post-infection data demonstrated differences, but mean daily QRS-I pairwise comparisons again downplays the meaningfulness of the statistical significance of the afebrile NHPs' QRS-I data. Whereas the QT-I of M169-16 diminished to 81% of its baseline value, that of M166-16 reduced to only 95% of the baseline value. The significance for M168-16 can be traced to an artifact that stems from missing data. Pairwise comparisons can be seen in Figure 39.

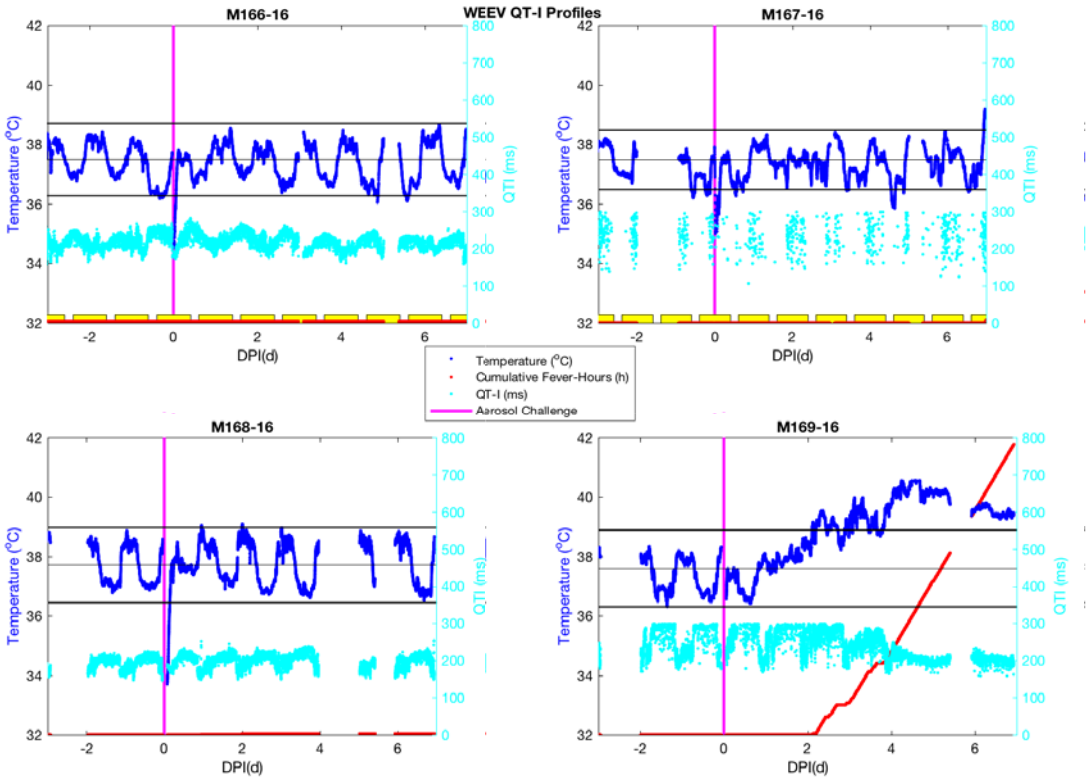

Figure 38. WEEV QT-I Profiles.

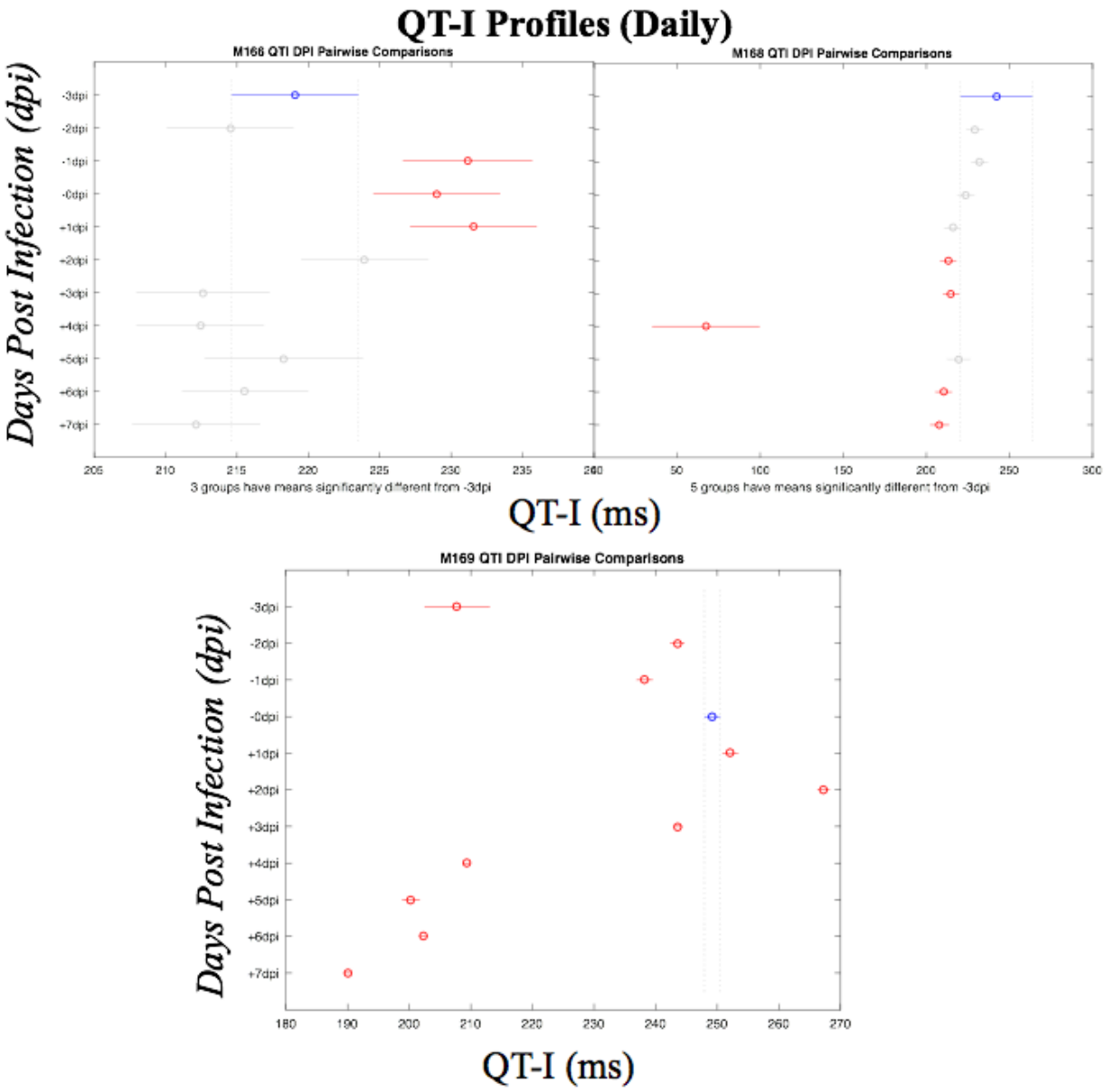

Figure 39. WEEV QT-I Changes (Mean Daily QT-I).

Finally, the last common metric for which significance was discovered was the RR-interval. The trend uncovered again mirrored that of HR; the data is plotted against disease course in Figure 40. The RR-I did not change to a significant degree in M166-16 nor M168-16; by contrast, by 2dpi, RR-I in M169-16 had decreased to 60% of baseline mean daily RR-I during the febrile period compared to 88% and 100% for M166-168-16, respectively. RR-I for M169-16

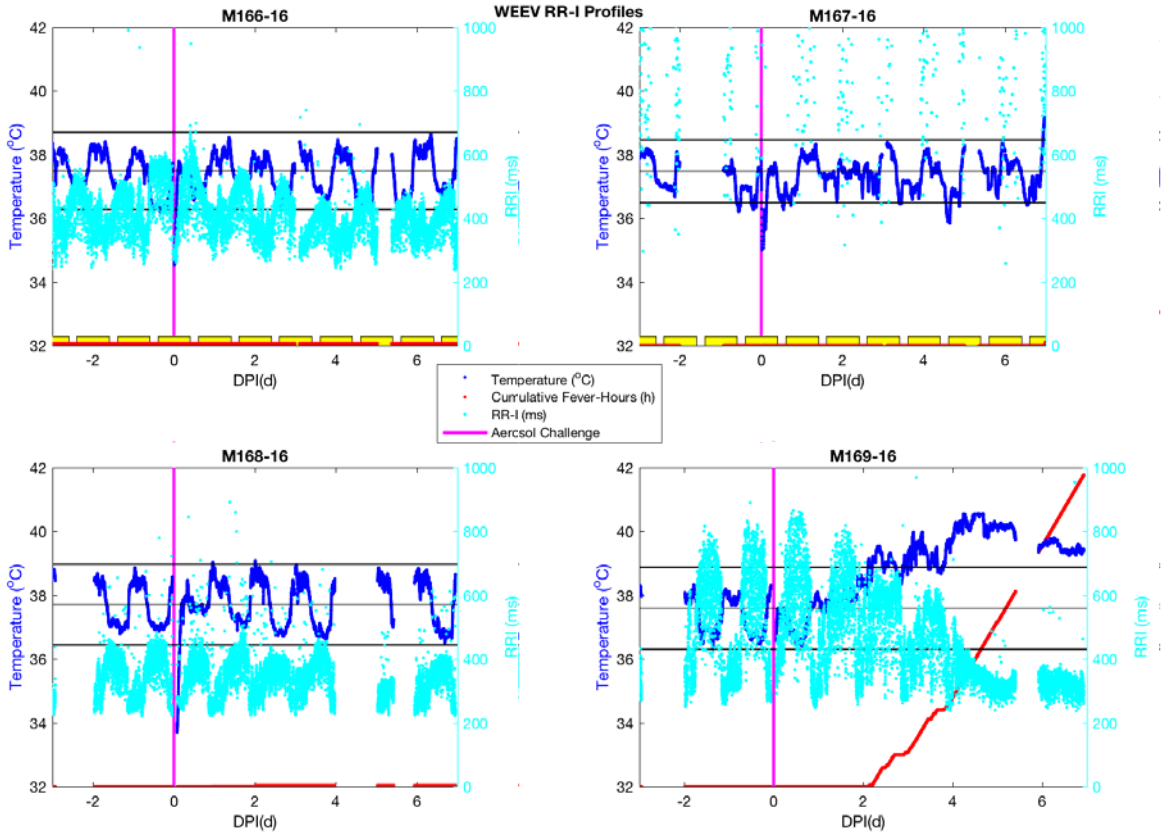

Figure 40. WEEV RR-I Profiles.

is plotted in Figure 41, as mean daily RR-I.

The findings for WEEV were remarkable in that the relevant ECG metrics here discussed only exhibited significant change after the onset of the febrile period. More variation in the baseline data, compounded by data loss, of the set of NHPs exposed to WEEV was experienced, leading to artifact generation in the results. In the case of M169-16, QRS-I appears to have decreased; the implications of this finding are unclear, though the literature points to this as a component of a poor prognosis, especially in the context of increased QRS-wave amplitude, which, though not

discussed, displayed significance in M169-16 [62]. The etiology behind the association with sudden death refers mainly to cardiogenic origins; however, recent investigation

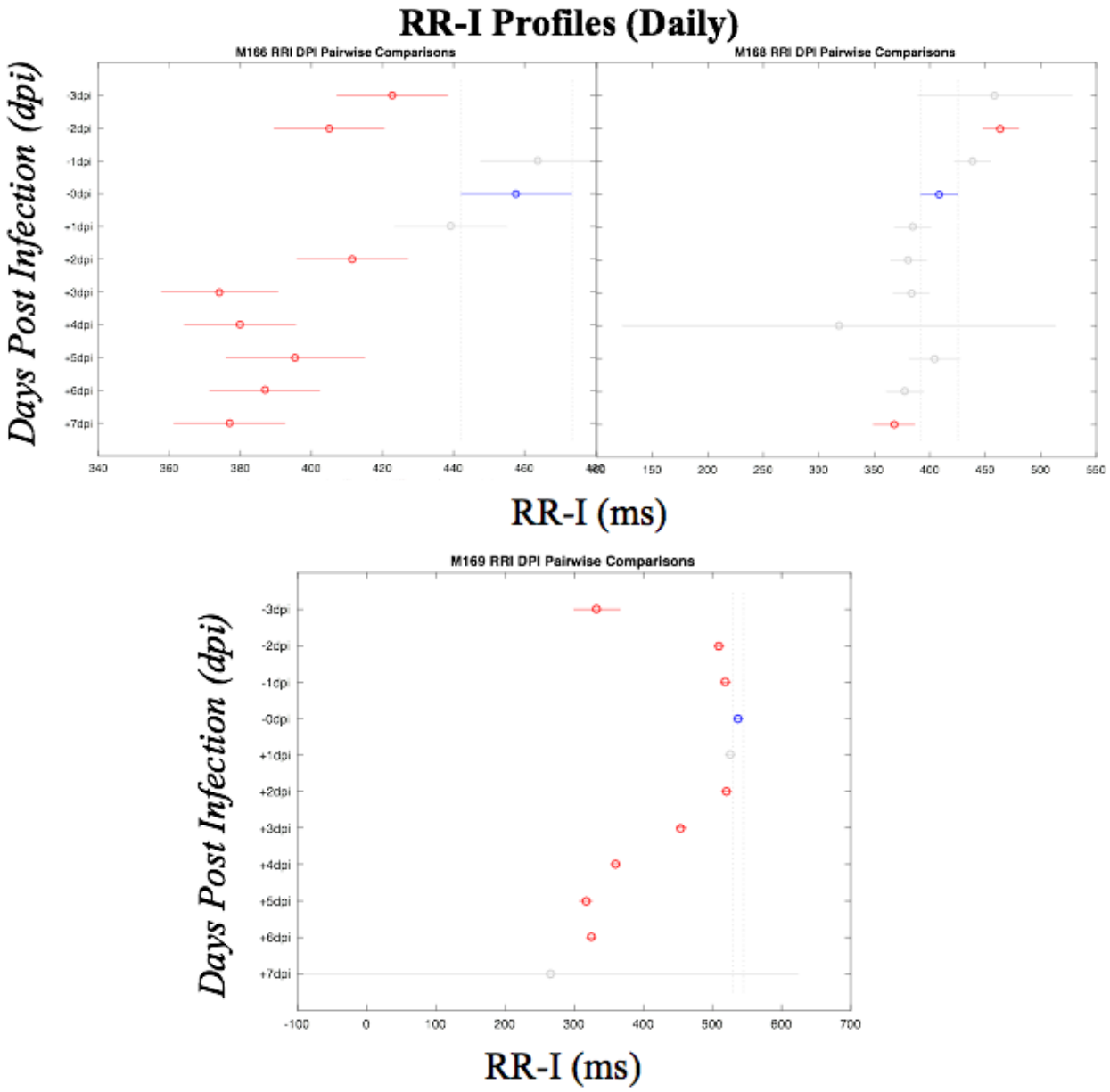

Figure 41. WEEV Mean Daily RR-I in Sickened NHPs.

has suggested that autonomic modulation of sympathetic/parasympathetic predominance of heart rate regulation can lead to morphological changes in the QRS-interval, with a narrower QRS-I

representing a shift towards sympathetic predominance [63]. The increase in QRS-amplitude, however, does not manifest until during the febrile period; QRSA data are plotted against disease progression in Figure 42.

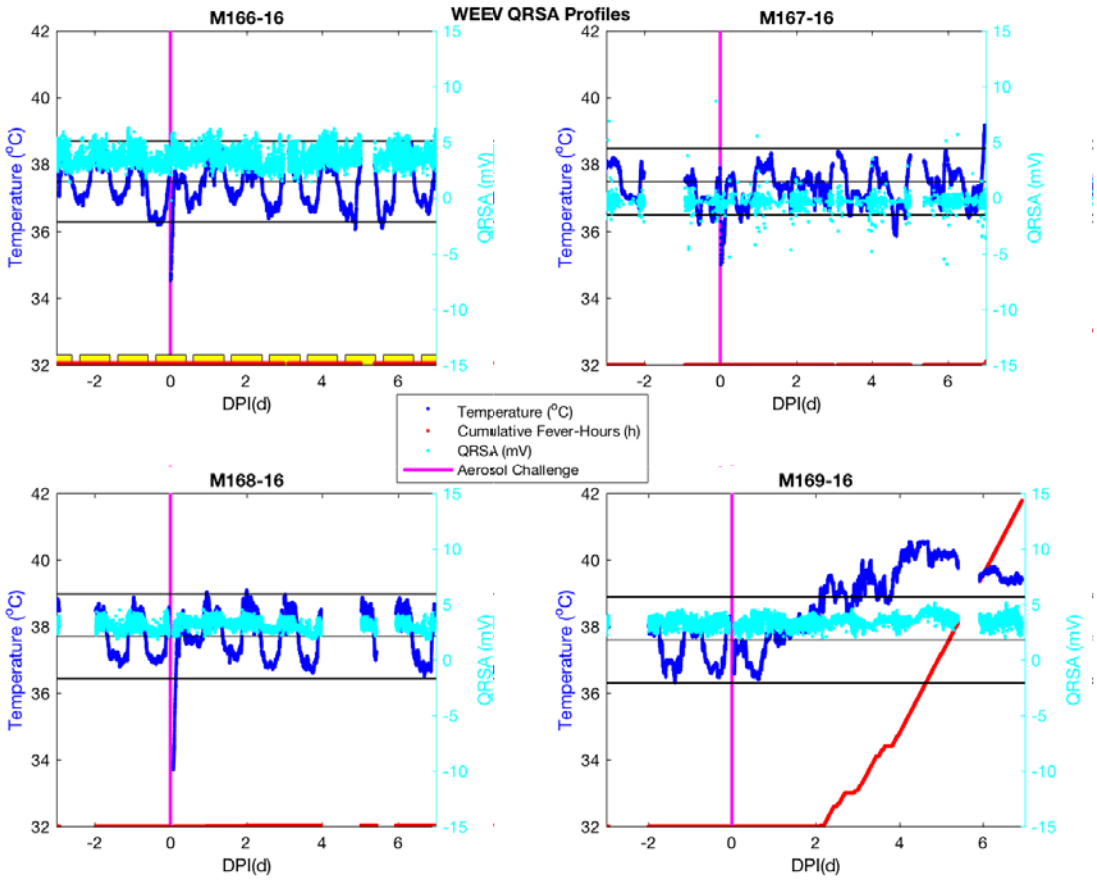

Figure 42. WEEV QRSA Profiles.

4.1.2.3 Frequency Spectrum Analyses

Frequency analysis of WEEV yields differences between fundamental frequencies that distinguish pre-/post-infection and febrile periods from each other. The frequency spectra again do not vary between covarying ECG metrics, and as such, RR-I was chosen as a representative sample of the frequency spectra of the WEEV-infected monkeys, shown in Figure 43.

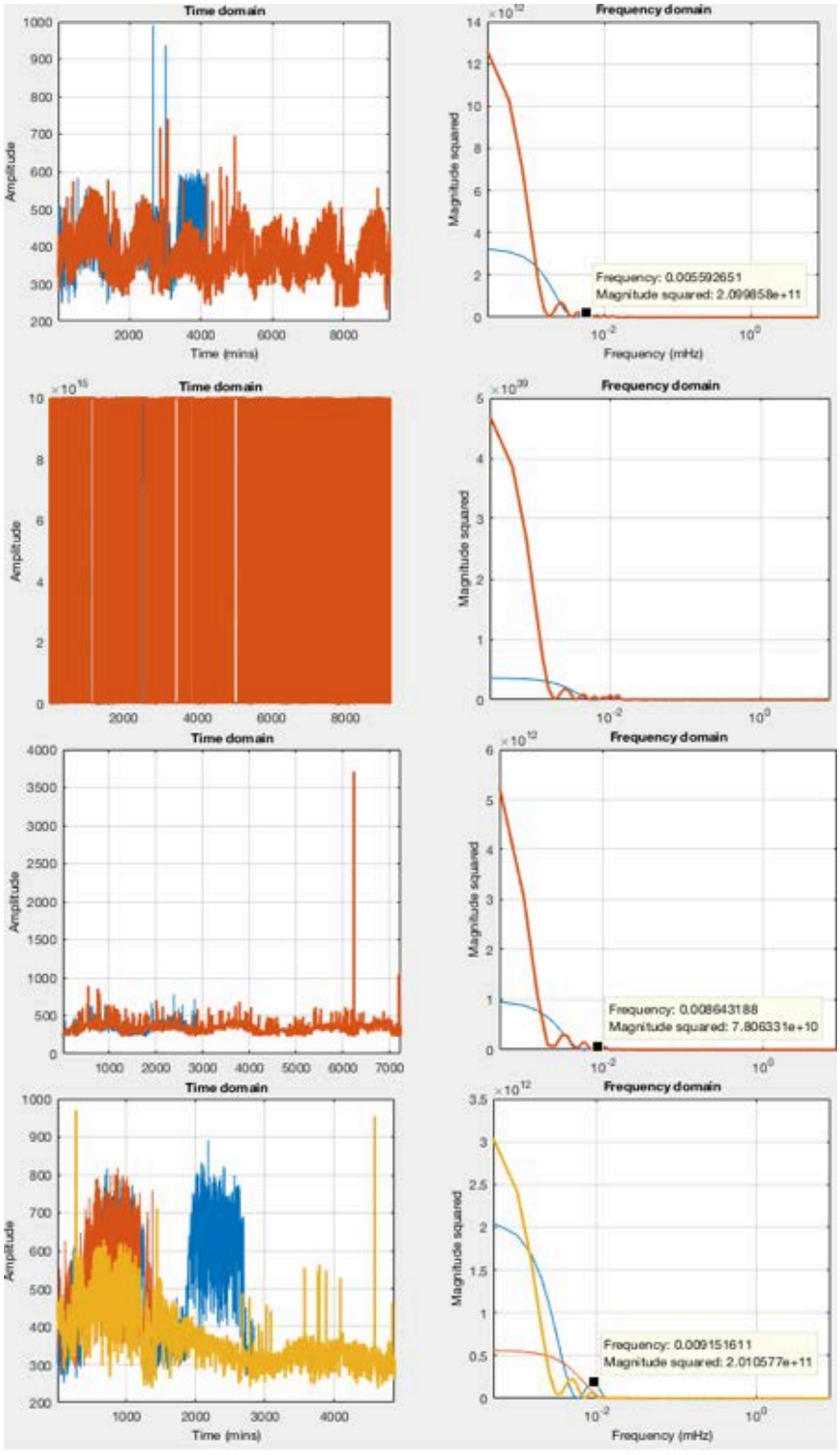

Figure 43. WEEV RR-I Frequency Spectra.

RR-Interval data plotted on the left, frequency spectra plotted on the right. From top to bottom: M166-16, M167-16, M168-16, M169-16. Blue for pre-infection, red for post-infection, and yellow for febrile period.

In the monkey that became ill, the fundamental frequency shifted to the right, then to the left as the febrile period approached; this stands in contrast to the fundamental frequencies observed for M166-16 and M168-16; though the post-infection period was defined by a shift of the fundamental frequency to a smaller frequency, variability between subjects was significant to the point that the magnitude of the change of fundamental frequency in M166-16 was twice that of M168-16. The fundamental frequencies of the WEEV frequency spectra data are summarized in Table 6.

Table 6. WEEV Frequency Analysis Results.

NHP	***Fundamental Frequency (cpd)***	***Post-Infection Frequency (cpd)***	***Febrile Period Frequency (cpd)***	***Differences (Pre-Post-Feb) (cpd)***
M166-16	0.748	0.220	N/A	(-0.528)
M168-16	0.483	0.264	N/A	(-0.219)
M169-16	0.791	1.537	0.439	(0.746, -1.098)

4.1.2.4 Heart Rate Variability

In the NHPs exposed to WEEV, HRV demonstrated a decrease during the febrile period in M169-16; the healthy NHPs manifested changes in HRV, but as the variability of the data for

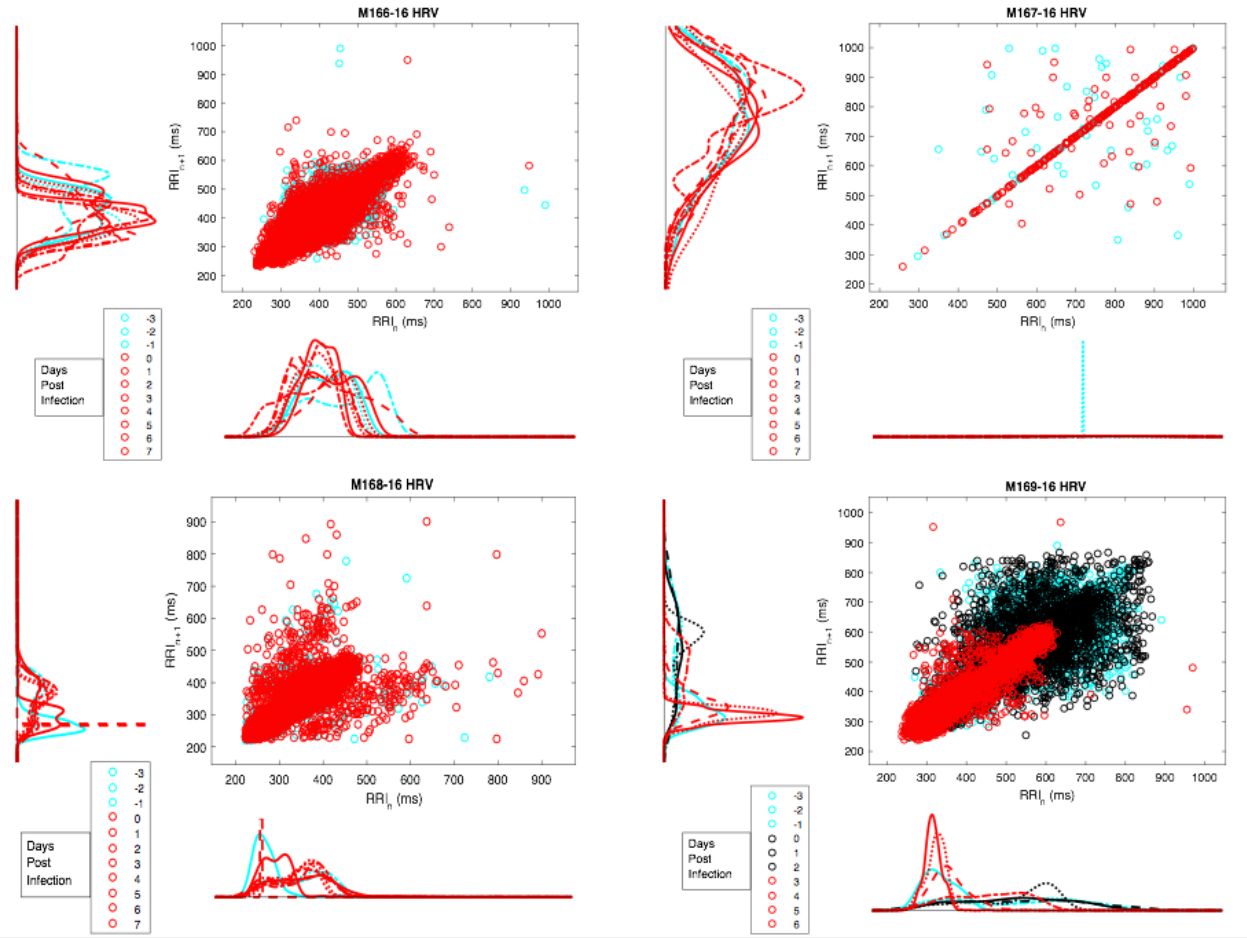

Figure 44. WEEV HRV Poincare Plot Overlays.

Poincare plots of HRV by day; cyan: pre-infection period, black: post-infection period, and red: febrile period.

M166-16 and M168-16 demonstrate no peaks comparable to the downshift observable in the HRV data of M169-16. These are plotted in Figure 44. One way ANOVA, in Table 7, demonstrated significant differences in daily HRV plots, such that the febrile period HRV data is distinguishable from post-infection and pre-infection period HRV.

Table 7. WEEV HRV Probability Density one-way ANOVA Results.

M166-16 HRV owANOVA

ANOVA Table

Source	SS	df	MS	F	Prob>F
Columns	0.00045	10	4.54018e-05	9.78	8.62413e-16
Error	0.00506	1089	4.64253e-06		
Total	0.00551	1099			

M167-16 HRV owANOVA

ANOVA Table

Source	SS	df	MS	F	Prob>F
Columns	1.13209e-06	10	1.13209e-07	143.49	6.77527e-191
Error	8.59214e-07	1089	7.88993e-10		
Total	1.9913e-06	1099			

M168-16 HRV owANOVA

ANOVA Table

Source	SS	df	MS	F	Prob>F
Columns	0.02369	10	0.00237	87.69	3.11469e-132
Error	0.02943	1089	0.00003		
Total	0.05312	1099			

M169-16 HRV owANOVA

ANOVA Table

Source	SS	df	MS	F	Prob>F
Columns	2.41078	10	0.24108	134.43	2.63287e-182
Error	1.95292	1089	0.00179		
Total	4.36371	1099			

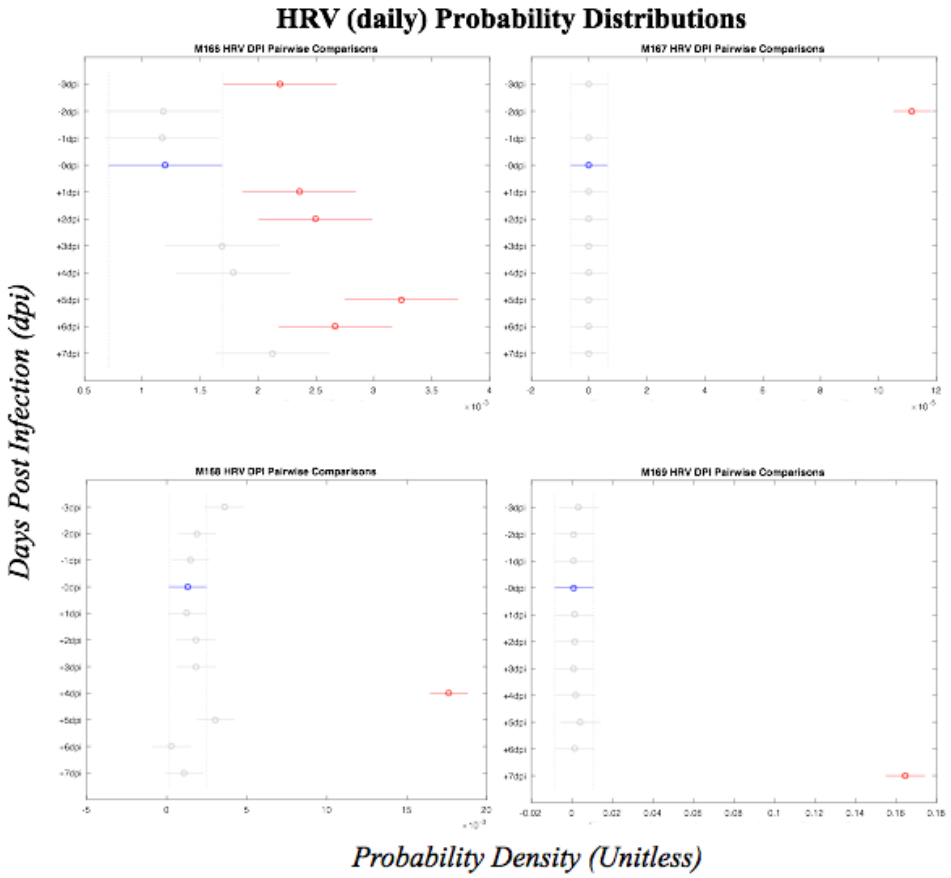

Figure 45. WEEV HRV post-hoc pairwise comparisons of probability density.

4.1.3 Venezuelan Equine Encephalitis Virus

4.1.3.1 Disease Course

The disease course in Venezuelan Equine Encephalitis Virus produced a very characteristic bimodal fever profile in the NHPs infected; none of the NHPs challenged with VEEV died from the disease, and all recovered from their fevers. Unlike the EEEV and WEEV cohort of NHPs, which were all-male and all-female, respectively, the VEEV NHP cohort was mixed-sex.

Post-challenge, the animals became febrile shortly at the 1dpi mark, with an initial fever peaking of 40-41ºC at approximately 1.3dpi, followed by a return to normal temperature range by 1.5dpi. A day later, at approximately 2.5dpi came the onset of a second fever, lasting four days until approximately 6.5dpi to 7dpi. The disease profiles are as detailed in Figure 46 and

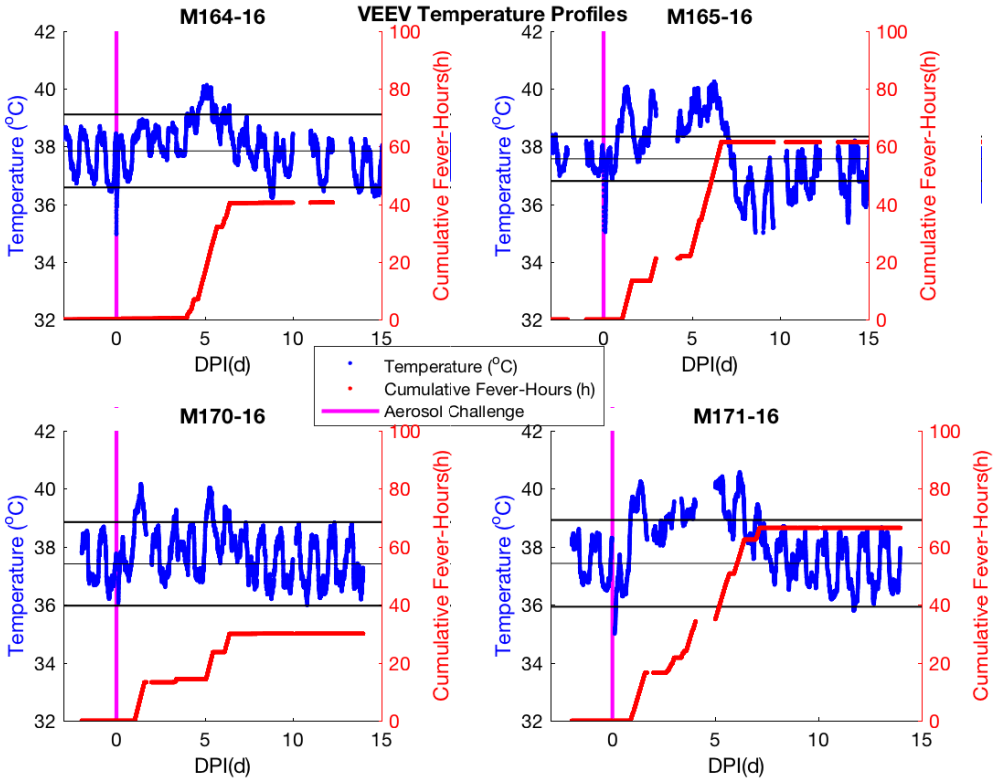

Figure 46. VEEV Disease Profiles.

modeled in Figure 47. Thus, four periods were initialized for analysis: pre-infection, post-infection, febrile period, and recovery period. VEEV is unique in this work due to the fact that all subjects experienced the same disease profile.

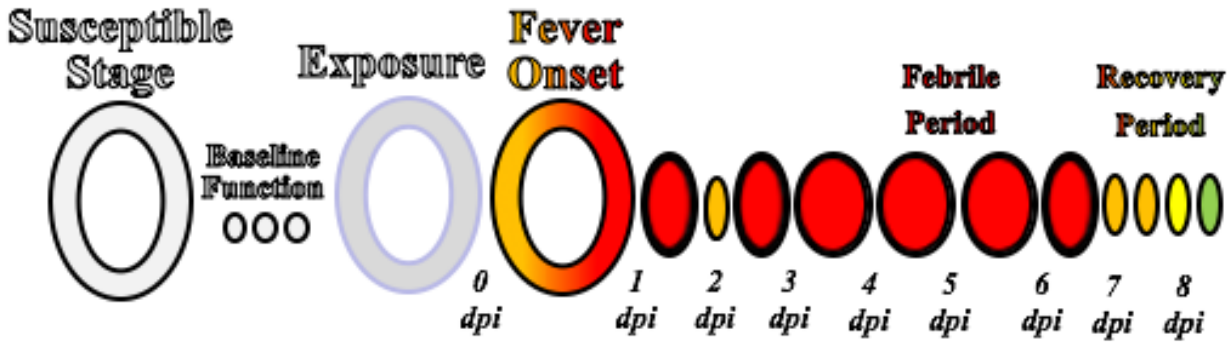

Figure 47. VEEV Disease Course.

Although the disease courses of the NHPs in this cohort fit the same archetype, some idiosyncrasies existed in individual NHP subjects. For instance, though M164-16 did not reach an initial fever as defined by baseline temperature by the 1dpi mark, a temperature elevation occurred which fit the pattern of the initial febrile peaks of the other NHPs in the cohort. The disease course of M165 was marred by a bout of hypothermia beginning at the recovery period, wherein the NHP's core temperature dropped below baseline.

Analysis by repeated measures ANOVA found nothing of significance in any and all metrics, follow-up one way ANOVAs were performed to analyze for differences between periods. The ECG metrics and their standard deviations (considered as ECG metrics in their own right) for which significant differences were found are summarized in Appendix A.1.

Data for each VEEV NHP subject was analyzed by one way ANOVA to compare pre-infection, post-infection, febrile period, and recovery ECG data for NHPs M164-16 and M165-16,

M170-16, and M171-16. As nearly every metric yielded significance when analyzed thus, only the metrics in common with EEEV and WEEV will be discussed in this segment. One way ANOVA tables can be found in the appendix.

Heart rate increased in all NHPs infected with VEEV from baseline, an effect that persisted through the biphasic febrile period through the recovery period. Heart rate data are plotted against disease profiles in Figure 48. As testament to the speed with which the febrile peak occurred, the heart rate was found to be significantly elevated by factors of 1.1x to 1.2x compared to baseline, depending upon the NHP, and peaked at a factor of approximately 1.3x baseline in all NHPs during the febrile period. Heart rate comparison by period is displayed in Figure 49. Although the heart rate reached an even higher period average for M165-16, this may have had to do with her episode of hypothermia, for which she received daily heat-lamp warming; this may have produced an effect on the heart rate. It should also be noted that the female NHPs (M164-16 and M165-16) exhibited higher baseline heart rates than the males, though this could be correlated to body size and not sex.

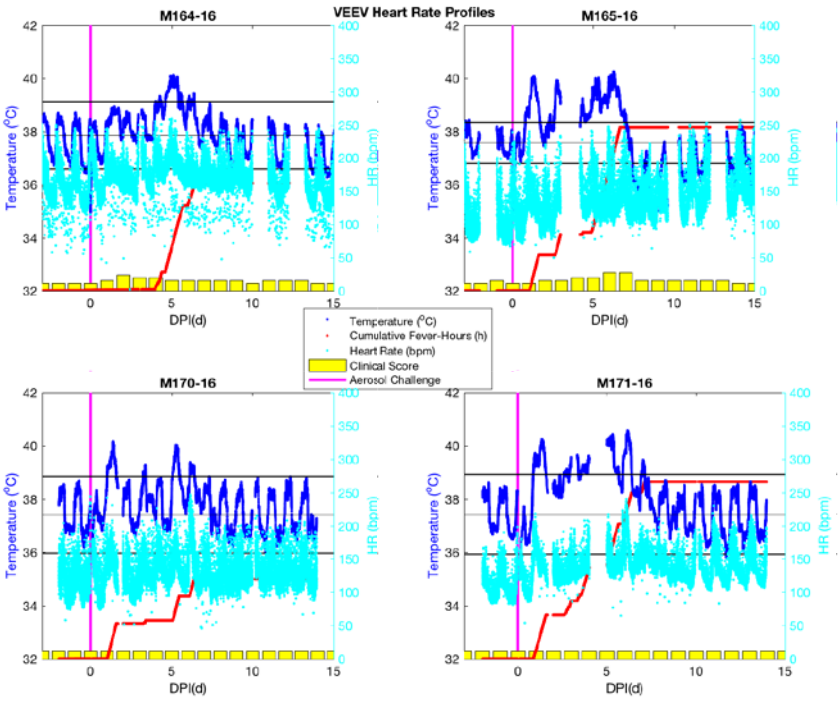

Figure 48. VEEV Heart Rate Profiles.

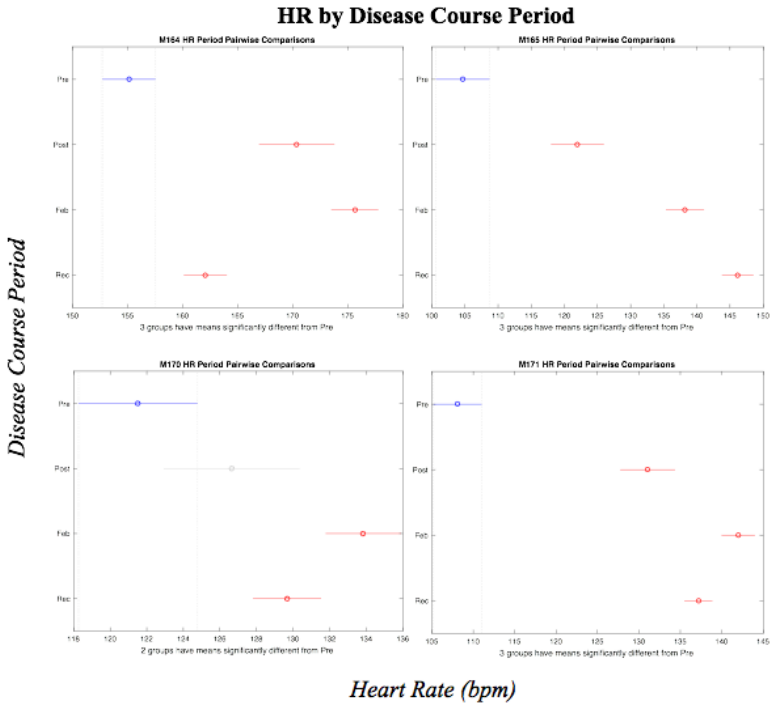

Figure 49. Heart Rate in VEEV-infected NHPs (period).

The QRS-interval in the VEEV infected NHPs against their disease courses are documented in Figure 50. An interesting effect observed was that by the recovery period, the QRS for the female NHPs were now higher than baseline, whereas the QRS for the male NHPs were decreased. These represented increases to 102% and 110% of baseline QRS for M164-16 and M165-16 respectively, and decreases to 95% for both M170-16 and M171-16, respectively. Differences by period can be seen in Figure 51.

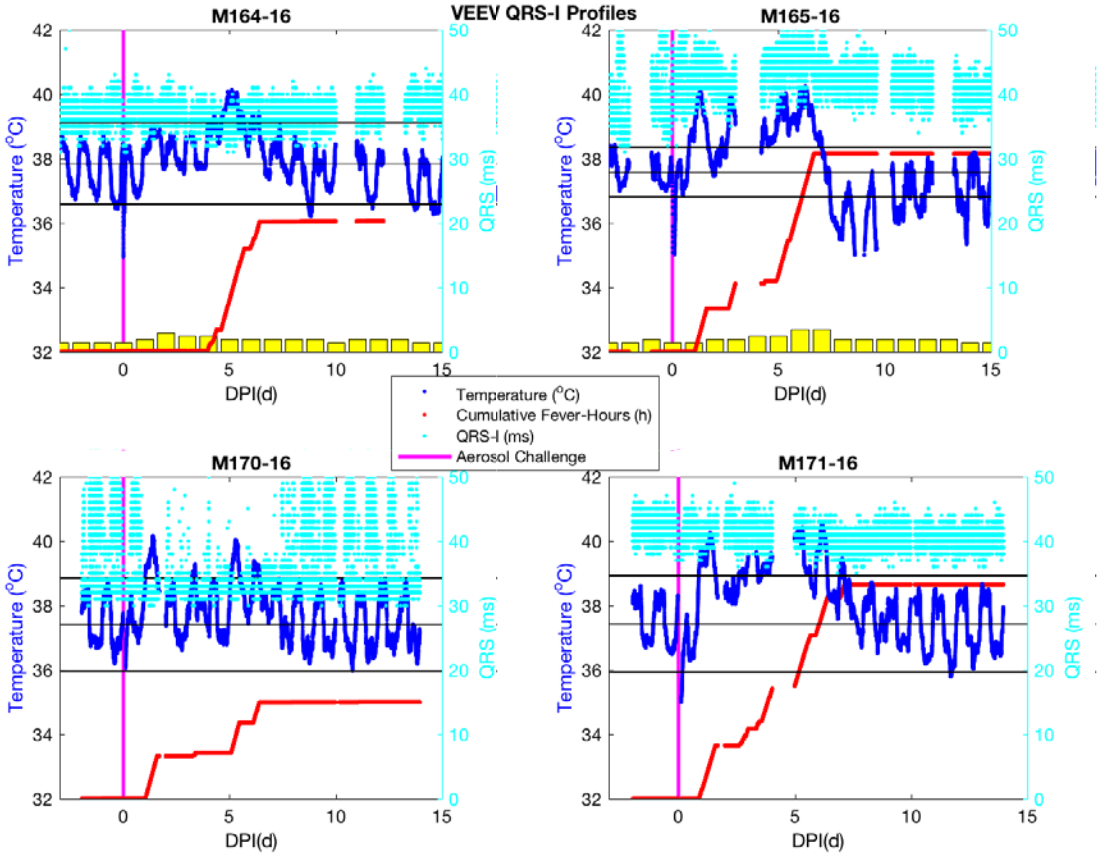

Figure 50. VEEV QRS Profiles.

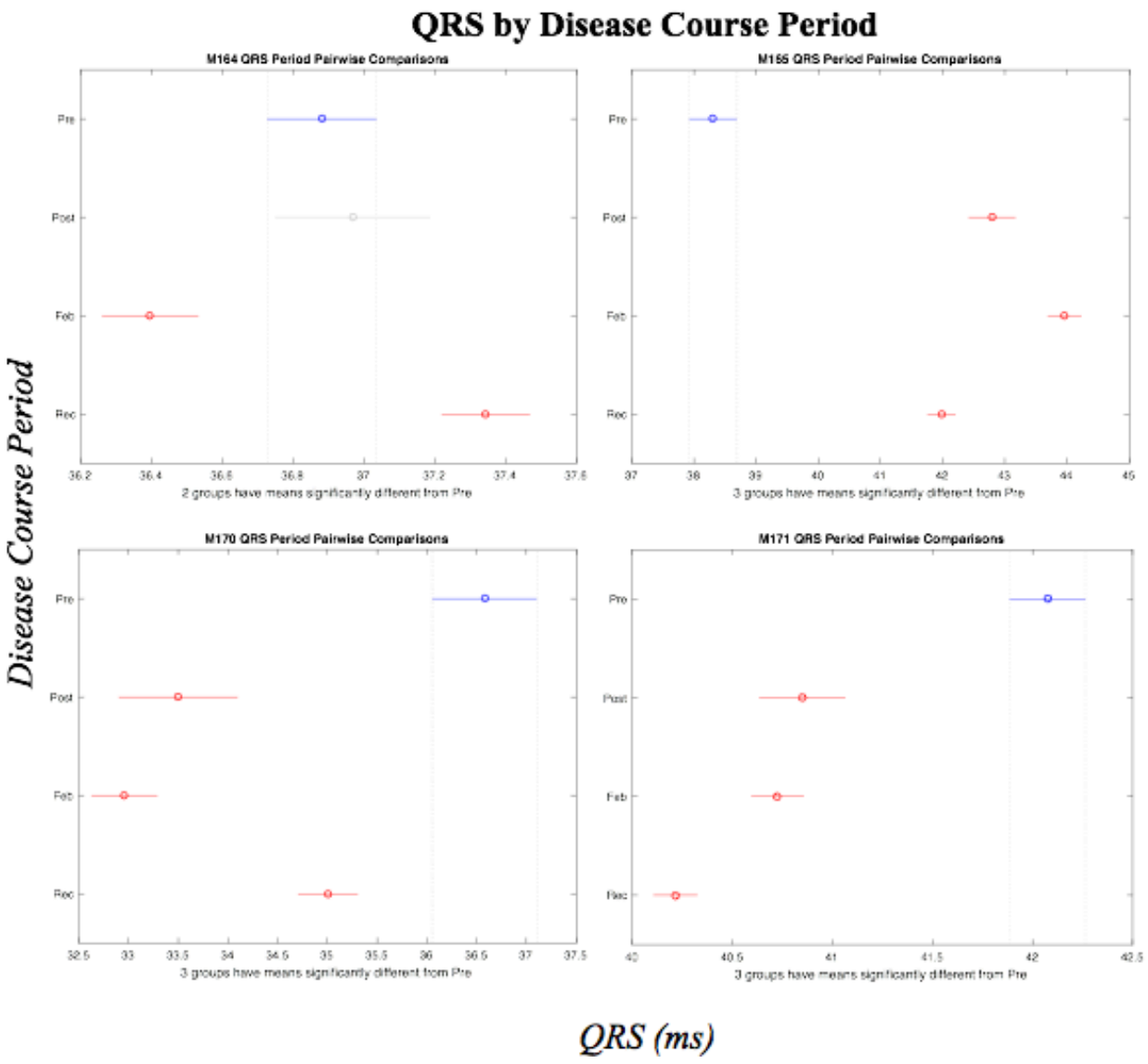

Figure 51. VEEV QRS Changes in Sickened NHPs.

When the amplitudes of the QRS intervals were examined (plotted in Figure 52), it was revealed that the QRSA for M164-16 and M165-16 decreased sharply during the post-infection period, and remained at a lower point than baseline through the febrile period and into recovery. The trend differed for QRSA in males M170-16 and M171-16, as the QRSA increased sharply during the post-infection period, decreased sharply during the febrile period, and increased during the recovery period, in the case of M171-16 returning to baseline, while M170-16's QRSA was

elevated above baseline to 105% of baseline values. Differences in QRSA by period are plotted in Figure 53. Of note is that M164-16, M165-16, M170-16, and M171-16 received progressively lower doses of virus; thus, not only could body weight and sex be correlates/confounders of such results, but the lowest dose received by M171-16 could have resulted in a faster physiologic recovery from disease. The fact that M171-16 had the fewest observable signs/symptoms of VEEV illness supports this.

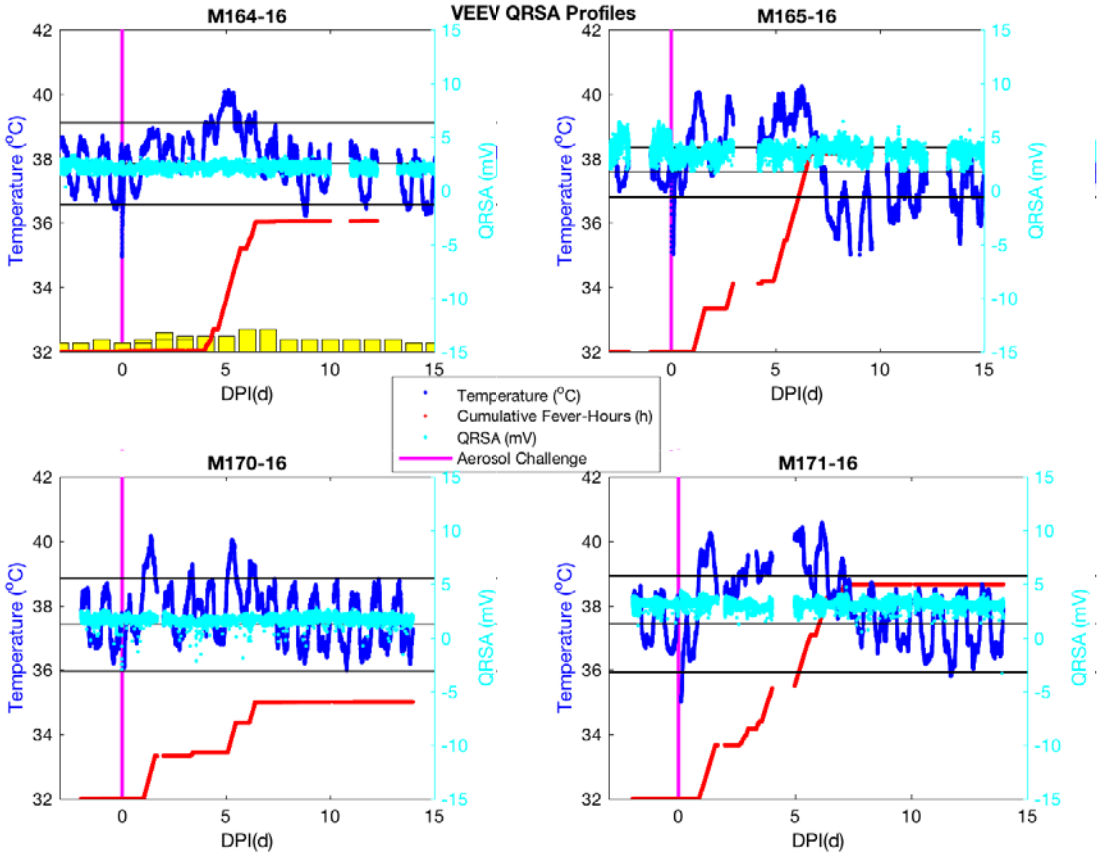

Figure 52. VEEV QRSA Profiles.

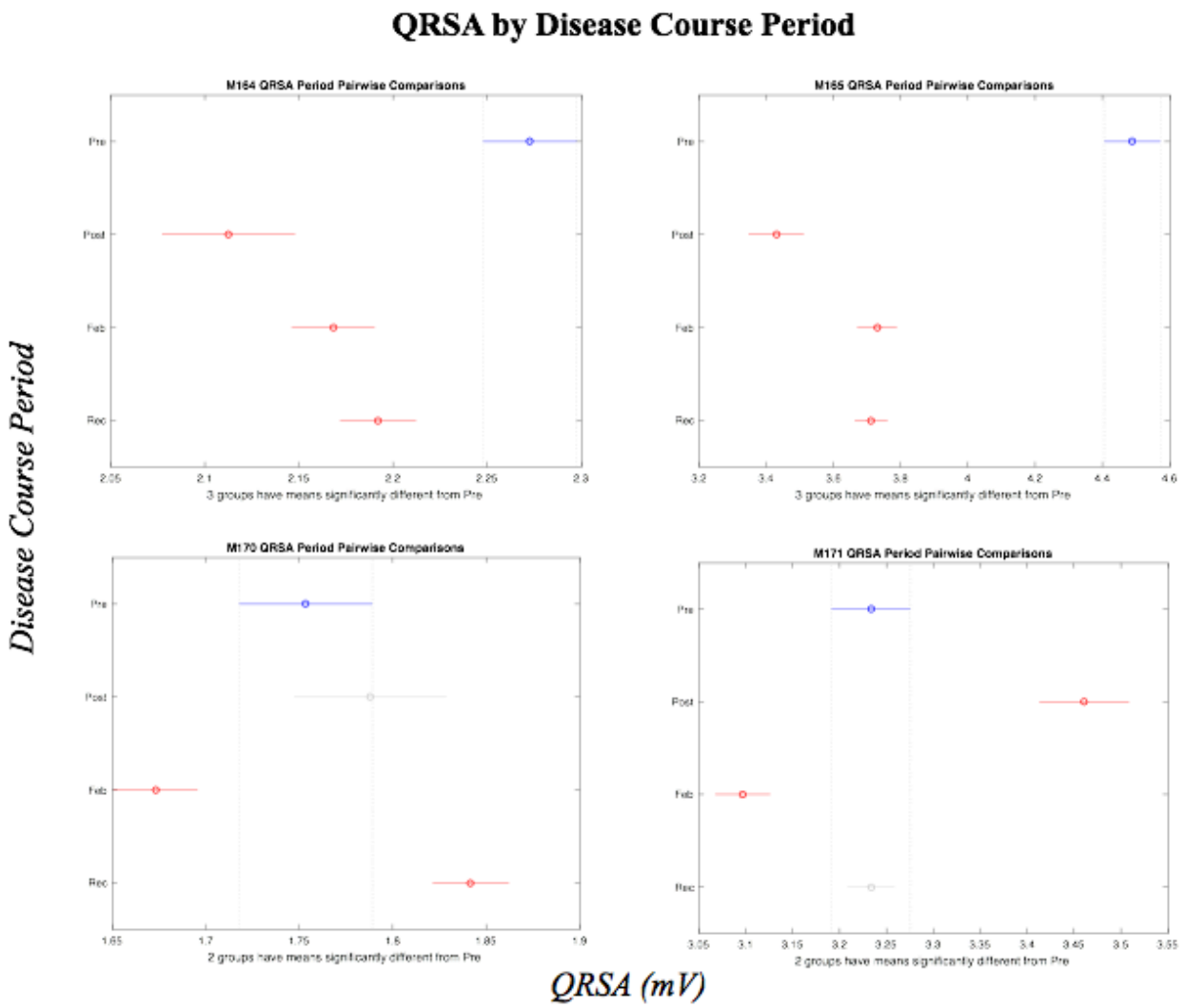

Figure 53. VEEV QRSA Changes in Sickened NHPs.

As the standard deviations for QRSA (QRSASD) were also significant, these trends were examined against the disease course (Figure 54); it appears that for female NHPs M164-16 and M165-16, the variability in QRS amplitude decreased following infection, and remained low; while the same trends in QRSASD appeared in M170-16 and M171-16, the results for M171-16 were not statistically significant, possibly due to a dose-dependent factor. Differences in QRSASD by period are plotted in Figure 55.

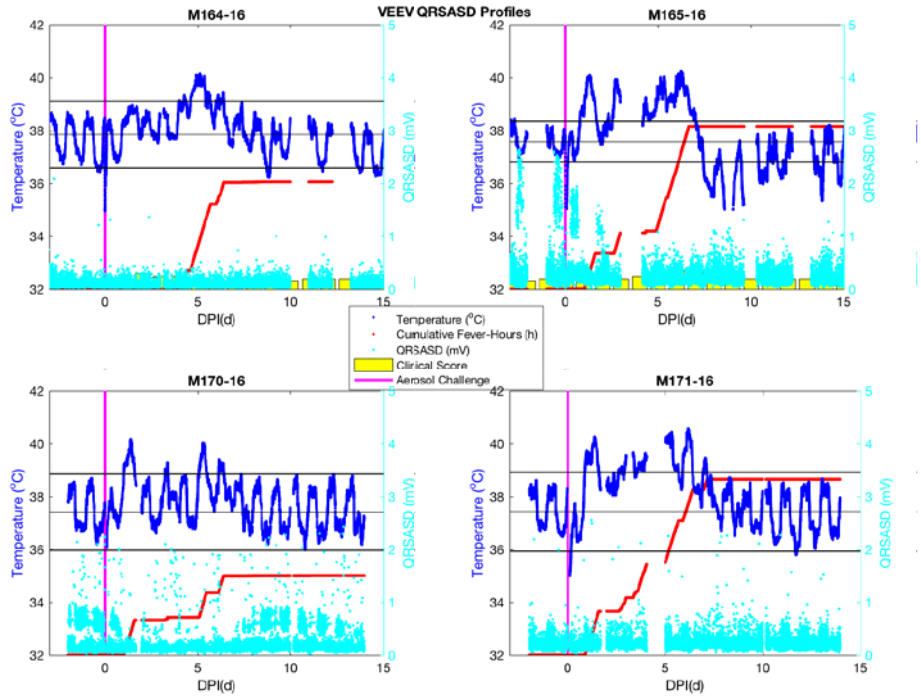

Figure 54. VEEV QRSASD Profiles.

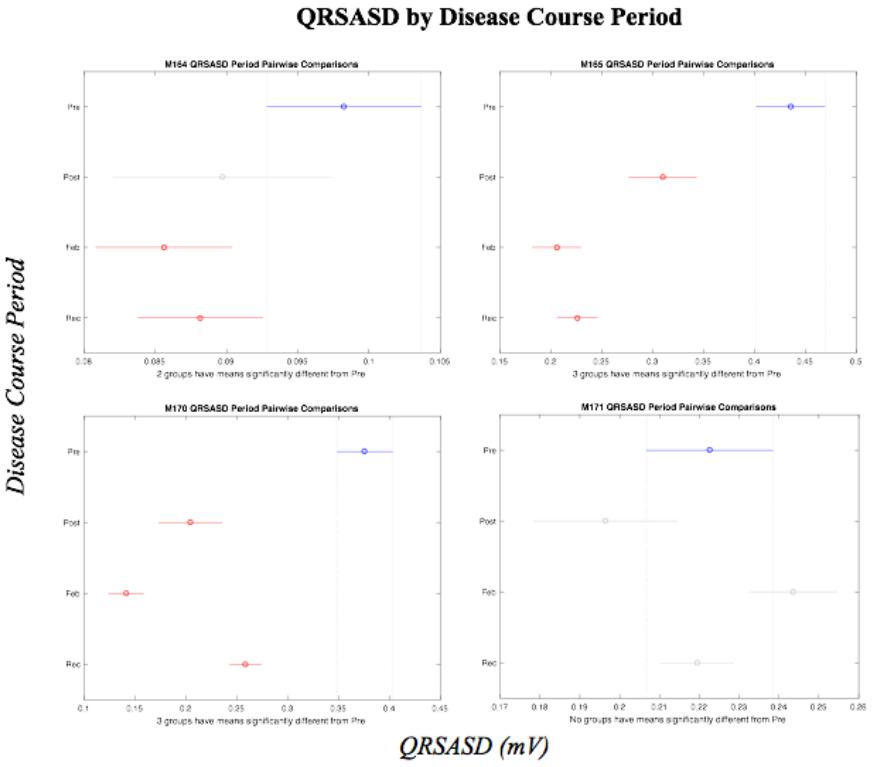

Figure 55. VEEV QRSASD Changes in Sickened NHPs.

Examination of the QT-interval data of VEEV infected NHPs demonstrated that, with the sole exception of M170-16, the QT-I decreased during the post-infection period, and remained decreased during the febrile period. In M165-16 and M171-16, the QT-I remained decreased during the recovery period, but for M164-16, the QT-I returned to baseline. In M171-16, the QT-interval manifested a consistent increase after the infection, through the febrile period and recovery. This can perhaps be explained by the fact that out of the four VEEV-infected NHPs, M170-16 had the lowest baseline QT-I; post-infection, one can visually inspect the QT-I data to determine that the range of QT-I values diminishes post-infection – the values decrease during the febrile period, then increase. QT-I is plotted over disease course in Figure 56, and differences in QT-I by period can be seen in Figure 57.

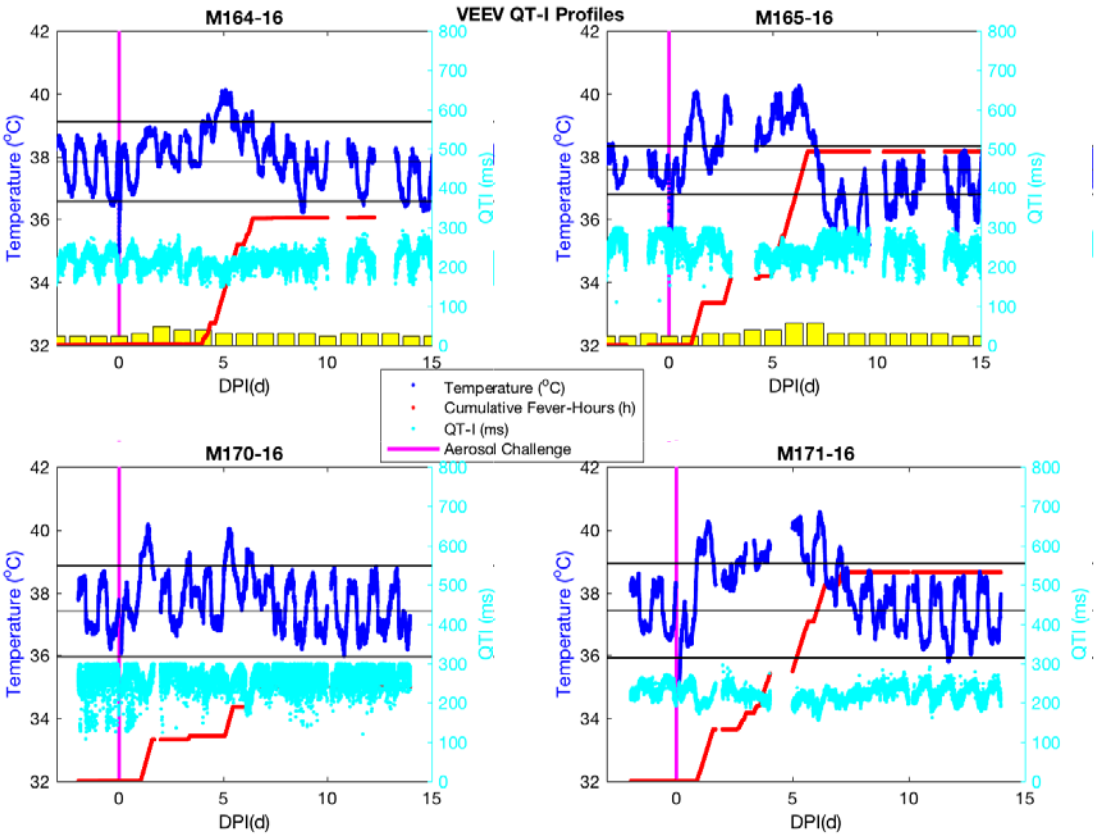

Figure 56. VEEV QT-I Profiles.

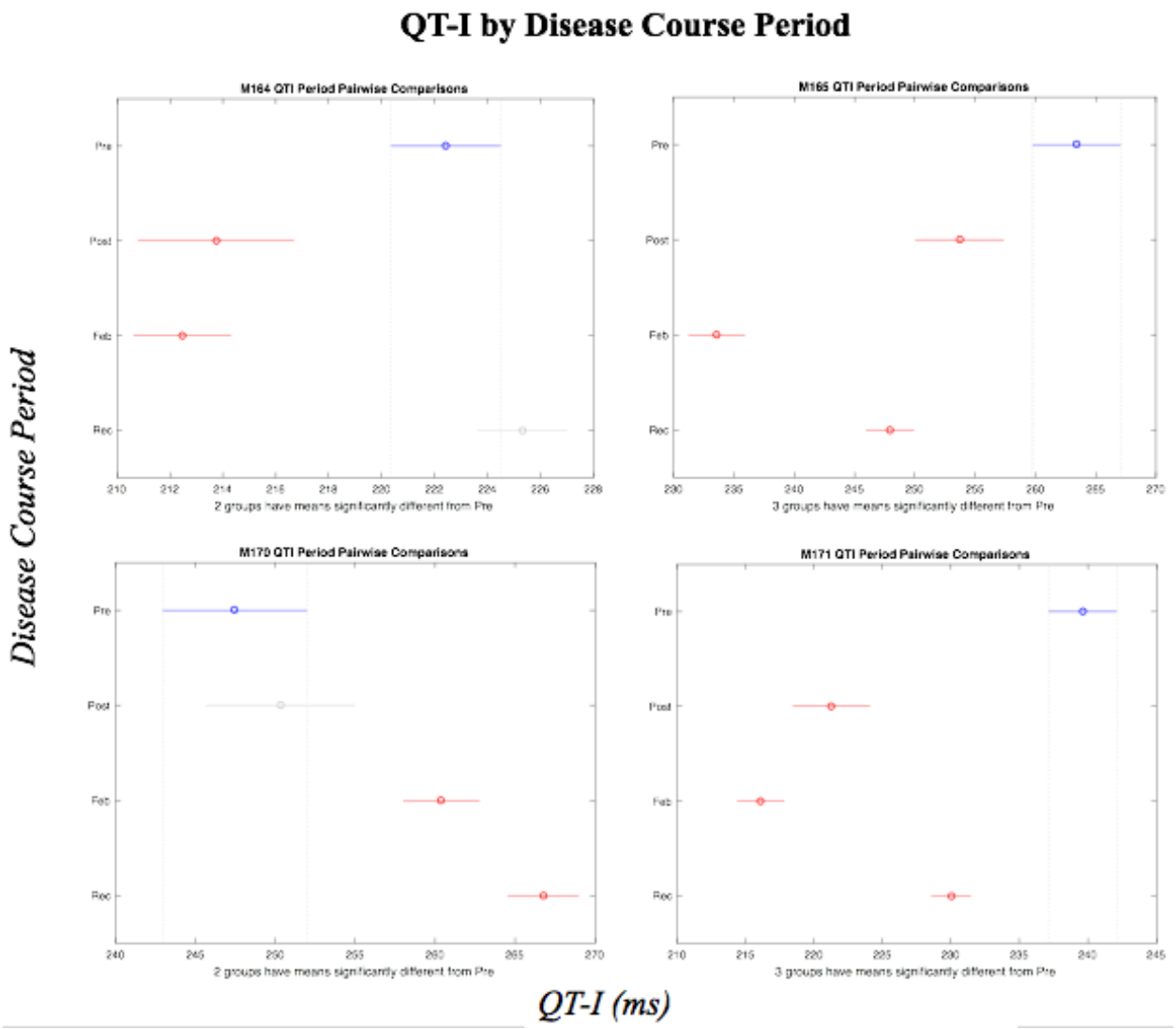

Figure 57. VEEV QT-I Changes in Sickened NHPs.

The RR-I decreased in all NHPs infected with VEEV post-infection, and remained persistently low through the recovery period. As expected, the trend in RR-I mirrors that of HR. The RR-I is plotted over disease courses in Figure 58, and differences by period in RR-I are plotted in Figure 59.

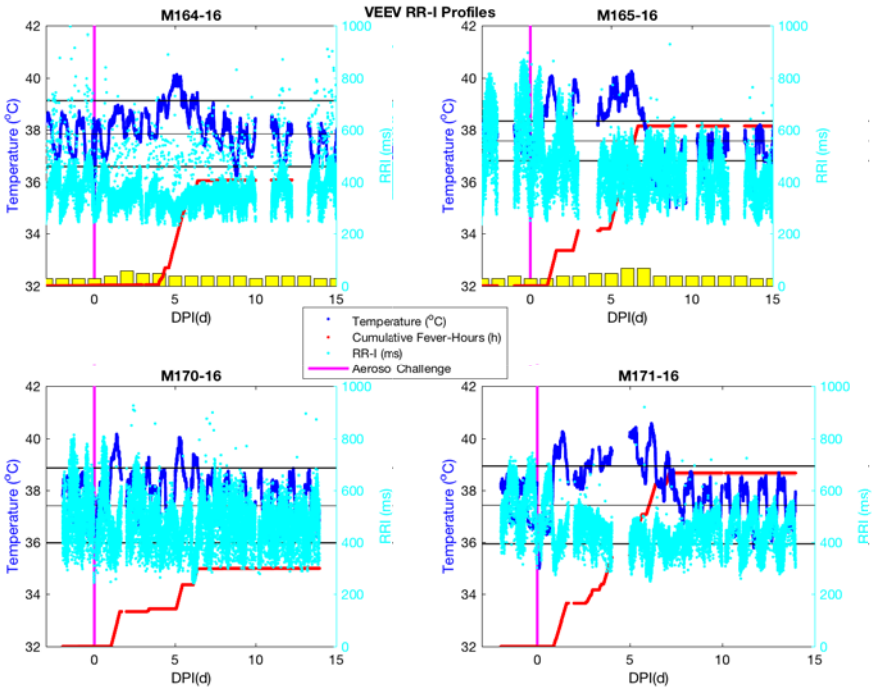

Figure 58. VEEV RR-I Profiles.

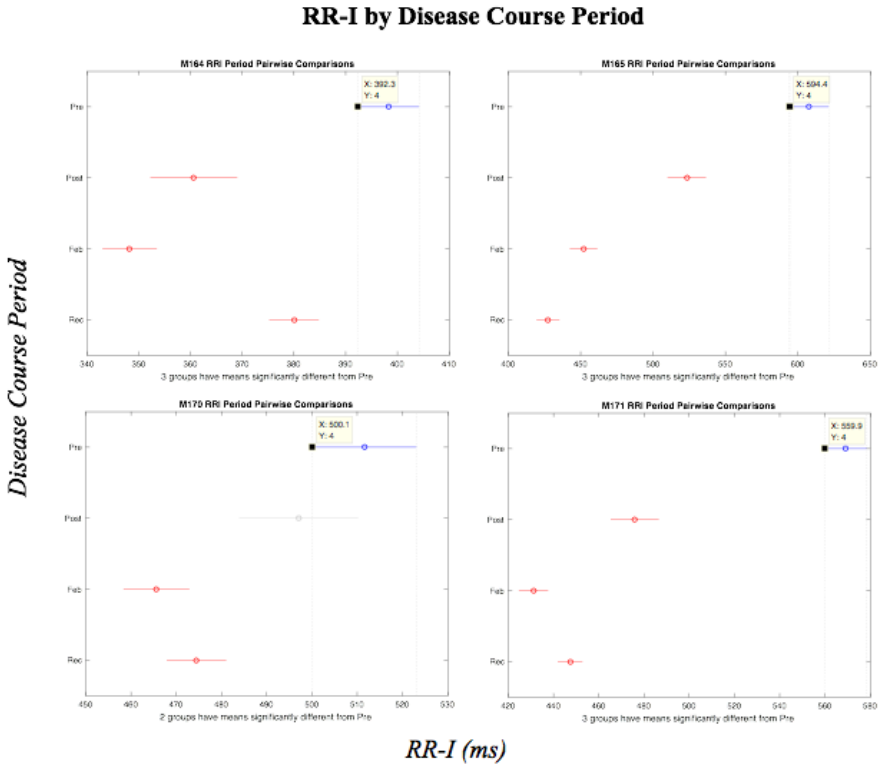

Figure 59. EEEV Mean Daily RR-I in Sickened NHPs.

The cohort of VEEV NHPs had no fatalities. The disease course was defined by a number of ECG metrics that became elevated/decreased and persisted even after the febrile illness had subsided. Whether or not this persistence, such as in the case of HR and related metrics, is reflective of a physiologic milieu favoring chemotaxis to infected areas, or else is indicative of persistent autonomic dysfunction remains to be seen [60, 61]. The latter case is supported by clinical scores for M164-16 and M165-16 that do not return to baseline values until 13-14dpi. The dichotomy in the behavior of the QRS interval reflects a dichotomy between several possible confounders: female/male sex, small/large body weight, and dose of VEEV received. Some literature demonstrates that menstrual cycles can precipitate effects on autonomic regulation that can manifest in ECG signal pattern disruption, though the focus of the study rested on HR and HRV [64]. From the ECG data alone it is impossible to determine conclusively the basis of the difference in the lengthening of the QRS interval during the febrile period. Examination of raw ECG trace obtained during the febrile period compared to the baseline ECG revealed no gross pathological signs, such as split or deformed QRS intervals, of direct cardiac pathology.

4.1.3.2 Frequency Spectrum Analyses

The frequency spectrum analysis of the NHP subjects in VEEV presents the finding that all periods discussed: pre-infection, post-infection, febrile, and recovery, can be distinguished in all NHPs in the VEEV cohort. Again, since covarying metrics displayed the same trends in the frequency spectra, only the RR-I plots will be displayed, as a representative sample in Figure 60.

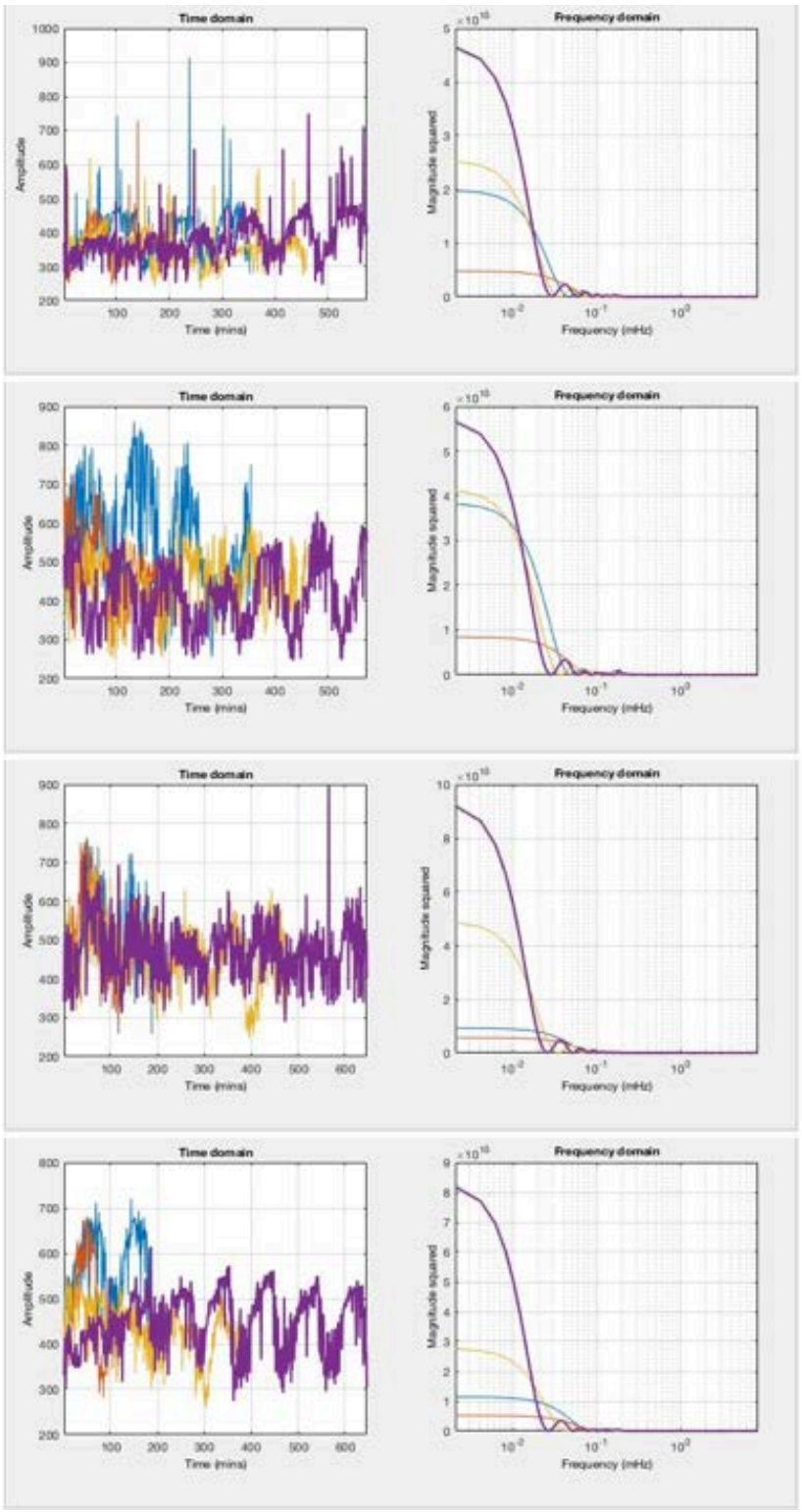

Figure 60. VEEV RR-I Frequency Spectra.

RR-Interval data plotted on the left, frequency spectra plotted on the right. From top to bottom: M164-16, M165-16, M170-16, M171-16. Blue: pre-infection, red: post-infection, yellow: febrile period, violet: recovery period.

As the cohort of NHPs displayed relatively similar disease profiles, the frequency analysis reflected this, and Table 8 lists the means of the fundamental frequencies, substratified by sex. The fundamental frequencies identified through the same method applied to the EEEV and WEEV cohorts yielded relatively high cyclic rates in the VEEV cohort, though the baseline values identified: 5.974 cpd and 11.245 cpd for female and male monkeys, represent the 17th and 32nd harmonics of an initial cyclic rate of 0.351 cpd, a value similar to the baseline values of EEEV frequency analysis. This points to the potential need for some kind of normalizing when comparing virus to virus. Values in parentheses are normalized to the first harmonic value.

Table 8. VEEV Frequency Analysis Results.

NHP	***Fundamental Frequency (cpd)***	***Post-Infection Frequency (cpd)***	***Febrile Period Frequency (cpd)***	***Recovery Period Frequency (cpd)***	***Differences (Pre-Post-Feb-Rec) (cpd)***
All	8.610	12.344	4.612	3.339	(3.734, -7.732, -1.273)
Male	11.245 (0.351)	13.793 (0.431)	4.744 (0.148)	3.163 (0.099)	(2.548, -9.049, -1.581) <0.080, -0.283, -0.049>
Female	5.974 (0.373)	10.894 (0.681)	4.481 (0.281)	3.514 (0.220)	(4.920, -6.413, -0.967) <0.080, -0.283, -0.049>
M164-16	5.974 (0.373)	11.070 (0.692)	4.393 (0.275)	3.514 (0.220)	(4.920, -6.413, -0.967) <0.319, -0.417, -0.055>
M165-16	5.974 (0.373)	10.718 (0.670)	4.568 (0.286)	3.514 (0.220)	(4.920, -6.413, -0.967) <0.297, -0.384, -0.066>
M170-16	11.245 (0.351)	13.881 (0.434)	4.217 (0.132)	3.163 (0.099)	(2.548, -9.049, -1.581) <0.083, -0.302, -0.033>
M171-16	11.245 (0.351)	13.705 (0.428)	5.271 (0.165)	3.163 (0.099)	(2.548, -9.049, -1.581) <0.077, -0.263, -0.066>

4.1.3.3 Heart Rate Variability

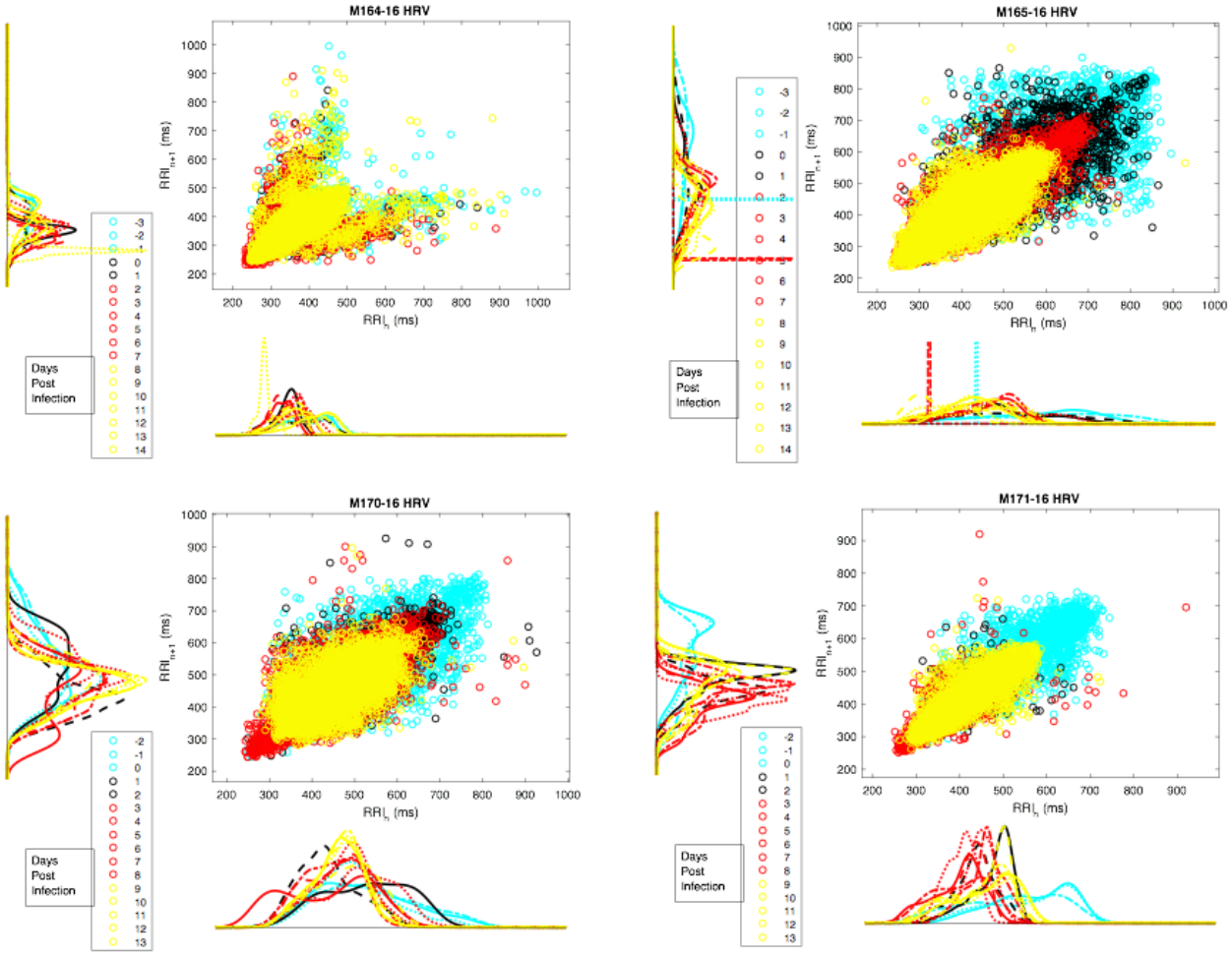

Figure 61. VEEV HRV Poincare Plot Overlays.

Poincare plots of HRV by day; cyan denotes the pre-infection period, black the post-infection period, red the febrile period, and yellow the recovery period.

HRV in VEEV-exposed NHPs downshifted in the post-infection period, which persisted through the recovery period; these profiles can be seen plotted in Figure 61. Although one way ANOVA demonstrated that these differences were significant, pairwise comparisons of the probability density functions composing the histograms of daily HRV distributions were not significantly different, and can be seen in Table 9; Figure 62 further illustrates these differences.

Table 9. VEEV HRV Probability Density one-way ANOVA Results.

M164-16 HRV owANOVA

ANOVA Table

Source	SS	df	MS	F	Prob>F
Columns	0.00016	17	9.67169e-06	3.89	1.39649e-07
Error	0.00443	1782	2.4847e-06		
Total	0.00459	1799			

M165-16 HRV owANOVA

ANOVA Table

Source	SS	df	MS	F	Prob>F
Columns	0.00017	17	9.82882e-06	3.13	1.576e-05
Error	0.00559	1782	3.13536e-06		
Total	0.00575	1799			

M170-16 HRV owANOVA

ANOVA Table

Source	SS	df	MS	F	Prob>F
Columns	0.00016	17	9.60992e-06	3.64	6.78572e-07
Error	0.0047	1782	2.63733e-06		
Total	0.00486	1799			

M171-16 HRV owANOVA

ANOVA Table

Source	SS	df	MS	F	Prob>F
Columns	0.00013	17	7.92579e-06	1.72	0.0334
Error	0.00821	1782	4.60815e-06		
Total	0.00835	1799			

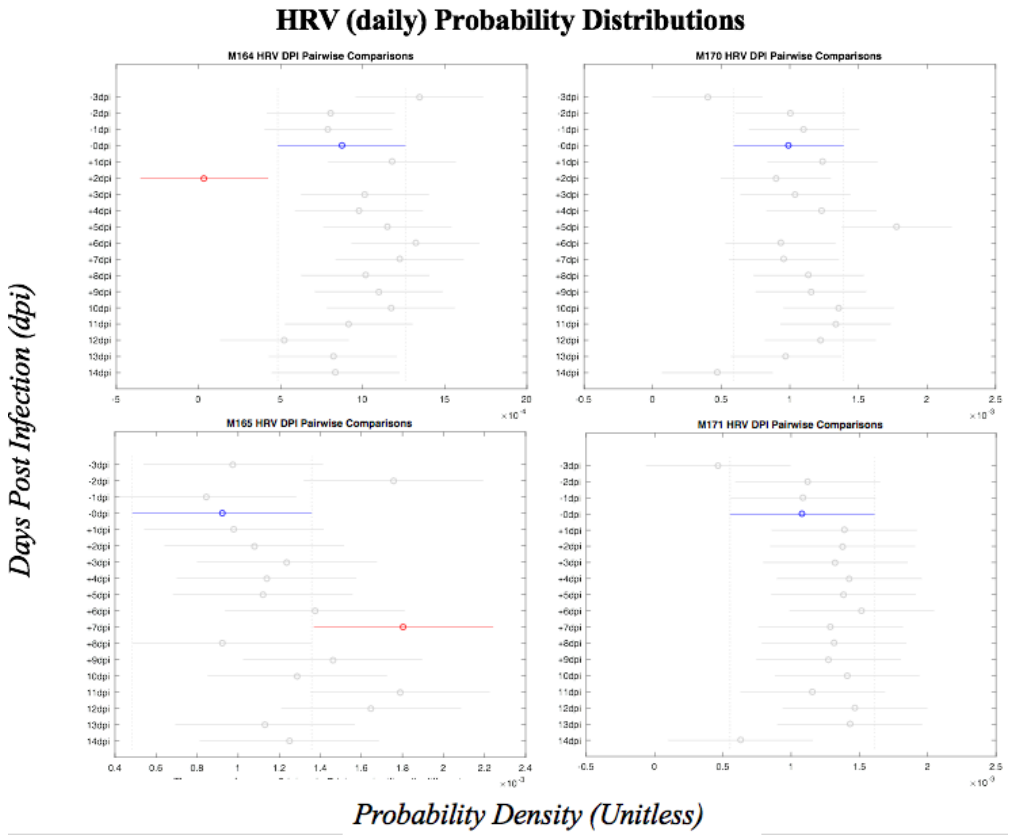

Figure 62. VEEV HRV post-hoc pairwise comparisons of probability density.

5.0 DISCUSSION

5.1 COMPARISONS BETWEEN EQUINE ENCEPHALITIS VIRUSES

The set of significant metrics shared between EEEV, WEEV, and VEEV consist of HR, PCt, PR-I, QRS, QRSA, QT-I, and RR-I. For those metrics in common, trends do not seem to manifest until febrile periods have been reached, with the exception of the QRS-interval. In EEEV, the QRS-interval widens, while in WEEV, the QRS-interval decreases. Though QRS-I exhibited consistent increases in NHPs sickened by EEEV, the results in WEEV were more inconsistent; however, when comparing QRS-I between fatal cases, the one fatal case of WEEV resulted in a reduced QRS-I. Globally, increases in mean daily metrics in diseased animals never exceeded approximately 1.5x baseline values, whereas decreased mean daily metrics in diseased animals never fell below 0.5x of baseline values, indicating potential thresholds for detection of anomalous patterns.

Frequency spectrum analysis reveals similar trends in different periods of disease course; post-infection, the fundamental frequency increases, then decreases post-infection, and remains relatively unchanged in individuals who do not present with signs of disease. In contrast, disease-free individuals often presented with little to no change in the fundamental frequencies post-challenge. Interestingly, the fact that fundamental frequency is shifted in sublethally infected NHPs is also relevant, as it can provide insight into whether or not an individual was recently infected, in concordance with a supporting clinical diagnosis. Heart rate variability, in the context of all three viruses, downshifted to lower RR-I_n-RR-I_{n+1} ordered pairs over the course of the disease; that is, as the disease progressed into the febrile period, the RR-intervals grew more

regular and also decreased, reflecting an increased heart rate during the febrile period. For EEEV and WEEV, day-to-day variations did not become readily apparent until the febrile period. However, for VEEV, an immediate shift of HRV occurred in the post-infection period and remained at a lower daily mean HRV which persisted into the recovery period.

5.2 CORRELATION OF TELEMETRIC READS TO DISEASE PATHOGENESIS

5.2.1 Determination of Core ECG Parameters

The metrics found to vary consistently post-infection for all EEVs comprise a core set of electrocardiography parameters that can be used to track and define disease progression. This set includes HR, PCt, P-Width, PR-I, QRS, QRSA, QT-I, R-H, RR-I, and ST-I. Although the metrics included in this set provide limited specificity to any single virus, they are very useful when establishing that an animal has been infected leading to a lethal infection, correlating with fever and possibly providing an additional basis for measuring encephalitic disease.

QRS appears to be a distinguishing variable whose effects are specific to each virus, though this remains to be tested. Examination of the VEEV data raises the question of whether or not the QRS-response was sex-specific. Male NHPs infected with VEEV exhibited a narrowed QRS interval while female NHPs infected with VEEV exhibited a widened QRS. However, with EEV the all-male cohort of NHPs exhibited widened QRS-interval in sick individuals, while the all-female cohort of WEEV-exposed NHPs exhibited a narrowed QRS-interval in the sick individual, though the difference could be virus-specific. Taken together, the core set of ECG metrics amenable to the tracking of disease include a number of covariant metrics based on heart rate and

its components, and the ECG amplitude of the R-Wave. Raw ECG traces were not assessed to a significant degree, and the small sample size of the NHP cohorts would have hindered generalizability.

5.2.2 Distinguishing Features of Equine Encephalitis Virus Disease Courses

A specific aim of this work sought to establish a basis of comparison within each virus challenge cohort and if possible, between viruses. As discussed previously, QRS-interval provided information specific to each virus, a unique feature among core metrics established. Over the course of the work, it became evident that frequency spectrum analysis of the core metrics provides a more powerful delineator and marker of clinical disease state/period. The fundamental frequency of the waveform presented by the Fourier transforms of the core metrics' time-domain data in each virus increased post-infection, then decreased during the onset of febrile illness. In the VEEV cohort, wherein a recovery period existed, the fundamental frequency proceeded to decrease again.

5.3 EVALUATION OF ELECTROCARDIOGRAPHY MODALITY AS A MODALITY OF TELEMETRIC SURVEILLANCE IN A NONHUMAN PRIMATE MODEL OF ALPHAVIRUS BY AEROSOL ROUTE

5.3.1 Use of Radiofrequency Electrocardiography for the Study of Disease Progression

The use of ECG telemetry in conjunction with traditional methods of observation of animal subjects for natural history studies provides a wealth of valuable information because animals

cannot be directly observed on a continuous basis. This modality allows for indirect monitoring of physiological status when lab staff are unavailable and can potentially prognosticate the onset of disease or moribund state in an animal. Not only does this aid decision-making regarding humane endpoints for such investigations, but the use of telemetry has the potential to provide more specific indicators as to which virus an animal is infected with, something a nonspecific indicator such as temperature cannot do.

Limitations of this work include the inability to investigate the electrocardiographic implications of the dose response relationship due to the small sample size of individual NHP subjects, and the inability to investigate differences in electrocardiography to a fine degree between NHPs who survived versus those who succumbed to aerosol EEV infection due to the variability between baseline parameters between subjects. Although relative changes from baseline within the same NHP could provide insight into disease course, as much of the data suggests marked deviations from baseline during illness, larger sample sizes are required to make a definitive judgment regarding the use of ECG telemetry in this manner. Likewise, the effects of the sex of the NHP upon the disease course also could not be investigated due to the small sample size of NHP subjects, and the relatively short course for which the disease was followed in them. With regard to ECG metrics, mean daily values do not appear to be the most robust unit of data to prognosticate disease, as metrics assessed in this manner give no indication of disease prior to the onset of clinically observable signs, with the notable exception of QRS intervals in the cohorts described.

The beauty of using frequency spectrum analysis is that it could provide for the identification of disease in the context of a known disease course. If an individual is being monitored continuously over a long period of time, samples of electrocardiography data can be

taken from the individual, and in this work, provided the clearest demarcation of the period of disease course. The limitation inherent in this method of prognostication lies in the fact that there exists a need for a lead-time such that the analysis can be conducted over a period of hours or days; in this work, variations in circadian rhythm were analyzed with a sampling frequency of minutes, to look at circadian variation; these trends may not hold for analyses in shorter time windows, perhaps limiting clinical applicability. Direct translation, however, would find better applicability in real-time analysis such that determinations to treat illness could be made. However, just as Holter monitors can detect cardiac arrhythmias in human patients in real time, ECG telemetry can perhaps become clinically relevant in the realm of infectious disease as well.

The same holds for the heart rate variability, but with one caveat – a method that went untested in this work was the use of different definitions of heart rate variability. While each RR-I measure was compared to the one immediately preceding it, one wonders how much the results would have differed should each ordered pair have consisted of (RR-I_n, RR-I_{n+5}) or (RR-I_n, RR-I_{n+12}), or any variant of such pairings. This could have identified more visually and statistically distinguishing differences between the variability data.

Although a large portion of the raw ECG traces went uninspected, no frank signs of direct cardiac pathology were observable from the raw ECG traces examined (data not shown). The findings of this work thus lend credence to the notion that changes in the autonomic nervous system as a response to infection, with or without immune system involvement, can mediate changes observable by electrocardiographic monitoring. Unpublished pathology data from the larger overarching NHP alphavirus study has demonstrated that the virus spreads diffusely into all areas of the brain, resulting in granulocytic infiltration and vasculitides in the brain, perhaps contributory to the development and manifestation of neurological signs and encephalitis. As the hypothalamus

is not excluded from the viral onslaught, it remains conceivable that changes in sympathetic and parasympathetic tone can modulate ECG metrics.

Questions that remain to be answered are as follows: Do sex-based differences in electrocardiographic signatures precipitate any effects on the response to infection by aerosol route, and if so, how does the periodicity of hormonal changes interfere or otherwise modify the outcome? Perhaps body weight, or animal size may exert an effect on the electrocardiographic trace not only in baseline data, but also in the post-infection period, through febrile illness. Finally, it may be helpful to determine whether or not a dose-dependent relationship exists between the manifestation of electrocardiographic changes and the dose of virus received, or even between electrocardiographic changes and the immune response observed.

5.3.2 Recommendations for Future Use and Analysis of ECG Data

Because there are problems with cross-reactivity among alphaviruses and possible interference between vaccines [13], evaluating vaccine candidates for efficacy would be easiest if the same NHP model were used for all 3 viruses. Thus, a set of recommendations for future work may improve the ability of the use of ECG data to help provide specific profiles and prognosticators of disease in the same animal when infected with different viruses.

As discussed previously, the majority of the metrics identified as a core set of electrocardiography metrics covary with each other. Dimension reduction can be carried out among covarying metrics for the purposes of principal component analysis. This could provide a more robust form of prognostication.

Another suggestion lies in the further implementation and standardization of normalization to the frequency spectrum analyses to occur as close to real time as possible. In this work, changes

in fundamental frequency were characterized by taking the difference in cycles per day from one period to another, whereas multiplicative methods of comparing frequency measures to baseline frequency measures may be more useful. The former additive/subtractive method does take into account the time-dependent nature of disease progression however, and differencing in this manner, albeit on a basis closer to real time may prove to be more effective in characterizing or prognosticating disease states before their onset.

Finally, for HRV, a goal to work towards would be as discussed previously: to analyze different series of ordered pairs for HRV. The construction of a 3D scatterplot as opposed to overlaid 2D scatterplots, such that a vector (as in principal component analysis) can be constructed in 3D space that can point to whether or not HRV, or in which direction, is changing on a daily (or more frequent) basis.

5.4 STATEMENT OF PUBLIC HEALTH SIGNIFICANCE: BIOSECURITY AND CLINICAL SURVEILLANCE OF INFECTIOUS DISEASE

A significant public health imperative that drives the study of EEVs lies in the potential of EEVs to be weaponized and to investigate the course and mitigation of natural illness as well. The production of EEV aerosols for the purposes of bioweapon deployment with modern technology has come within reach of well-funded non-state actors and is entirely within the means of the military-industrial complexes of post-industrial nation-states [65, 66]. Research and development of such bioweapons in the case of the first description have historical precedents [67]. It behooves clinicians and researchers to explore new methods of disease detection and disease

prognostication, not only to protect against biological weapons attacks, but also to improve the surveillance, detection, and prognostication of disease courses.

5.4.1 Historical and Contemporary Concerns for Equine Encephalitis Viruses

During the Cold War, the USA and the USSR both sponsored programs intended to investigate and develop EEVs as a tactical tool to induce nonlethal casualties such that a conventional attacking force might be compelled to commit time and resources to attend to downed combatants. Specifically, the US first identified aerosolized VEEV as an ideal agent, due to its low mortality, fast growth, low infectious dose, stability in aerosol form, and propensity for infection by inhalation; it then began a program to simultaneously generate offensive bioweapon stockpiles and a vaccine as a countermeasure. Much groundbreaking work on aerobiology and the associated agents came as a result of these programs. Discovery of the US programs by Soviet espionage led the USSR to respond by beginning a VEEV program of its own[68].

Détente in the 1970s and the end of the Cold War saw international bans enacted on bioweapon production, and the decreasing probability of use of such weapons in conflicts between nation-states [68]. Likewise, the fact that international norms and espionage have made secrecy a requirement for bioweapons programs significantly reduces the deterrent value of offensive bioweapon stockpiles. However, several nation-states have since continued offensive bioweapon production in violation of international law, and the 21st Century has witnessed the emergence of powerful non-state actors who have become alarmingly adept at asymmetric warfare to the extent that fragile nation-states remain embattled with them in prolonged conflicts [66]. This development, coupled with the tendency of more powerful nation-states to achieve long-term geopolitical goals by surreptitiously collaborating with non-state actors such that the latter achieve

the former's goals by proxy, create an environment conducive to the development, proliferation, and deployment of bioweapons as preemptive or vengeance strikes by both state- and non-state actors.

The United States faced a harrowing new set of challenges in the months and years following the September 11th 2001 attacks coupled with the Amerithrax *B. anthracis* spore attacks; these events underscored the need for effective contingency plans for ensuring national security in the face of widespread vulnerability to attack, culminating in the establishment of risk-stratified Category A, B, and C agent lists (in decreasing order of risk priority) by the CDC; the EEVs discussed rank in Category B [69]. The relatively low technical requirements and ease with which the EEVs may be manufactured, stored, and dispersed, combined with the difficulty of large-scale defense against such attacks, belie the EEVs' Category B status; the very nature of the decreased infectiousness and virulence may make the application of EEV all the more attractive to those who seek to employ the pathogen for nefarious purposes [66, 70, 71].

5.4.2 Surveillance, Detection, and Prognostication of Infectious Disease

The foremost takeaway from this work, however, lies in the exploration of nontraditional methods of disease detection in the context of infectious disease. For a wide spectrum of infectious diseases spanning the pantheon of microbiological pathogens, clinicians are presented with an equally great array of information regarding the differential diagnosis of an afflicted individual upon presentation to the clinical setting. In the event of a large outbreak of an uncommon disease, the burden of a large influx of patients presenting with an unfamiliar set of symptoms can stretch a healthcare system beyond its capacity to effectively fulfill its mission of diagnosing and treating patients. The promise of studying alphaviruses in a well-defined animal model, not only in the

context of aerobiology for the sake of biosecurity, biodefense, lies also in the prospect of vaccine development and the establishment and improvement of better biotechnology that can achieve clinical applicability for both chronic and acute disease surveillance. As much work is currently underway to make feasible the use of blood tests that can identify viruses, the applications of the work described here can be used as a delimiter of whether or not to treat, and can be applied to prognostication of the severity of illness.

APPENDIX A: ANOVA TABLES

A.1 SIGNIFICANT ECG METRICS FOR EQUINE ENCEPHALITIS VIRUSES

Table 10. Repeated Measures ANOVA Summary for EEEV.

Electrocardiography Metric	*NHP*	*Metric Significance*	*SD Significance*
BAD	M160-16	ns	ns
	M161-16	ns	ns
	M162-16	ns	ns
	M163-16	ns	ns
HR	***M160-16***	***ns***	***ns***
	M161-16	**	***ns***
	M162-16	***ns***	***ns***
	M163-16	***	***ns***
MxdV	M160-16	ns	ns
	M161-16	ns	ns
	M162-16	ns	ns
	M163-16	*	ns
Noise	M160-16	ns	ns
	M161-16	ns	ns
	M162-16	ns	ns
	M163-16	*	ns
PCt	***M160-16***	***ns***	ns
	M161-16	*	ns
	M162-16	***ns***	ns

Table 10 (cont'd)			
	M163-16	*****	ns
P-H	M160-16	*	ns
	M161-16	*	ns
	M162-16	ns	ns
	M163-16	ns	ns
PR-I	***M160-16***	***ns***	ns
	M161-16	*****	ns
	M162-16	***ns***	ns
	M163-16	******	ns
P-Width	***M160-16***	***ns***	ns
	M161-16	*****	ns
	M162-16	***ns***	ns
	M163-16	*****	ns
QATN	M160-16	*	*
	M161-16	ns	ns
	M162-16	ns	ns
	M163-16	***	ns
QR-I	M160-16	ns	ns
	M161-16	ns	ns
	M162-16	ns	ns
	M163-16	*	ns
QRS	***M160-16***	***ns***	***ns***
	M161-16	*****	***ns***
	M162-16	***ns***	***ns***
	M163-16	*****	***ns***
QRSA	***M160-16***	***ns***	***ns***

Table 10 (cont'd)	***M161-16***	*****	***ns***
	M162-16	***ns***	***ns***
	M163-16	*****	***ns***
QT-I	***M160-16***	*****	*
	M161-16	***ns***	ns
	M162-16	***ns***	ns
	M163-16	******	ns
R-H	***M160-16***	***ns***	ns
	M161-16	*****	ns
	M162-16	***ns***	ns
	M163-16	**	ns
RR-I	***M160-16***	***ns***	ns
	M161-16	*****	ns
	M162-16	***ns***	ns
	M163-16	***	ns
ST-E	M160-16	ns	*
	M161-16	*	ns
	M162-16	ns	ns
	M163-16	*****	ns
ST-I	M160-16	*	*
	M161-16	ns	ns
	M162-16	ns	ns
	M163-16	******	ns
T-H	M160-16	ns	*
	M161-16	ns	ns
	M162-16	ns	ns
	M163-16	ns	ns

Table 10 (cont'd)			
T-HN	M160-16	ns	ns
	M161-16	ns	ns
	M162-16	ns	ns
	M163-16	*	ns
T-P	M160-16	ns	ns
	M161-16	ns	ns
	M162-16	ns	ns
	M163-16	ns	ns
T-Pe	M160-16	ns	*
	M161-16	ns	ns
	M162-16	ns	ns
	M163-16	***	ns

Table 11. Repeated Measures ANOVA Summary for WEEV.

Electrocardiography Metric	***NHP***	***Metric Significance***	***SD Significance***
BAD	M166-16	ns	ns
	M168-16	ns	ns
	M169-16	ns	ns
HR	M166-16	***ns***	ns
	M168-16	***ns***	ns
	M169-16	***	ns
MxdV	***M166-16***	***ns***	**ns**
	M168-16	***ns***	**ns**
	M169-16	***	*
Noise	***M166-16***	***ns***	ns

Table 11 (cont'd)	***M168-16***	***ns***	ns
	M169-16	**	ns
PCt	M166-16	*	ns
	M168-16	**********	ns
	M169-16	***	ns
P-H	***M166-16***	***ns***	ns
	M168-16	***ns***	ns
	M169-16	*	ns
PR-I	M166-16	***ns***	ns
	M168-16	***ns***	ns
	M169-16	**	ns
P-Width	M166-16	ns	ns
	M168-16	ns	ns
	M169-16	ns	ns
QATN	M166-16	ns	ns
	M168-16	ns	ns
	M169-16	ns	ns
QR-I	M166-16	ns	ns
	M168-16	ns	ns
	M169-16	ns	Ns
QRS	M166-16	*	***ns***
	M168-16	**********	***ns***
	M169-16	**	*
QRSA	M166-16	***ns***	***ns***
	M168-16	**	***ns***
	M169-16	**	**
QT-I	***M166-16***	***ns***	ns

Table 11 (cont'd)	***M168-16***	***ns***	ns
	M169-16	*****	ns
R-H	M166-16	ns	ns
	M168-16	ns	ns
	M169-16	ns	ns
RR-I	M166-16	***ns***	ns
	M168-16	***ns***	ns
	M169-16	***	ns
ST-E	M166-16	ns	ns
	M168-16	ns	ns
	M169-16	ns	ns
ST-I	***M166-16***	***	ns
	M168-16	**********	ns
	M169-16	*****	ns
T-H	***M166-16***	***ns***	***ns***
	M168-16	***ns***	***ns***
	M169-16	*	**
T-HN	M166-16	ns	ns
	M168-16	ns	ns
	M169-16	ns	ns
T-P	M166-16	ns	ns
	M168-16	ns	ns
	M169-16	ns	ns
T-Pe	M166-16	ns	ns
	M168-16	ns	ns
	M169-16	ns	ns

Table 12. One Way ANOVA Summary for VEEV, by Period.

Electrocardiography Metric	*NHP*	*Metric Significance*	*SD Significance*
BAD	M164-16	ns	ns
	M165-16	ns	ns
	M170-16	ns	ns
	M171-16	ns	ns
HR	***M164-16***	****x31***	ns
	M165-16	****x60***	*x30
	M170-16	*********	*x36
	M171-16	****x64***	**
MxdV	***M164-16***	****x35***	Ns
	M165-16	****x27***	*x29
	M170-16	****x17***	*x26
	M171-16	*********	**
Noise	M164-16	ns	ns
	M165-16	ns	ns
	M170-16	ns	ns
	M171-16	ns	ns
PCt	***M164-16***	****x23***	ns
	M165-16	****x45***	ns
	M170-16	**********	ns
	M171-16	****x30***	ns
P-H	***M164-16***	ns	**
	M165-16	ns	*******
	M170-16	*x22	********

Table 12 (cont'd)	***M171-16***	ns	****x36***
PR-I	***M164-16***	*x67	*****
	M165-16	ns	******
	M170-16	*x45	****x14***
	M171-16	*x62	*******
P-Width	***M164-16***	********	*****
	M165-16	****x22***	*******
	M170-16	*****	****x16***
	M171-16	****x26***	*******
QATN	***M164-16***	****x38***	**********
	M165-16	****x88***	****x24***
	M170-16	****x37***	******
	M171-16	****x92***	****x62***
QR-I	***M164-16***	**********	ns
	M165-16	****x28***	**********
	M170-16	****x24***	*x23
	M171-16	****x26***	****
QRS	***M164-16***	****x18***	ns
	M165-16	****x91***	*x18
	M170-16	****x30***	*x36
	M171-16	****x50***	*****
QRSA	***M164-16***	**********	*****
	M165-16	****x61***	****x26***
	M170-16	****x23***	****x40***
	M171-16	****x30***	******
QT-I	***M164-16***	****x22***	********
	M165-16	****x37***	**

Table 12 (cont'd)	***M170-16***	**********	ns
	M171-16	***x49***	ns
R-H	***M164-16***	**********	**
	M165-16	***x59***	***x26***
	M170-16	***x26***	***x43***
	M171-16	***x30***	****
RR-I	***M164-16***	***x30***	ns
	M165-16	***x96***	*x82
	M170-16	**********	*x23
	M171-16	***x100***	**
ST-E	***M164-16***	***x34***	ns
	M165-16	***x36***	**********
	M170-16	********	*x46
	M171-16	***x35***	*x10
ST-I	***M164-16***	***x22***	**
	M165-16	***x38***	*********
	M170-16	*******	*
	M171-16	***x48***	*
T-H	M164-16	ns	ns
	M165-16	*x39	****
	M170-16	*x34	*
	M171-16	*x98	****
T-HN	***M164-16***	*******	ns
	M165-16	**********	*******
	M170-16	****	*
	M171-16	***x45***	ns
T-P	***M164-16***	***x40***	ns

Table 12 (cont'd)	***M165-16***	****x73***	****
	M170-16	***********	*
	M171-16	****x49***	*
T-Pe	***M164-16***	****x44***	*
	M165-16	****x44***	*******
	M170-16	*************	ns
	M171-16	****x35***	*

A.2 EEEV ANOVA RESULTS

Table 13. Repeated Measures ANOVA for EEEV HR.

M160-16 HR rmANOVA

	SumSq	DF	MeanSq	F	pValue	pValueGG	pValueHF	pValueLB
(Intercept):HR	14794	11	1344.9	2.9651	0.00087861	0.0080281	0.0039173	0.094441
Time:HR	18917	11	1719.7	3.7915	3.6302e-05	0.0012164	0.00039098	0.060066
Error(HR)	1.6465e+05	363	453.58					

M161-16 HR rmANOVA

	SumSq	DF	MeanSq	F	pValue	pValueGG	pValueHF	pValueLB
(Intercept):HR	21476	11	1952.4	6.1858	1.7293e-09	1.0452e-07	2.2535e-09	0.017148
Time:HR	38139	11	3467.2	10.985	4.9535e-18	2.7838e-14	8.6551e-18	0.0019585
Error(HR)	1.3888e+05	440	315.63					

M162-16 HR rmANOVA

	SumSq	DF	MeanSq	F	pValue	pValueGG	pValueHF	pValueLB
(Intercept):HR	10659	11	969.04	4.831	0.0073473	0.27182	0.27182	0.27182
Time:HR	7534.5	11	684.95	3.4148	0.026526	0.31578	0.31578	0.31578
Error(HR)	2206.4	11	200.59					

M163-16 HR rmANOVA

	SumSq	DF	MeanSq	F	pValue	pValueGG	pValueHF	pValueLB
(Intercept):HR	45511	11	4137.3	15.219	1.2117e-26	7.513e-22	1.9202e-25	0.00024134
Time:HR	43590	11	3962.7	14.577	1.7773e-25	6.5357e-21	2.471e-24	0.00031718
Error(HR)	1.8241e+05	671	271.85					

Table 14. Repeated Measures ANOVA for EEEV PCt.

M160-16 PCt rmANOVA	SumSq	DF	MeanSq	F	pValue	pValueGG	pValueHF	pValueLB
(Intercept):PCt	96.254	11	8.7503	2.3875	0.0072718	0.027629	0.017256	0.13185
Time:PCt	141.07	11	12.825	3.4991	0.00011383	0.0021733	0.0007728	0.070292
Error(PCt)	1330.4	363	3.6651					

M161-16 PCt rmANOVA	SumSq	DF	MeanSq	F	pValue	pValueGG	pValueHF	pValueLB
(Intercept):PCt	780.87	11	70.989	9.6973	8.0816e-16	3.0329e-11	1.9824e-13	0.0033604
Time:PCt	299.37	11	27.215	3.7177	4.3001e-05	0.00057151	0.00016539	0.060785
Error(PCt)	3301.5	451	7.3205					

M162-16 PCt rmANOVA	SumSq	DF	MeanSq	F	pValue	pValueGG	pValueHF	pValueLB
(Intercept):PCt	109.76	11	9.9784	2.2788	0.093843	0.37247	0.37247	0.37247
Time:PCt	168.5	11	15.318	3.4983	0.024394	0.31257	0.31257	0.31257
Error(PCt)	48.167	11	4.3788					

M163-16 PCt rmANOVA	SumSq	DF	MeanSq	F	pValue	pValueGG	pValueHF	pValueLB
(Intercept):PCt	305.78	11	27.799	13.152	7.2633e-23	1.0697e-18	1.0703e-21	0.00058769
Time:PCt	287.1	11	26.1	12.349	2.2317e-21	1.6608e-17	2.7156e-20	0.00083798
Error(PCt)	1418.2	671	2.1136					

Table 15. Repeated Measures ANOVA for EEEV PR-I.

M160-16 PRI rmANOVA	SumSq	DF	MeanSq	F	pValue	pValueGG	pValueHF	pValueLB
(Intercept):PRI	936.15	11	85.105	2.4598	0.0056232	0.018358	0.0095886	0.12634
Time:PRI	1297.8	11	117.98	3.4099	0.00016085	0.0016484	0.00046107	0.07379
Error(PRI)	12559	363	34.599					

M161-16 PRI rmANOVA	SumSq	DF	MeanSq	F	pValue	pValueGG	pValueHF	pValueLB
(Intercept):PRI	1.7694e+33	11	1.6086e+32	85.784	3.7727e-103	7.4051e-24	3.1783e-25	1.3252e-11
Time:PRI	1.3918e+32	11	1.2653e+31	6.7476	1.5963e-10	0.0010424	0.00078888	0.012979
Error(PRI)	8.4568e+32	451	1.8751e+30					

M162-16 PRI rmANOVA	SumSq	DF	MeanSq	F	pValue	pValueGG	pValueHF	pValueLB
(Intercept):PRI	755.25	11	68.659	0.56855	0.81847	0.5887	0.5887	0.5887
Time:PRI	4204.5	11	382.22	3.1651	0.034317	0.326	0.326	0.326
Error(PRI)	1328.4	11	120.76					

M163-16 PRI rmANOVA	SumSq	DF	MeanSq	F	pValue	pValueGG	pValueHF	pValueLB
(Intercept):PRI	936.19	11	85.108	7.2937	7.6686e-12	7.527e-10	2.8347e-11	0.0089445
Time:PRI	1319.8	11	119.98	10.283	1.6448e-17	2.1521e-14	1.2736e-16	0.0021394
Error(PRI)	7829.7	671	11.669					

Table 16. Repeated Measures ANOVA for EEEV P-Width.

M160-16 PWidth rmANOVA

	SumSq	DF	MeanSq	F	pValue	pValueGG	pValueHF	pValueLB
(Intercept):PWdth	384.65	11	34.968	1.1471	0.32331	0.33367	0.32725	0.29193
Time:PWdth	797.19	11	72.472	2.3773	0.0075374	0.020705	0.010786	0.13264
Error(PWdth)	11066	363	30.485					

M161-16 PWidth rmANOVA

	SumSq	DF	MeanSq	F	pValue	pValueGG	pValueHF	pValueLB
(Intercept):PWdth	1.7694e+33	11	1.6086e+32	85.784	3.7727e-103	7.4051e-24	3.1783e-25	1.3252e-11
Time:PWdth	1.3918e+32	11	1.2653e+31	6.7476	1.5963e-10	0.0010424	0.00078888	0.012979
Error(PWdth)	8.4568e+32	451	1.8751e+30					

M162-16 PWidth rmANOVA

	SumSq	DF	MeanSq	F	pValue	pValueGG	pValueHF	pValueLB
(Intercept):PWdth	351.92	11	31.992	0.69452	0.72219	0.5577	0.5577	0.5577
Time:PWdth	1382.5	11	125.68	2.7283	0.055301	0.34657	0.34657	0.34657
Error(PWdth)	506.71	11	46.064					

M163-16 PWidth rmANOVA

	SumSq	DF	MeanSq	F	pValue	pValueGG	pValueHF	pValueLB
(Intercept):PWdth	2051.6	11	186.51	8.6616	1.9242e-14	3.4162e-12	4.386e-14	0.004591
Time:PWdth	1442.1	11	131.1	6.0883	1.4841e-09	3.5923e-08	2.4631e-09	0.01643
Error(PWdth)	14448	671	21.533					

Table 17. Repeated Measures ANOVA for EEEV QRS.

M160-16 QRS rmANOVA

	SumSq	DF	MeanSq	F	pValue	pValueGG	pValueHF	pValueLB
(Intercept):QRS	152.88	11	13.898	4.1407	9.1242e-06	0.00032937	6.641e-05	0.049961
Time:QRS	141.59	11	12.872	3.835	3.0586e-05	0.00071042	0.00017426	0.05869
Error(QRS)	1218.4	363	3.3564					

M161-16 QRS rmANOVA

	SumSq	DF	MeanSq	F	pValue	pValueGG	pValueHF	pValueLB
(Intercept):QRS	317.18	11	28.834	11.082	2.9675e-18	3.3357e-13	6.1828e-16	0.0018503
Time:QRS	136.8	11	12.436	4.7795	5.7157e-07	2.3325e-05	3.1253e-06	0.034565
Error(QRS)	1173.5	451	2.602					

M162-16 QRS rmANOVA

	SumSq	DF	MeanSq	F	pValue	pValueGG	pValueHF	pValueLB
(Intercept):QRS	158.43	11	14.403	0.59476	0.79892	0.58178	0.58178	0.58178
Time:QRS	811.46	11	73.769	3.0463	0.038939	0.33123	0.33123	0.33123
Error(QRS)	266.37	11	24.216					

M163-16 QRS rmANOVA

	SumSq	DF	MeanSq	F	pValue	pValueGG	pValueHF	pValueLB
(Intercept):QRS	226.75	11	20.614	4.8422	3.2259e-07	5.0223e-06	9.1668e-07	0.031568
Time:QRS	188.9	11	17.173	4.034	9.8075e-06	7.4403e-05	2.1189e-05	0.049025
Error(QRS)	2856.5	671	4.2571					

Table 18. Repeated Measures ANOVA for EEEV QT-I.

M160-16 QT-I rmANOVA

	SumSq	DF	MeanSq	F	pValue	pValueGG	pValueHF	pValueLB
(Intercept):QTI	9848.4	11	895.31	5.2135	1.2335e-07	6.8874e-05	1.2946e-05	0.028984
Time:QTI	12225	11	1111.4	6.4716	7.6358e-10	4.3321e-06	4.4323e-07	0.015828
Error(QTI)	62338	363	171.73					

M161-16 QT-I rmANOVA

	SumSq	DF	MeanSq	F	pValue	pValueGG	pValueHF	pValueLB
(Intercept):QTI	1.6102e+33	11	1.4638e+32	55.861	4.2786e-77	1.6578e-18	1.4807e-19	3.5592e-09
Time:QTI	1.1196e+32	11	1.0178e+31	3.8842	2.2041e-05	0.01816	0.016013	0.055518
Error(QTI)	1.1818e+33	451	2.6204e+30					

M162-16 QT-I rmANOVA

	SumSq	DF	MeanSq	F	pValue	pValueGG	pValueHF	pValueLB
(Intercept):QTI	3871.5	11	351.96	0.57184	0.81604	0.58782	0.58782	0.58782
Time:QTI	20056	11	1823.3	2.9624	0.042638	0.33508	0.33508	0.33508
Error(QTI)	6770.3	11	615.48					

M163-16 QT-I rmANOVA

	SumSq	DF	MeanSq	F	pValue	pValueGG	pValueHF	pValueLB
(Intercept):QTI	14377	11	1307	7.9184	4.9753e-13	8.5775e-10	5.0092e-11	0.0065776
Time:QTI	45314	11	4119.4	24.956	1.9411e-43	2.4177e-31	6.0269e-36	5.2195e-06
Error(QTI)	1.1076e+05	671	165.06					

Table 19. Repeated Measures ANOVA for EEEV RR-I.

M160-16 RR-I rmANOVA

	SumSq	DF	MeanSq	F	pValue	pValueGG	pValueHF	pValueLB
(Intercept):RRI	1.3084e+05	11	11894	2.7203	0.0021849	0.016321	0.0097119	0.10857
Time:RRI	1.6449e+05	11	14954	3.4199	0.00015473	0.0036855	0.0016316	0.073388
Error(RRI)	1.5872e+06	363	4372.5					

M161-16 RR-I rmANOVA

	SumSq	DF	MeanSq	F	pValue	pValueGG	pValueHF	pValueLB
(Intercept):RRI	3.4176e+05	11	31069	3.0953	0.00049763	0.013321	0.009632	0.085978
Time:RRI	7.3164e+05	11	66512	6.6264	2.646e-10	2.3653e-05	7.8294e-06	0.013758
Error(RRI)	4.5269e+06	451	10037					

M162-16 RR-I rmANOVA

	SumSq	DF	MeanSq	F	pValue	pValueGG	pValueHF	pValueLB
(Intercept):RRI	1.4037e+05	11	12761	2.2336	0.099184	0.37541	0.37541	0.37541
Time:RRI	1.3998e+05	11	12725	2.2273	0.099957	0.37583	0.37583	0.37583
Error(RRI)	62846	11	5713.3					

M163-16 RR-I rmANOVA

	SumSq	DF	MeanSq	F	pValue	pValueGG	pValueHF	pValueLB
(Intercept):RRI	3.0763e+05	11	27966	10.505	6.2647e-18	4.5995e-15	1.7589e-17	0.0019304
Time:RRI	4.0762e+05	11	37056	13.92	2.8209e-24	2.8382e-20	1.1933e-23	0.00042079
Error(RRI)	1.7863e+06	671	2662.1					

A.3 WEEV ANOVA RESULTS

Table 20. Repeated Measures ANOVA and One Way ANOVA for WEEV HR.

M166-16 HR owANOVA

```
pHRper166 =

    0.1679

ciHRper166 =

   -7.5387
    1.3135

statsHRper166 =

    tstat: -1.3800
       df: 990
       sd: 27.8984
```

M168-16 HR owANOVA

```
pHRper168 =

    0.6295

ciHRper168 =

   -5.4347
    8.9777

statsHRper168 =

    tstat: 0.4826
       df: 757
       sd: 33.9122
```

M169-16 HR rmANOVA

	SumSq	DF	MeanSq	F	pValue	pValueGG	pValueHF	pValueLB
(Intercept):HR	1.5294e+05	10	15294	51.913	1.6328e-78	8.0255e-51	6.6773e-56	4.3324e-10
Time:HR	46634	10	4663.4	15.829	6.2606e-26	2.618e-17	6.8288e-19	0.00016173
Error(HR)	2.1506e+05	730	294.61					

Table 21. Repeated Measures ANOVA and One Way ANOVA for WEEV PCt.

M166-16 PCt owANOVA

```
pPCtper166 =

    0.1729

ciPCtper166 =

   -0.6327
    0.1138

statsPCtper166 =

    tstat: -1.3640
       df: 990
       sd: 2.3526
```

M168-16 PCt owANOVA

```
pPCtper168 =

    0.6951

ciPCtper168 =

   -0.4806
    0.7205

statsPCtper168 =

    tstat: 0.3920
       df: 757
       sd: 2.8262
```

M169-16 PCt rmANOVA

	SumSq	DF	MeanSq	F	pValue	pValueGG	pValueHF	pValueLB
(Intercept):PCt	1108.7	10	110.87	47.158	1.8466e-72	3.4088e-46	1.0515e-50	1.835e-09
Time:PCt	322.34	10	32.234	13.71	2.6286e-22	9.1355e-15	4.6079e-16	0.00041142
Error(PCt)	1716.3	730	2.3511					

Table 22. Repeated Measures ANOVA and One Way ANOVA for WEEV QRS.

M166-16 QRS owANOVA

```
pQRSper166 =

    0.0342

ciQRSper166 =

   -0.5385
   -0.0209

statsQRSper166 =

    tstat: -2.1211
       df: 990
       sd: 1.6313
```

M168-16 QRS owANOVA

```
pQRSper168 =

    1.1708e-21

ciQRSper168 =

   -2.6626
   -1.7784

statsQRSper168 =

    tstat: -9.8600
       df: 757
       sd: 2.0805
```

M169-16 QRS rmANOVA

	SumSq	DF	MeanSq	F	pValue	pValueGG	pValueHF	pValueLB
(Intercept):QRS	253.19	10	25.319	30.185	7.9524e-49	1.1888e-34	2.276e-38	5.4576e-07
Time:QRS	43.988	10	4.3988	5.2442	1.8071e-07	9.2708e-06	3.2869e-06	0.024911
Error(QRS)	612.32	730	0.8388					

Table 23. Repeated Measures ANOVA and One Way ANOVA for WEEV QT-I.

M166-16 QT-I owANOVA

```
pQTIper166 =

    0.0079

ciQTIper166 =

   -7.6296
   -1.1519

statsQTIper166 =

    tstat: -2.6603
       df: 990
       sd: 20.4145
```

M168-16 QT-I owANOVA

```
pQTIper168 =

    3.8527e-04

ciQTIper168 =

  -10.6004
   -3.0731

statsQTIper168 =

    tstat: -3.5660
       df: 756
       sd: 17.7099
```

M169-16 QT-I rmANOVA

	SumSq	DF	MeanSq	F	pValue	pValueGG	pValueHF	pValueLB
(Intercept):QTI	1.3687e+05	10	13687	92.458	1.463e-122	8.8852e-57	8.9824e-61	1.3178e-14
Time:QTI	30541	10	3054.1	20.631	6.5387e-34	1.3533e-16	1.1934e-17	2.1539e-05
Error(QTI)	1.0807e+05	730	148.04					

Table 24. Repeated Measures ANOVA and One Way ANOVA for WEEV RR-I.

M166-16 RR-I owANOVA

```
pRRIper166 =

    0.5252

ciRRIper166 =

   -7.8991
   15.4658

statsRRIper166 =

    tstat: 0.6355
       df: 990
       sd: 73.6358
```

M168-16 RR-I owANOVA

```
pRRIper168 =

    0.6186

ciRRIper168 =

   -17.5454
    10.4446

statsRRIper168 =

    tstat: -0.4980
       df: 757
       sd: 65.8602
```

M169-16 RR-I rmANOVA

	SumSq	DF	MeanSq	F	pValue	pValueGG	pValueHF	pValueLB
(Intercept):RRI	8.2149e+05	10	82149	48.211	8.0673e-74	5.8522e-44	6.2495e-48	1.3263e-09
Time:RRI	2.8729e+05	10	28729	16.86	1.1377e-27	4.8642e-17	1.8658e-18	0.00010376
Error(RRI)	1.2439e+06	730	1704					

A.4 VEEV ANOVA RESULTS

Table 25. One Way ANOVA for VEEV HR.

M164-16 HR owANOVA

ANOVA Table

Source	SS	df	MS	F	Prob>F
Groups	96620.2	3	32206.7	50.59	3.24961e-31
Error	1001347	1573	636.6		
Total	1097967.3	1576			

M165-16 HR owANOVA

ANOVA Table

Source	SS	df	MS	F	Prob>F
Groups	283093.5	3	94364.5	103.8	2.11588e-60
Error	1213634.2	1335	909.1		
Total	1496727.7	1338			

M170-16 HR owANOVA

ANOVA Table

Source	SS	df	MS	F	Prob>F
Groups	22159.1	3	7386.37	12.47	4.72301e-08
Error	863721	1458	592.4		
Total	885880.1	1461			

M171-16 HR owANOVA

ANOVA Table

Source	SS	df	MS	F	Prob>F
Groups	158518.3	3	52839.4	110.73	3.45726e-64
Error	652788.6	1368	477.2		
Total	811306.9	1371			

Table 26. One Way ANOVA for VEEV QRS.

M164-16 QRS owANOVA

ANOVA Table

Source	SS	df	MS	F	Prob>F
Groups	229.79	3	76.5982	29.55	1.39072e-18
Error	4077.82	1573	2.5924		
Total	4307.61	1576			

M165-16 QRS owANOVA

ANOVA Table

Source	SS	df	MS	F	Prob>F
Groups	4045.2	3	1348.39	164.71	7.80954e-91
Error	10929	1335	8.19		
Total	14974.1	1338			

M170-16 QRS owANOVA

ANOVA Table

Source	SS	df	MS	F	Prob>F
Groups	2242	3	747.339	48.4	8.13092e-30
Error	22513.9	1458	15.442		
Total	24756	1461			

M171-16 QRS owANOVA

ANOVA Table

Source	SS	df	MS	F	Prob>F
Groups	510.25	3	170.085	84.17	5.6369e-50
Error	2764.46	1368	2.021		
Total	3274.71	1371			

Table 27. One Way ANOVA for VEEV QRSA.

M164-16 QRSA owANOVA

ANOVA Table

Source	SS	df	MS	F	Prob>F
Groups	3.774	3	1.25817	18.54	8.0452e-12
Error	106.746	1573	0.06786		
Total	110.52	1576			

M165-16 QRSA owANOVA

ANOVA Table

Source	SS	df	MS	F	Prob>F
Groups	121.311	3	40.437	105.22	3.78558e-61
Error	513.042	1335	0.3843		
Total	634.353	1338			

M170-16 QRSA owANOVA

ANOVA Table

Source	SS	df	MS	F	Prob>F
Groups	7.889	3	2.62967	36.94	5.20711e-23
Error	103.781	1458	0.07118		
Total	111.67	1461			

M171-16 QRSA owANOVA

ANOVA Table

Source	SS	df	MS	F	Prob>F
Groups	14.833	3	4.94443	49.6	1.97462e-30
Error	136.364	1368	0.09968		
Total	151.197	1371			

Table 28. One Way ANOVA for VEEV QRSASD.

M164-16 QRSASD owANOVA

ANOVA Table

Source	SS	df	MS	F	Prob>F
Groups	0.03489	3	0.01163	3.64	0.0123
Error	5.02498	1573	0.00319		
Total	5.05987	1576			

M165-16 QRSASD owANOVA

ANOVA Table

Source	SS	df	MS	F	Prob>F
Groups	7.9968	3	2.66558	41.99	6.23675e-26
Error	84.7413	1335	0.06348		
Total	92.7381	1338			

M170-16 QRSASD owANOVA

ANOVA Table

Source	SS	df	MS	F	Prob>F
Groups	8.3735	3	2.79116	66.27	3.58539e-40
Error	61.407	1458	0.04212		
Total	69.7805	1461			

M171-16 QRSASD owANOVA

ANOVA Table

Source	SS	df	MS	F	Prob>F
Groups	0.2771	3	0.09238	6.51	0.0002
Error	19.4265	1368	0.0142		
Total	19.7036	1371			

Table 29. One Way ANOVA for VEEV QT-I.

M164-16 QT-I owANOVA

ANOVA Table

Source	SS	df	MS	F	Prob>F
Groups	51551.8	3	17183.9	36.3	1.11653e-22
Error	744721.7	1573	473.4		
Total	796273.5	1576			

M165-16 QT-I owANOVA

ANOVA Table

Source	SS	df	MS	F	Prob>F
Groups	113973.4	3	37991.1	62.56	1.07373e-37
Error	762784.9	1256	607.3		
Total	876758.2	1259			

M170-16 QT-I owANOVA

ANOVA Table

Source	SS	df	MS	F	Prob>F
Groups	54651.3	3	18217.1	25.46	5.48709e-16
Error	890811.4	1245	715.5		
Total	945462.7	1248			

M171-16 QT-I owANOVA

ANOVA Table

Source	SS	df	MS	F	Prob>F
Groups	85890.5	3	28630.2	82.35	5.66532e-49
Error	474905.9	1366	347.7		
Total	560796.4	1369			

Table 30. One Way ANOVA for VEEV RR-I.

M164-16 RR-I owANOVA

ANOVA Table

Source	SS	df	MS	F	Prob>F
Groups	564845.4	3	188281.8	49.07	2.56677e-30
Error	6035080.5	1573	3836.7		
Total	6599925.9	1576			

M165-16 RR-I owANOVA

ANOVA Table

Source	SS	df	MS	F	Prob>F
Groups	5.29021e+06	3	1763403.6	175.92	4.19924e-96
Error	1.33823e+07	1335	10024.2		
Total	1.86725e+07	1338			

M170-16 RR-I owANOVA

ANOVA Table

Source	SS	df	MS	F	Prob>F
Groups	347295.2	3	115765.1	15.65	5.08876e-10
Error	10786026.1	1458	7397.8		
Total	11133321.3	1461			

M171-16 RR-I owANOVA

ANOVA Table

Source	SS	df	MS	F	Prob>F
Groups	2.69589e+06	3	898629.9	182.96	9.68756e-100
Error	6.719e+06	1368	4911.6		
Total	9.41489e+06	1371			

APPENDIX B: PERTINENT MATLAB CODE FOR ANALYSES

Designation “M1XX-16_(M/F)_(E/W/V)_(L/D)_Var” used as a placeholder for a given NHP.

B.1 DATA PROCESSING AND PROFILE GENERATON

B.1.1 Data Processing and Filtration

```
%% Temperature Profiles
   %Temperature Profiles Plotted with Cumulative Fever Hours
for i= 1:1
figure(1);
Htemp = gcf;
hold on;

   %M1xx

      ii = 1;
   while ii < length(M1XX-16_DPI')+1
      if ((M1XX-16_(M/F)_(E/W/V)_(L/D)_T_Mean(ii,1))>42) || (M1XX-16_(M/F)_(E/W/V)_(L/D)_T_Mean(ii,1)<22)
         M1XX-16_(M/F)_(E/W/V)_(L/D)_T_MeanCens(ii,1) = NaN;
      else
         M1XX-16_(M/F)_(E/W/V)_(L/D)_T_MeanCens(ii,1) = M1XX-16_(M/F)_(E/W/V)_(L/D)_T_Mean(ii,1);
      end
         ii= ii+1;
   end
   M1XX-16_ARIMA = [(mean(M1XX-16_(M/F)_(E/W/V)_(L/D)_T_MeanCens(1:2881),'omitnan')-(2*std(M1XX-
16_(M/F)_(E/W/V)_(L/D)_T_MeanCens(1:2881),'omitnan'))) (mean(M1XX-16_(M/F)_(E/W/V)_(L/D)_T_MeanCens(1:2881),'omitnan')) (mean(M1XX-
16_(M/F)_(E/W/V)_(L/D)_T_MeanCens(1:2881),'omitnan')+(2*std(M1XX-16_(M/F)_(E/W/V)_(L/D)_T_MeanCens(1:2881),'omitnan')))];

   subplot(n,m,p),
      aero1 = line([0 0], [-100 100],'LineWidth',2,'Color','m');
      hold;
      title('M1XX-16');
      yyaxis left
      pt1 = plot(M1XX-16_DPI, M1XX-16_(M/F)_(E/W/V)_(L/D)_T_MeanCens,'.b');
      xlim([-3 15]);
      ylim([32 42]);
      line([-6 30], [M1XX-16_ARIMA(1,1) M1XX-16_ARIMA(1,1)],'LineWidth',1);
      line([-6 30], [M1XX-16_ARIMA(1,2) M1XX-16_ARIMA(1,2)],'LineWidth',0.5);
      line([-6 30], [M1XX-16_ARIMA(1,3) M1XX-16_ARIMA(1,3)],'LineWidth',1);
      xlabel ('DPI(d)');
      ylabel ('Temperature (^oC)','Color','b');
      yyaxis right
      pc1 = plot(M1XX-16_DPI, M1XX-16_(M/F)_(E/W/V)_(L/D)_CumFH,'.r');
      ylim([0 100]);
      ylabel ('Cumulative Fever-Hours(h)', 'Color','r');
      subplotobj = subplot(n,m,p,'Parent',Htemp);
      set(subplotobj,'XColor',[0 0 0],'YColor',[1 0 0],'ZColor',[0 0 0]);
end
```

%% Clinical Scores

```
%% Clinical Scores – Daily Clinical Score, scaled to temperature curve
```

```
for i=1:1
   M1XX_Clin = [3 3 3 3 4 6 5 5 4 4 4 4 4 3 4 4 4 3 3];
     M1XXModClin = 32+(42-32).*(M1XX_Clin./100);
end
```

B.1.2 Profile Generation

Case: Heart Rate, M166-16, M167-16, M168-16, M169-16

Metric

```
%HR - Heart Rate
        for i=1:1
        disp('HR-Run');
        SubtitleHR = {'M166-16', 'M167-16','M168-16','M169-16'};
        figure(5)
        HHR = gcf;
        hold on;

        jj = 1;
        while jj<5
           switch jj
                case 1
                   M166_F_W_L_HRCens = [];
                   ii = 1;
                   while ii < length(M166_DPI')+1
                       if (M166_F_W_L_HR(ii,1)>400) || (M166_F_W_L_HR(ii,1)<40)
                         M166_F_W_L_HRCens(ii,1) = M166_F_W_L_HR(ii-1,1);
                       else
                         M166_F_W_L_HRCens(ii,1) = M166_F_W_L_HR(ii,1);
                       end
                          ii= ii+1;
                   end
                   subplot(2,2,jj)
                   hold;
                   aero1 = line([0 0], [-100 100],'LineWidth',2,'Color','m');
                   hold on;
                   title(SubtitleHR(1,jj));
                   yyaxis left
                   b1 = bar([-3 -2 -1 0 1 2 3 4 5 6 7], M166ModClin,'y');
                   hold on;
                   M166ModCumFH = 32+(42-32).*(M166_F_W_L_CumFH./100);
                   pc1 = plot(M166_DPI, M166ModCumFH,'.r');
                   hold on;
                   pt1 = plot(M166_DPI, M166_F_W_L_T_MeanCens,'.b');
                   hold on;
                   line([-6 30], [M166_ARIMA(1,1) M166_ARIMA(1,1)],'LineWidth',1);
                   hold on;
                   line([-6 30], [M166_ARIMA(1,2) M166_ARIMA(1,2)],'LineWidth',0.5);
                   hold on;
                   line([-6 30], [M166_ARIMA(1,3) M166_ARIMA(1,3)],'LineWidth',1);
                   hold on;
                   xlim([-3 7]);
                   ylim([32 42]);
                   xlabel ('DPI(d)');
                   ylabel ('Temperature (^oC)','Color','b');
                   hold;
                   yyaxis right
                   phr1= plot(M166_DPI, M166_F_W_L_HRCens,'.c');
                   ylim([0 400]);
                   ylabel ('HR (bpm)','Color','c');
                   hold;
                   subplotobj = subplot(2,2,jj,'Parent',HHR);
                set(subplotobj,'XColor',[0 0 0],'YColor',[0 1 1],'ZColor',[0 0 0]);

                case 2
```

```
    M167_F_W_L_T_HRCens = [];
    ii = 1;
    while ii < length(M167_DPI')+1
        if (M167_F_W_L_HR(ii,1)>400) || (M167_F_W_L_HR(ii,1)<40)
          M167_F_W_L_HRCens(ii,1) = NaN;
        else
          M167_F_W_L_HRCens(ii,1) = M167_F_W_L_HR(ii,1);
        end
           ii= ii+1;
    end
    subplot(2,2,jj)
    hold;
    aero2 = line([0 0], [-100 100],'LineWidth',2,'Color','m');
    hold on;
    title(SubtitleHR(1,jj));
    yyaxis left
    b2 = bar([-3 -2 -1 0 1 2 3 4 5 6 7], M167ModClin,'y');
    hold on;
    M167ModCumFH = 32+(42-32).*(M167_F_W_L_CumFH./100);
    pc2 = plot(M167_DPI, M167ModCumFH,'.r');
    hold on;
    pt2 = plot(M167_DPI, M167_F_W_L_T_MeanCens,'.b');
    hold on;
    line([-6 30], [M167_ARIMA(1,1) M167_ARIMA(1,1)],'LineWidth',1);
    hold on;
    line([-6 30], [M167_ARIMA(1,2) M167_ARIMA(1,2)],'LineWidth',0.5);
    hold on;
    line([-6 30], [M167_ARIMA(1,3) M167_ARIMA(1,3)],'LineWidth',1);
    hold on;
    xlim([-3 7]);
    ylim([32 42]);
    xlabel ('DPI(d)');
    ylabel ('Temperature (^oC)','Color','b');
    hold;
    yyaxis right
    phr2= plot(M167_DPI, M167_F_W_L_HRCens,'.c');
    ylim([0 400]);
    ylabel ('HR (bpm)','Color','c');
    hold;
    subplotobj = subplot(2,2,jj,'Parent',HHR);
set(subplotobj,'XColor',[0 0 0],'YColor',[0 1 1],'ZColor',[0 0 0]);

case 3
    M168_F_W_L_T_HRCens = [];
    ii = 1;
    while ii < length(M168_DPI')+1
        if (M168_F_W_L_HR(ii,1)>400) || (M168_F_W_L_HR(ii,1)<40)
          M168_F_W_L_HRCens(ii,1) = M168_F_W_L_HR(ii-1,1);
        else
          M168_F_W_L_HRCens(ii,1) = M168_F_W_L_HR(ii,1);
        end
           ii= ii+1;
    end
     subplot(2,2,jj)
    hold;
    aero3 = line([0 0], [-100 100],'LineWidth',2,'Color','m');
    hold on;
    title(SubtitleHR(1,jj));
    yyaxis left
    b3 =  bar([-3 -2 -1 0 1 2 3 4 5 6 7], M168ModClin,'y');
    hold on;
    M168ModCumFH = 32+(42-32).*(M168_F_W_L_CumFH./100);
    pc3 = plot(M168_DPI, M168ModCumFH,'.r');
    hold on;
    pt3 = plot(M168_DPI, M168_F_W_L_T_MeanCens,'.b');
    hold on;
    line([-6 30], [M168_ARIMA(1,1) M168_ARIMA(1,1)],'LineWidth',1);
    hold on;
    line([-6 30], [M168_ARIMA(1,2) M168_ARIMA(1,2)],'LineWidth',0.5);
    hold on;
    line([-6 30], [M168_ARIMA(1,3) M168_ARIMA(1,3)],'LineWidth',1);
    hold on;
    xlim([-3 7]);
    ylim([32 42]);
    xlabel ('DPI(d)');
```

```
                    ylabel ('Temperature (^oC)','Color','b');
                    hold;
                    yyaxis right
                    phr3= plot(M168_DPI, M168_F_W_L_HRCens,'.c');
                    ylim([0 400]);
                    ylabel ('HR (bpm)','Color','c');
                    hold;
                    subplotobj = subplot(2,2,jj,'Parent',HHR);
                set(subplotobj,'XColor',[0 0 0],'YColor',[0 1 1],'ZColor',[0 0 0]);

                case 4
                    M169_F_W_D_T_HRCens = [];
                    ii = 1;
                    while ii < length(M169_DPI')+1
                        if (M169_F_W_D_HR(ii,1)>400) || (M169_F_W_D_HR(ii,1)<40)
                          M169_F_W_D_HRCens(ii,1) = M169_F_W_D_HR(ii-1,1);
                        else
                          M169_F_W_D_HRCens(ii,1) = M169_F_W_D_HR(ii,1);
                        end
                           ii= ii+1;
                    end
                     subplot(2,2,jj)
                    hold;
                    aero4 = line([0 0], [-100 100],'LineWidth',2,'Color','m');
                    hold on;
                    title(SubtitleHR(1,jj));
                    yyaxis left
                    b4 =  bar([-3 -2 -1 0 1 2 3 4 5 6 7], M169ModClin,'y');
                    hold on;
                     M169ModCumFH = 32+(42-32).*(M169_F_W_D_CumFH./100);
                    pc3 = plot(M169_DPI, M169ModCumFH,'.r');
                    hold on;
                    pt4 = plot(M169_DPI, M169_F_W_D_T_MeanCens,'.b');
                    hold on;
                    line([-6 30], [M169_ARIMA(1,1) M169_ARIMA(1,1)],'LineWidth',1);
                    hold on;
                    line([-6 30], [M169_ARIMA(1,2) M169_ARIMA(1,2)],'LineWidth',0.5);
                    hold on;
                    line([-6 30], [M169_ARIMA(1,3) M169_ARIMA(1,3)],'LineWidth',1);
                    hold on;
                    xlim([-3 7]);legend([pt1 pc1 phr1 b1 aero1], {'Temperature (^oC)', 'Cumulative Fever-Hours (h)', 'Heart Rate (bpm)', 'Clinical
Score', 'Aerosol Challenge'}); %legend
                    ylim([32 42]);
                    xlabel ('DPI(d)');
                    ylabel ('Temperature (^oC)','Color','b');
                    hold;
                    yyaxis right
                    phr4= plot(M169_DPI, M169_F_W_D_HRCens,'.c');
                    ylim([0 400]);
                    ylabel ('HR (bpm)','Color','c');
                    hold;
                    subplotobj = subplot(2,2,jj,'Parent',HHR);
                set(subplotobj,'XColor',[0 0 0],'YColor',[0 1 1],'ZColor',[0 0 0]);
            end
            jj=jj+1;
        end

          mtit(HHR,'WEEV Heart Rate Profiles'); %overtitle
        legend([pt1 pc1 phr1 b1 aero1], {'Temperature (^oC)', 'Cumulative Fever-Hours (h)', 'Heart Rate (bpm)', 'Clinical Score', 'Aerosol
Challenge'}); %legend

        disp('HR-done')
        %%unfold
        end
```

SD

```
%HRSD - Heart Rate
        for i=1:1
        disp('HRSD-Run');
        SubtitleHRSD = {'M166-16', 'M167-16','M168-16','M169-16'};
        figure(28)
        HHRSD = gcf;
        hold on;

        jj = 1;
        while jj<5
           switch jj
                case 1
                   M166_F_W_L_HRSDCens = [];
                   ii = 1;
                   while ii < length(M166_DPI')+1
                       if (M166_F_W_L_HRSD(ii,1)>400) || (M166_F_W_L_HRSD(ii,1)<0)
                         M166_F_W_L_HRSDCens(ii,1) = M166_F_W_L_HRSD(ii-1,1);
                       else
                         M166_F_W_L_HRSDCens(ii,1) = M166_F_W_L_HRSD(ii,1);
                       end
                          ii= ii+1;
                   end
                   subplot(2,2,jj)
                   hold;
                   aero1 = line([0 0], [-100 100],'LineWidth',2,'Color','m');
                   hold on;
                   title(SubtitleHRSD(1,jj));
                   yyaxis left
                    b1 = bar([-3 -2 -1 0 1 2 3 4 5 6 7], M166ModClin,'y');
                   hold on;
                   M166ModCumFH = 32+(42-32).*(M166_F_W_L_CumFH./100);
                   pc1 = plot(M166_DPI, M166ModCumFH,'.r');
                   hold on;
                   pt1 = plot(M166_DPI, M166_F_W_L_T_MeanCens,'.b');
                   hold on;
                   line([-6 30], [M166_ARIMA(1,1) M166_ARIMA(1,1)],'LineWidth',1);
                   hold on;
                   line([-6 30], [M166_ARIMA(1,2) M166_ARIMA(1,2)],'LineWidth',0.5);
                   hold on;
                   line([-6 30], [M166_ARIMA(1,3) M166_ARIMA(1,3)],'LineWidth',1);
                   hold on;
                   xlim([-3 7]);
                   ylim([32 42]);
                   xlabel ('DPI(d)');
                   ylabel ('Temperature (^oC)','Color','b');
                   hold;
                   yyaxis right
                   phr1= plot(M166_DPI, M166_F_W_L_HRSDCens,'.c');
                   ylim([0 50]);
                   ylabel ('HRSD (bpm)','Color','c');
                   hold;
                   subplotobj = subplot(2,2,jj,'Parent',HHRSD);
                set(subplotobj,'XColor',[0 0 0],'YColor',[0 1 1],'ZColor',[0 0 0]);

                case 2
                   M167_F_W_L_T_HRSDCens = [];
                   ii = 1;
                   while ii < length(M167_DPI')+1
                       if (M167_F_W_L_HRSD(ii,1)>400) || (M167_F_W_L_HRSD(ii,1)<0)
                         M167_F_W_L_HRSDCens(ii,1) = M167_F_W_L_HRSD(ii-1,1);
                       else
                         M167_F_W_L_HRSDCens(ii,1) = M167_F_W_L_HRSD(ii,1);
                       end
                          ii= ii+1;
                   end
                   subplot(2,2,jj)
                   hold;
                   aero2 = line([0 0], [-100 100],'LineWidth',2,'Color','m');
```

```
    hold on;
    title(SubtitleHRSD(1,jj));
    yyaxis left
      b2 = bar([-3 -2 -1 0 1 2 3 4 5 6 7], M167ModClin,'y');
    hold on;
    M167ModCumFH = 32+(42-32).*(M167_F_W_L_CumFH./100);
    pc2 = plot(M167_DPI, M167ModCumFH,'.r');
    hold on;
    pt2 = plot(M167_DPI, M167_F_W_L_T_MeanCens,'.b');
    hold on;
    line([-6 30], [M167_ARIMA(1,1) M167_ARIMA(1,1)],'LineWidth',1);
    hold on;
    line([-6 30], [M167_ARIMA(1,2) M167_ARIMA(1,2)],'LineWidth',0.5);
    hold on;
    line([-6 30], [M167_ARIMA(1,3) M167_ARIMA(1,3)],'LineWidth',1);
    hold on;
    xlim([-3 7]);
    ylim([32 42]);
    xlabel ('DPI(d)');
    ylabel ('Temperature (^oC)','Color','b');
    hold;
    yyaxis right
    phr2= plot(M167_DPI, M167_F_W_L_HRSDCens,'.c');
    ylim([0 50]);
    ylabel ('HRSD (bpm)','Color','c');
    hold;
    subplotobj = subplot(2,2,jj,'Parent',HHRSD);
set(subplotobj,'XColor',[0 0 0],'YColor',[0 1 1],'ZColor',[0 0 0]);

case 3
    M168_F_W_L_T_HRSDCens = [];
    ii = 1;
    while ii < length(M168_DPI')+1
        if (M168_F_W_L_HRSD(ii,1)>400) || (M168_F_W_L_HRSD(ii,1)<0)
          M168_F_W_L_HRSDCens(ii,1) = M168_F_W_L_HRSD(ii-1,1);
        else
          M168_F_W_L_HRSDCens(ii,1) = M168_F_W_L_HRSD(ii,1);
        end
           ii= ii+1;
    end
     subplot(2,2,jj)
    hold;
    aero3 = line([0 0], [-100 100],'LineWidth',2,'Color','m');
    hold on;
    title(SubtitleHRSD(1,jj));
    yyaxis left
     M168ModCumFH = 32+(42-32).*(M168_F_W_L_CumFH./100);
    pc3 = plot(M168_DPI, M168ModCumFH,'.r');
    hold on;
    pt3 = plot(M168_DPI, M168_F_W_L_T_MeanCens,'.b');
    hold on;
    line([-6 30], [M168_ARIMA(1,1) M168_ARIMA(1,1)],'LineWidth',1);
    hold on;
    line([-6 30], [M168_ARIMA(1,2) M168_ARIMA(1,2)],'LineWidth',0.5);
    hold on;
    line([-6 30], [M168_ARIMA(1,3) M168_ARIMA(1,3)],'LineWidth',1);
    hold on;
    xlim([-3 7]);
    ylim([32 42]);
    xlabel ('DPI(d)');
    ylabel ('Temperature (^oC)','Color','b');
    hold;
    yyaxis right
    phr3= plot(M168_DPI, M168_F_W_L_HRSDCens,'.c');
    ylim([0 50]);
    ylabel ('HRSD (bpm)','Color','c');
    hold;
    subplotobj = subplot(2,2,jj,'Parent',HHRSD);
set(subplotobj,'XColor',[0 0 0],'YColor',[0 1 1],'ZColor',[0 0 0]);

case 4
    M169_F_W_D_T_HRSDCens = [];
    ii = 1;
    while ii < length(M169_DPI')+1
        if (M169_F_W_D_HRSD(ii,1)>400) || (M169_F_W_D_HRSD(ii,1)<0)
```

```
                M169_F_W_D_HRSDCens(ii,1) = M169_F_W_D_HRSD(ii-1,1);
            else
                M169_F_W_D_HRSDCens(ii,1) = M169_F_W_D_HRSD(ii,1);
            end
                ii= ii+1;
        end
         subplot(2,2,jj)
        hold;
        aero4 = line([0 0], [-100 100],'LineWidth',2,'Color','m');
        hold on;
        title(SubtitleHRSD(1,jj));
        yyaxis left
         M169ModCumFH = 32+(42-32).*(M169_F_W_D_CumFH./100);
        pc3 = plot(M169_DPI, M169ModCumFH,'.r');
        hold on;
        pt4 = plot(M169_DPI, M169_F_W_D_T_MeanCens,'.b');
        hold on;
        line([-6 30], [M169_ARIMA(1,1) M169_ARIMA(1,1)],'LineWidth',1);
        hold on;
        line([-6 30], [M169_ARIMA(1,2) M169_ARIMA(1,2)],'LineWidth',0.5);
        hold on;
        line([-6 30], [M169_ARIMA(1,3) M169_ARIMA(1,3)],'LineWidth',1);
        hold on;
        xlim([-3 7]);
        ylim([32 42]);
        xlabel ('DPI(d)');
        ylabel ('Temperature (^oC)','Color','b');
        hold;
        yyaxis right
        phr4= plot(M169_DPI, M169_F_W_D_HRSDCens,'.c');
        ylim([0 50]);
        ylabel ('HRSD (bpm)','Color','c');
        hold;
        subplotobj = subplot(2,2,jj,'Parent',HHRSD);
      set(subplotobj,'XColor',[0 0 0],'YColor',[0 1 1],'ZColor',[0 0 0]);
    end
    jj=jj+1;
end

  mtit(HHRSD,'WEEV Heart Rate SD Profiles'); %overtitle
legend([pt1 pc1 phr1 aero1], {'Temperature (^oC)', 'Cumulative Fever-Hours (h)', 'HR-SD (bpm)', 'Aerosol Challenge'}); %legend

disp('HRSD-done')
%%unfold
end
```

B.2 STATISTICAL ANALYSIS AUTOMATION

Case: M166-16, M167-16, M168-16, M169-16

```
%A - M166-16 - rows; see doc.
   A = {M166_ARIMA; M166_DPI; M166_F_W_L_BAD; M166_F_W_L_BADCens; M166_F_W_L_BADSD; M166_F_W_L_CumFH;
M166_F_W_L_CumFHCens; M166_F_W_L_EQTM; M166_F_W_L_EQTMce; M166_F_W_L_EQTMCens; M166_F_W_L_EQTMceSD;
M166_F_W_L_EQTMcs; M166_F_W_L_EQTMcsSD; M166_F_W_L_EQTMSD; M166_F_W_L_EQTS; M166_F_W_L_EQTSc;
M166_F_W_L_EQTScSD; M166_F_W_L_EQTSSD; M166_F_W_L_GW; M166_F_W_L_GWSD; M166_F_W_L_HR;
M166_F_W_L_HRCens; M166_F_W_L_HRSD; M166_F_W_L_Match; M166_F_W_L_MatchSD; M166_F_W_L_MxdV;
M166_F_W_L_MxdVCens; M166_F_W_L_MxdVSD; M166_F_W_L_Noise; M166_F_W_L_NoiseCens; M166_F_W_L_NoiseSD;
M166_F_W_L_Num; M166_F_W_L_NumSD; M166_F_W_L_PCt; M166_F_W_L_PCtSD; M166_F_W_L_PH; M166_F_W_L_PHSD;
M166_F_W_L_PMatch; M166_F_W_L_PMatchSD; M166_F_W_L_PRI; M166_F_W_L_PRISD; M166_F_W_L_PWdth;
M166_F_W_L_PWdthSD; M166_F_W_L_QAT; M166_F_W_L_QATN; M166_F_W_L_QATNSD; M166_F_W_L_QATSD;
M166_F_W_L_QMatch; M166_F_W_L_QMatchSD; M166_F_W_L_QRI; M166_F_W_L_QRISD; M166_F_W_L_QRS;
M166_F_W_L_QRSA; M166_F_W_L_QRSASD; M166_F_W_L_QRSSD; M166_F_W_L_QTcb; M166_F_W_L_QTcbSD;
M166_F_W_L_QTcf; M166_F_W_L_QTcfSD; M166_F_W_L_QTck; M166_F_W_L_QTckSD; M166_F_W_L_QTcm;
M166_F_W_L_QTcmSD; M166_F_W_L_QTCt; M166_F_W_L_QTCtSD; M166_F_W_L_QTcv; M166_F_W_L_QTcvSD;
M166_F_W_L_QTD; M166_F_W_L_QTDSD; M166_F_W_L_QTI; M166_F_W_L_QTISD; M166_F_W_L_QTMc; M166_F_W_L_QTMcSD;
```

```
M166_F_W_L_RH; M166_F_W_L_RHSD; M166_F_W_L_RRI; M166_F_W_L_RRISD; M166_F_W_L_SMatch; M166_F_W_L_SMatchSD;
M166_F_W_L_STE; M166_F_W_L_STESD; M166_F_W_L_STI; M166_F_W_L_STISD; M166_F_W_L_T_Area;
M166_F_W_L_T_AreaSD;  M166_F_W_L_T_Mean; M166_F_W_L_T_MeanCens; M166_F_W_L_T_MeanSD;  M166_F_W_L_TCt;
M166_F_W_L_TCtSD; M166_F_W_L_TH; M166_F_W_L_THN; M166_F_W_L_THNSD; M166_F_W_L_THSD; M166_F_W_L_TMatch;
M166_F_W_L_TMatchSD; M166_F_W_L_TP; M166_F_W_L_TpeI; M166_F_W_L_TpeISD; M166_F_W_L_TPSD; M166_F_W_L_TW;
M166_F_W_L_TWSD; M166ModCumFH};
   %B - M167-16 - rows; see doc.
   B = {M167_ARIMA; M167_DPI; M167_F_W_L_BAD; M167_F_W_L_BADCens; M167_F_W_L_BADSD; M167_F_W_L_CumFH;
M167_F_W_L_CumFHCens; M167_F_W_L_EQTM; M167_F_W_L_EQTMce; M167_F_W_L_EQTMCens; M167_F_W_L_EQTMceSD;
M167_F_W_L_EQTMcs; M167_F_W_L_EQTMcsSD; M167_F_W_L_EQTMSD; M167_F_W_L_EQTS; M167_F_W_L_EQTSc;
M167_F_W_L_EQTScSD; M167_F_W_L_EQTSSD; M167_F_W_L_GW; M167_F_W_L_GWSD; M167_F_W_L_HR;
M167_F_W_L_HRCens; M167_F_W_L_HRSD; M167_F_W_L_Match; M167_F_W_L_MatchSD; M167_F_W_L_MxdV;
M167_F_W_L_MxdVCens; M167_F_W_L_MxdVSD; M167_F_W_L_Noise; M167_F_W_L_NoiseCens; M167_F_W_L_NoiseSD;
M167_F_W_L_Num; M167_F_W_L_NumSD; M167_F_W_L_PCt; M167_F_W_L_PCtSD; M167_F_W_L_PH; M167_F_W_L_PHSD;
M167_F_W_L_PMatch; M167_F_W_L_PMatchSD; M167_F_W_L_PRI; M167_F_W_L_PRISD; M167_F_W_L_PWdth;
M167_F_W_L_PWdthSD; M167_F_W_L_QAT; M167_F_W_L_QATN; M167_F_W_L_QATNSD; M167_F_W_L_QATSD;
M167_F_W_L_QMatch; M167_F_W_L_QMatchSD; M167_F_W_L_QRI; M167_F_W_L_QRISD; M167_F_W_L_QRS;
M167_F_W_L_QRSA; M167_F_W_L_QRSASD; M167_F_W_L_QRSSD; M167_F_W_L_QTcb; M167_F_W_L_QTcbSD;
M167_F_W_L_QTcf; M167_F_W_L_QTcfSD; M167_F_W_L_QTck; M167_F_W_L_QTckSD; M167_F_W_L_QTcm;
M167_F_W_L_QTcmSD; M167_F_W_L_QTCt; M167_F_W_L_QTCtSD; M167_F_W_L_QTcv; M167_F_W_L_QTcvSD;
M167_F_W_L_QTD; M167_F_W_L_QTDSD; M167_F_W_L_QTI;  M167_F_W_L_QTISD; M167_F_W_L_QTMc; M167_F_W_L_QTMcSD;
M167_F_W_L_RH; M167_F_W_L_RHSD; M167_F_W_L_RRI; M167_F_W_L_RRISD; M167_F_W_L_SMatch; M167_F_W_L_SMatchSD;
M167_F_W_L_STE; M167_F_W_L_STESD; M167_F_W_L_STI; M167_F_W_L_STISD; M167_F_W_L_T_Area;
M167_F_W_L_T_AreaSD;  M167_F_W_L_T_Mean; M167_F_W_L_T_MeanCens; M167_F_W_L_T_MeanSD; M167_F_W_L_TCt;
M167_F_W_L_TCtSD; M167_F_W_L_TH; M167_F_W_L_THN; M167_F_W_L_THNSD; M167_F_W_L_THSD; M167_F_W_L_TMatch;
M167_F_W_L_TMatchSD; M167_F_W_L_TP; M167_F_W_L_TpeI; M167_F_W_L_TpeISD; M167_F_W_L_TPSD; M167_F_W_L_TW;
M167_F_W_L_TWSD; M167ModCumFH};
   %C - M168-16 - rows; see doc.
   C = {M168_ARIMA; M168_DPI; M168_F_W_L_BAD; M168_F_W_L_BADCens; M168_F_W_L_BADSD; M168_F_W_L_CumFH;
M168_F_W_L_CumFHCens; M168_F_W_L_EQTM; M168_F_W_L_EQTMce; M168_F_W_L_EQTMCens; M168_F_W_L_EQTMceSD;
M168_F_W_L_EQTMcs; M168_F_W_L_EQTMcsSD; M168_F_W_L_EQTMSD; M168_F_W_L_EQTS; M168_F_W_L_EQTSc;
M168_F_W_L_EQTScSD; M168_F_W_L_EQTSSD; M168_F_W_L_GW; M168_F_W_L_GWSD; M168_F_W_L_HR;
M168_F_W_L_HRCens; M168_F_W_L_HRSD; M168_F_W_L_Match; M168_F_W_L_MatchSD; M168_F_W_L_MxdV;
M168_F_W_L_MxdVCens; M168_F_W_L_MxdVSD; M168_F_W_L_Noise; M168_F_W_L_NoiseCens; M168_F_W_L_NoiseSD;
M168_F_W_L_Num; M168_F_W_L_NumSD; M168_F_W_L_PCt; M168_F_W_L_PCtSD; M168_F_W_L_PH; M168_F_W_L_PHSD;
M168_F_W_L_PMatch; M168_F_W_L_PMatchSD; M168_F_W_L_PRI; M168_F_W_L_PRISD; M168_F_W_L_PWdth;
M168_F_W_L_PWdthSD; M168_F_W_L_QAT; M168_F_W_L_QATN; M168_F_W_L_QATNSD; M168_F_W_L_QATSD;
M168_F_W_L_QMatch; M168_F_W_L_QMatchSD; M168_F_W_L_QRI; M168_F_W_L_QRISD; M168_F_W_L_QRS;
M168_F_W_L_QRSA; M168_F_W_L_QRSASD; M168_F_W_L_QRSSD; M168_F_W_L_QTcb; M168_F_W_L_QTcbSD;
M168_F_W_L_QTcf; M168_F_W_L_QTcfSD; M168_F_W_L_QTck; M168_F_W_L_QTckSD; M168_F_W_L_QTcm;
M168_F_W_L_QTcmSD; M168_F_W_L_QTCt; M168_F_W_L_QTCtSD; M168_F_W_L_QTcv; M168_F_W_L_QTcvSD;
M168_F_W_L_QTD; M168_F_W_L_QTDSD; M168_F_W_L_QTI; M168_F_W_L_QTISD; M168_F_W_L_QTMc; M168_F_W_L_QTMcSD;
M168_F_W_L_RH; M168_F_W_L_RHSD; M168_F_W_L_RRI; M168_F_W_L_RRISD; M168_F_W_L_SMatch; M168_F_W_L_SMatchSD;
M168_F_W_L_STE; M168_F_W_L_STESD; M168_F_W_L_STI; M168_F_W_L_STISD; M168_F_W_L_T_Area; M168_F_W_L_T_AreaSD;
M168_F_W_L_T_Mean; M168_F_W_L_T_MeanCens; M168_F_W_L_T_MeanSD;  M168_F_W_L_TCt; M168_F_W_L_TCtSD;
M168_F_W_L_TH; M168_F_W_L_THN; M168_F_W_L_THNSD; M168_F_W_L_THSD; M168_F_W_L_TMatch; M168_F_W_L_TMatchSD;
M168_F_W_L_TP; M168_F_W_L_TpeI; M168_F_W_L_TpeISD; M168_F_W_L_TPSD; M168_F_W_L_TW; M168_F_W_L_TWSD;
M168ModCumFH};
   %C - M168-16 - rows; see doc.
   D = {M169_ARIMA; M169_DPI; M169_F_W_D_BAD; M169_F_W_D_BADCens; M169_F_W_D_BADSD; M169_F_W_D_CumFH;
M169_F_W_D_CumFHCens; M169_F_W_D_EQTM; M169_F_W_D_EQTMce; M169_F_W_D_EQTMCens; M169_F_W_D_EQTMceSD;
M169_F_W_D_EQTMcs; M169_F_W_D_EQTMcsSD; M169_F_W_D_EQTMSD; M169_F_W_D_EQTS; M169_F_W_D_EQTSc;
M169_F_W_D_EQTScSD; M169_F_W_D_EQTSSD; M169_F_W_D_GW; M169_F_W_D_GWSD; M169_F_W_D_HR;
M169_F_W_D_HRCens; M169_F_W_D_HRSD; M169_F_W_D_Match; M169_F_W_D_MatchSD;  M169_F_W_D_MxdV;
M169_F_W_D_MxdVCens; M169_F_W_D_MxdVSD; M169_F_W_D_Noise; M169_F_W_D_NoiseCens; M169_F_W_D_NoiseSD;
M169_F_W_D_Num; M169_F_W_D_NumSD; M169_F_W_D_PCt; M169_F_W_D_PCtSD; M169_F_W_D_PH; M169_F_W_D_PHSD;
M169_F_W_D_PMatch; M169_F_W_D_PMatchSD; M169_F_W_D_PRI; M169_F_W_D_PRISD; M169_F_W_D_PWdth;
M169_F_W_D_PWdthSD; M169_F_W_D_QAT; M169_F_W_D_QATN; M169_F_W_D_QATNSD; M169_F_W_D_QATSD;
M169_F_W_D_QMatch; M169_F_W_D_QMatchSD; M169_F_W_D_QRI; M169_F_W_D_QRISD; M169_F_W_D_QRS;
M169_F_W_D_QRSA; M169_F_W_D_QRSASD; M169_F_W_D_QRSSD; M169_F_W_D_QTcb; M169_F_W_D_QTcbSD;
M169_F_W_D_QTcf; M169_F_W_D_QTcfSD; M169_F_W_D_QTck; M169_F_W_D_QTckSD; M169_F_W_D_QTcm;
M169_F_W_D_QTcmSD; M169_F_W_D_QTCt; M169_F_W_D_QTCtSD; M169_F_W_D_QTcv; M169_F_W_D_QTcvSD;
M169_F_W_D_QTD; M169_F_W_D_QTDSD; M169_F_W_D_QTI; M169_F_W_D_QTISD; M169_F_W_D_QTMc; M169_F_W_D_QTMcSD;
M169_F_W_D_RH; M169_F_W_D_RHSD; M169_F_W_D_RRI; M169_F_W_D_RRISD; M169_F_W_D_SMatch; M169_F_W_D_SMatchSD;
M169_F_W_D_STE; M169_F_W_D_STESD; M169_F_W_D_STI; M169_F_W_D_STISD; M169_F_W_D_T_Area;
M169_F_W_D_T_AreaSD;  M169_F_W_D_T_Mean; M169_F_W_D_T_MeanCens; M169_F_W_D_T_MeanSD;  M169_F_W_D_TCt;
M169_F_W_D_TCtSD; M169_F_W_D_TH; M169_F_W_D_THN; M169_F_W_D_THNSD; M169_F_W_D_THSD; M169_F_W_D_TMatch;
M169_F_W_D_TMatchSD; M169_F_W_D_TP; M169_F_W_D_TpeI; M169_F_W_D_TpeISD; M169_F_W_D_TPSD; M169_F_W_D_TW;
M169_F_W_D_TWSD; M169ModCumFH};

      %Period Generation
         %Days
         for i = 1:1
               disDPI_166 = [-3 -2 -1 0 1 2 3 4 5 6 7 8];
               realDPI_167 =[];
```

```
        indexGenericDayMat_166 = [];
        for i=1:1:length(disDPI_166)
        desDay = disDPI_166(i);
        tmp = abs(A{2}-desDay);
        [idx1 idxa] = min(tmp);
        indexGenericDayMat_166(i) = idxa;
        closest = A{2}(idxa);
        realDPI_167(i) = closest;
        end
       disDPI_167 = [-3 -2 -1 0 1 2 3 4 5 6 7 8];
       realDPI_167 =[];
       indexGenericDayMat_167 = [];
       for i=1:1:length(disDPI_167)
       desDay = disDPI_167(i);
       tmp = abs(B{2}-desDay);
       [idx1 idxb] = min(tmp);
       indexGenericDayMat_167(i) = idxb;
       closest = B{2}(idxb);
       realDPI_167(i) = closest;
       end
       disDPI_168 = [-3 -2 -1 0 1 2 3 4 5 6 7 8];
       realDPI_168 =[];
       indexGenericDayMat_168 = [];
       for i=1:1:length(disDPI_168)
       desDay = disDPI_168(i);
       tmp = abs(C{2}-desDay);
       [idx1 idxc] = min(tmp);
       indexGenericDayMat_168(i) = idxc;
       closest = C{2}(idxc);
       realDPI_168(i) = closest;
       end
       disDPI_169 = [-3 -2 -1 0 1 2 3 4 5 6 7 8];
       realDPI_169 =[];
       indexGenericDayMat_169 = [];
       for i=1:1:length(disDPI_169)
       desDay = disDPI_169(i);
       tmp = abs(D{2}-desDay);
       [idx1 idxd] = min(tmp);
       indexGenericDayMat_169(i) = idxd;
       closest = D{2}(idxd);
       realDPI_169(i) = closest;
       end
end
%Periods
kk = 1;
while kk<5
switch kk
   case 1
       disPre_166 = [-3 -2 -1];
         Pre166 = M166_DPI(indexGenericDayMat_166(1):indexGenericDayMat_166(3));
       disPost_166 = [0 1 2 3 4 5 6 7 8];
         Post166 = M166_DPI(indexGenericDayMat_166(3):indexGenericDayMat_166(12));
   case 2
       disPre_167 = [-3 -2 -1];
         Pre167 = M167_DPI(indexGenericDayMat_167(1):indexGenericDayMat_167(3));
       disPost_167 = [0 1 2 3 4 5 6 7 8];
         Post167 = M167_DPI(indexGenericDayMat_167(3)+1:indexGenericDayMat_167(12));
   case 3
       disPre_168 = [-3 -2 -1];
         Pre168 = M168_DPI(indexGenericDayMat_168(1):indexGenericDayMat_168(3));
       disPost_168 = [0 1 2 3 4 5 6 7 8];
         Post168 = M168_DPI(indexGenericDayMat_168(3)+1:indexGenericDayMat_168(12));
   case 4
       disPre_169 = [-3 -2 -1];
         Pre169 = M169_DPI(indexGenericDayMat_169(1):indexGenericDayMat_169(3));
       disPost_169 = [0 1 2];
         Post169 = M169_DPI(indexGenericDayMat_169(3)+1:indexGenericDayMat_169(6));
       disFeb_169 = [3 4 5 6 7 8];
         Feb169 = M169_DPI(indexGenericDayMat_169(6)+1:indexGenericDayMat_169(12));
end
kk = kk+1;
end
```

B.2.1 One Way ANOVA and T-Tests

Case: Heart Rate, M166-16, M168-16, M169-16

```
%values,means,stdev
            for i=1:1
            HR_166_DPIly = zeros(length(indexGenericDayMat_166)-1,3);
            for i=1:1:length(indexGenericDayMat_166)-1
              HR_166_DPIly(i,1) = mean(M166_F_W_L_HRCens(indexGenericDayMat_166(i):indexGenericDayMat_166(i+1)));
              HR_166_DPIly(i,2) = std(M166_F_W_L_HRCens(indexGenericDayMat_166(i):indexGenericDayMat_166(i+1)));
              HR_166_DPIly(i,3) =  indexGenericDayMat_166(i+1)-indexGenericDayMat_166(i);
            end
            HR_167_DPIly = zeros(length(indexGenericDayMat_167)-1,3);
            for i=1:1:length(indexGenericDayMat_167)-1
              HR_167_DPIly(i,1) = mean(M167_F_W_L_HRCens(indexGenericDayMat_167(i):indexGenericDayMat_167(i+1)));
              HR_167_DPIly(i,2) = std(M167_F_W_L_HRCens(indexGenericDayMat_167(i):indexGenericDayMat_167(i+1)));
              HR_167_DPIly(i,3) =  indexGenericDayMat_167(i+1)-indexGenericDayMat_167(i);
            end
            HR_168_DPIly = zeros(length(indexGenericDayMat_168)-1,3);
            for i=1:1:length(indexGenericDayMat_168)-1
              HR_168_DPIly(i,1) = mean(M168_F_W_L_HRCens(indexGenericDayMat_168(i):indexGenericDayMat_168(i+1)));
              HR_168_DPIly(i,2) = std(M168_F_W_L_HRCens(indexGenericDayMat_168(i):indexGenericDayMat_168(i+1)));
              HR_168_DPIly(i,3) =  indexGenericDayMat_168(i+1)-indexGenericDayMat_168(i);
            end
             HR_169_DPIly = zeros(length(indexGenericDayMat_169)-1,3);
            for i=1:1:length(indexGenericDayMat_169)-1
              HR_169_DPIly(i,1) = mean(M169_F_W_D_HRCens(indexGenericDayMat_169(i):indexGenericDayMat_169(i+1)));
              HR_169_DPIly(i,2) = std(M169_F_W_D_HRCens(indexGenericDayMat_169(i):indexGenericDayMat_169(i+1)));
              HR_169_DPIly(i,3) =  indexGenericDayMat_169(i+1)-indexGenericDayMat_169(i);
            end
            %values
            HR_DPIlyMaster = [HR_166_DPIly(:,1), HR_167_DPIly(:,1), HR_168_DPIly(:,1), HR_169_DPIly(:,1)];
            HR_166 = {};
            for i=1:1:length(indexGenericDayMat_166)-1
              HR_166{i} = (M166_F_W_L_HRCens(indexGenericDayMat_166(i):15:indexGenericDayMat_166(i+1)));
            end
            HR_167 = {};
            for i=1:1:length(indexGenericDayMat_167)-1
              HR_167{i} = (M167_F_W_L_HRCens(indexGenericDayMat_167(i):15:indexGenericDayMat_167(i+1)));
            end
              HR_168 = {};
            for i=1:1:length(indexGenericDayMat_168)-1
              HR_168{i} = (M166_F_W_L_HRCens(indexGenericDayMat_168(i):15:indexGenericDayMat_168(i+1)));
            end
            HR_169 = {};
            for i=1:1:length(indexGenericDayMat_169)-1
              HR_169{i} = (M169_F_W_D_HRCens(indexGenericDayMat_169(i):indexGenericDayMat_169(i+1)));
            end
          end
            %per-diem-analysis-ANOVA
            for i=1:1

            for  i = 1:1:11
            transpose = HR_166{1,i}';
            padHR166 = 5000-length(HR_166{1,i});
            NaNHR166 = NaN(1,padHR166);
            transpose = [transpose NaNHR166];
            HR_166{1,i} = transpose';
            i = i+1;
            end
            HR166 = [HR_166{1,1}, HR_166{1,2}, HR_166{1,3}, HR_166{1,4}, HR_166{1,5}, HR_166{1,6}, HR_166{1,7}, HR_166{1,8},
HR_166{1,9}, HR_166{1,10}, HR_166{1,11}];
            Time166 = disDPI_166(1:11)';
            [pHR166 tblHR166 statsHR166] = anova1(HR166)
            statsHR166.gnames = ['-3dpi'; '-2dpi'; '-1dpi'; '-0dpi'; '+1dpi'; '+2dpi'; '+3dpi'; '+4dpi'; '+5dpi'; '+6dpi'; '+7dpi'];
            multcompare(statsHR166);
            title('M166 HR DPI Pairwise Comparisons')

            for  i = 1:1:11
```

```
transpose = HR_168{1,i}';
padHR168 = 5000-length(HR_168{1,i});
NaNHR168 = NaN(1,padHR168);
transpose = [transpose NaNHR168];
HR_168{1,i} = transpose';
i = i+1;
end
HR168 = [HR_168{1,1}, HR_168{1,2}, HR_168{1,3}, HR_168{1,4}, HR_168{1,5}, HR_168{1,6}, HR_168{1,7}, HR_168{1,8},
HR_168{1,9}, HR_168{1,10}, HR_168{1,11}];
Time168 = disDPI_168(1:11)';
[pHR168 tblHR168 statsHR168] = anova1(HR168)
statsHR168.gnames = ['-3dpi'; '-2dpi'; '-1dpi'; '-0dpi'; '+1dpi'; '+2dpi'; '+3dpi'; '+4dpi'; '+5dpi'; '+6dpi'; '+7dpi'];
multcompare(statsHR168);
title('M168 HR DPI Pairwise Comparisons')

for  i = 1:1:11
transpose = HR_169{1,i}';
padHR169 = 5000-length(HR_169{1,i});
NaNHR169 = NaN(1,padHR169);
transpose = [transpose NaNHR169];
HR_169{1,i} = transpose';
i = i+1;
end
HR169 = [HR_169{1,1}, HR_169{1,2}, HR_169{1,3}, HR_169{1,4}, HR_169{1,5}, HR_169{1,6}, HR_169{1,7}, HR_169{1,8},
HR_169{1,9}, HR_169{1,10}, HR_169{1,11}];
Time169 = disDPI_169(1:11)';
[pHR169 tblHR169 statsHR169] = anova1(HR169)
statsHR169.gnames = ['-3dpi'; '-2dpi'; '-1dpi'; '-0dpi'; '+1dpi'; '+2dpi'; '+3dpi'; '+4dpi'; '+5dpi'; '+6dpi'; '+7dpi'];
multcompare(statsHR169);
title('M169 HR DPI Pairwise Comparisons')

PreHRper166 = M166_F_W_L_HRCens(indexGenericDayMat_166(1):15:indexGenericDayMat_166(3));
    PostHRper166 = M166_F_W_L_HRCens(indexGenericDayMat_166(3)+1:15:indexGenericDayMat_166(12));
    [hHRper166,pHRper166,ciHRper166,statsHRper166] = ttest2(PreHRper166,PostHRper166)

    PreHRper168 = M168_F_W_L_HRCens(indexGenericDayMat_168(1):15:indexGenericDayMat_168(3));
    PostHRper168 = M168_F_W_L_HRCens(indexGenericDayMat_168(3)+1:15:indexGenericDayMat_168(12));
    [hHRper168,pHRper168,ciHRper168,statsHRper168] = ttest2(PreHRper168,PostHRper168)

    PreHRper169 = M169_F_W_D_HRCens(indexGenericDayMat_169(1):15:indexGenericDayMat_169(3));
    PostHRper169 = M169_F_W_D_HRCens(indexGenericDayMat_169(3)+1:15:indexGenericDayMat_169(6));
    FebHRper169 = M169_F_W_D_HRCens(indexGenericDayMat_169(6)+1:15:indexGenericDayMat_169(12));

        transpose = PreHRper169';
        padHR169 = 500-length(PreHRper169);
        NaNHR169 = NaN(1,padHR169);
        transpose = [transpose NaNHR169];
        PreHRper169 = transpose';
        transpose = PostHRper169';
        padHR169 = 500-length(PostHRper169);
        NaNHR169 = NaN(1,padHR169);
        transpose = [transpose NaNHR169];
        PostHRper169 = transpose';
        transpose = FebHRper169';
        padHR169 = 500-length(FebHRper169);
        NaNHR169 = NaN(1,padHR169);
        transpose = [transpose NaNHR169];
        FebHRper169 = transpose';

    HRper169 = [PreHRper169 PostHRper169 FebHRper169];
    [pHRper169 tblHRper169 statsHRper169] = anova1(HRper169)
    statsHRper169.gnames = ['Pre '; 'Post'; 'Feb '];
    figure;
    multcompare(statsHRper169);
    title('M169 HR Period Pairwise Comparisons')
```

B.2.2 Repeated Measures ANOVA

Case: Heart Rate, M166-16, M168-16, M169-16

```
TimeVec = (1:1:5000)';
	tHR166 = table(TimeVec, HR_166{1,1}, HR_166{1,2}, HR_166{1,3}, HR_166{1,4}, HR_166{1,5}, HR_166{1,6}, HR_166{1,7},
HR_166{1,8}, HR_166{1,9}, HR_166{1,10}, HR_166{1,11},'VariableNames',
{'Time','dpin3','dpin2','dpin1','dpin0','dpip1','dpip2','dpip3','dpip4','dpip5','dpip6', 'dpip7'});
	MeasHR166 = table([1 2 3 4 5 6 7 8 9 10 11]', 'Variablenames', {'HR'});
	rmHR166 = fitrm(tHR166, 'dpin3-dpip7~Time', 'WithinDesign', MeasHR166);
	ranovatbl = ranova(rmHR166)
	rmHR166.Coefficients
	rmHR166.Covariance

	HR_168{1,8}(1,1) = 0;
	HR_168{1,8}(2,1) = 0;
	HR_168{1,8}(3,1) = 0;
	tHR168 = table(TimeVec, HR_168{1,1}, HR_168{1,2}, HR_168{1,3}, HR_168{1,4}, HR_168{1,5}, HR_168{1,6}, HR_168{1,7},
HR_168{1,8}, HR_168{1,9}, HR_168{1,10}, HR_168{1,11},'VariableNames',
{'Time','dpin3','dpin2','dpin1','dpin0','dpip1','dpip2','dpip3','dpip4','dpip5','dpip6', 'dpip7'});
	MeasHR168 = table([1 2 3 4 5 6 7 8 9 10 11]', 'Variablenames', {'HR'});
	rmHR168 = fitrm(tHR168, 'dpin3-dpip7~Time', 'WithinDesign', MeasHR168);
	ranovatbl = ranova(rmHR168)
	rmHR168.Coefficients
	rmHR168.Covariance

	tHR169 = table(TimeVec, HR_169{1,1}, HR_169{1,2}, HR_169{1,3}, HR_169{1,4}, HR_169{1,5}, HR_169{1,6}, HR_169{1,7},
HR_169{1,8}, HR_169{1,9}, HR_169{1,10}, HR_169{1,11},'VariableNames',
{'Time','dpin3','dpin2','dpin1','dpin0','dpip1','dpip2','dpip3','dpip4','dpip5','dpip6', 'dpip7'});
	MeasHR169 = table([1 2 3 4 5 6 7 8 9 10 11]', 'Variablenames', {'HR'});
	rmHR169 = fitrm(tHR169, 'dpin3-dpip7~Time', 'WithinDesign', MeasHR169);
	ranovatbl = ranova(rmHR169)
	rmHR169.Coefficients
	rmHR169.Covariance
```

B.3 FREQUENCY SPECTRUM ANALYSIS

B.3.1 Window Visualization Tool

Case: Heart Rate, M166-16, M168-16, M169-16

```
M166_HRfft_Pre = M166_F_W_L_HRCens(indexGenericDayMat_166(1):indexGenericDayMat_166(4));
M166_HRfft_Post = M166_F_W_L_HRCens(indexGenericDayMat_166(5):indexGenericDayMat_166(12));
wvtool(M166_HRfft_Pre,M166_HRfft_Post)
M167_HRfft_Pre = M167_F_W_L_HRCens(indexGenericDayMat_167(1):indexGenericDayMat_167(4));
M167_HRfft_Post = M167_F_W_L_HRCens(indexGenericDayMat_167(5):indexGenericDayMat_167(12));
wvtool(M167_HRfft_Pre,M167_HRfft_Post)
M168_HRfft_Pre = M168_F_W_L_HRCens(indexGenericDayMat_168(1):indexGenericDayMat_168(4));
```

```
M168_HRfft_Post = M168_F_W_L_HRCens(indexGenericDayMat_168(5):indexGenericDayMat_168(12));
wvtool(M168_HRfft_Pre,M168_HRfft_Post)
M169_HRfft_Pre = M169_F_W_D_HRCens(indexGenericDayMat_169(1):indexGenericDayMat_169(4));
M169_HRfft_Post = M169_F_W_D_HRCens(indexGenericDayMat_169(5):indexGenericDayMat_169(6));
M169_HRfft_Feb = M169_F_W_D_HRCens(indexGenericDayMat_169(7):indexGenericDayMat_169(12));
wvtool(M169_HRfft_Pre,M169_HRfft_Post,M169_HRfft_Feb);
```

B.4 HEART RATE VARIABILITY

B.4.1 Poincare Plot Overlay Generation

Case: HRV, M169-16

```
        M169HRVser = {};
    transpose1 = M169_F_W_D_HRV1';
    transpose2 = M169_F_W_D_HRV2';
    M169HRVX = nan(1440,11);
    M169HRVY  = nan(1440,11);
    M169HRVDPIgrpser = ['-3dpi','-2dpi','-1dpi','0dpi','1dpi','2dpi','3dpi','4dpi','5dpi','6dpi','7dpi'];
    for i=1:1:11
    M169HRVser{1,i} =   transpose1(indexGenericDayMat_169(i):indexGenericDayMat_169(i+1));
    M169HRVser{2,i} =   transpose2(indexGenericDayMat_169(i):indexGenericDayMat_169(i+1));
      for j = 1:1:length(M169HRVser{1,i})
          M169HRVX(j,i) = M169HRVser{1,i}(1,j);
      end

      for k = 1:1:length(M169HRVser{2,i})
          M169HRVY(k,i) = M169HRVser{2,i}(1,k);
      end
    end
  M169HRV = [];
    transpose1 = M169_F_W_D_HRV1';
    transpose2 = M169_F_W_D_HRV2';
    M169HRV(:,1) = transpose1(indexGenericDayMat_169(1)+1:indexGenericDayMat_169(12))';
    M169HRV(:,2) = transpose2(indexGenericDayMat_169(1)+1:indexGenericDayMat_169(12))';
    M169HRVDPIgrp = zeros(length(M169HRV(:,1)'),1);
    for j = 1:1:11
    for i= indexGenericDayMat_169(j):1:(indexGenericDayMat_169(j+1)-1)
      M169HRVDPIgrp(i,1) = j-4;
    end
    end
    transposegrp = M169HRVDPIgrp';
    M169HRVDPIgrp = transposegrp(indexGenericDayMat_169(1):1:length(transposegrp))';
    figure;
    scatterhist(M169HRV(:,1),M169HRV(:,2),'Group',M169HRVDPIgrp,'Kernel','on', 'Color','ccckkkrrrrr','Legend','on');
    hold on;
    xlabel('RRI_n (ms)');
    ylabel('RRI_n_+_1 (ms)');
    title('M169-16 HRV');
    annotation('textbox',[0.063 0.107142857142857 0.0829285714285714
0.104761904761905],'String',{'Days','Post','Infection'},'FitBoxToText','on');
```

B.4.2 Probability Density – One Way ANOVA

Case: HRV, M169-16

```
    M169HRVoneWay= zeros(100,11);
for i = 1:1:11
   M169HRVoneWay(:,i) = ksdensity(M169HRVX(:,i))';

end
   [pHRV169 tblHRV169 statsHRV169] = anova1(M169HRVoneWay)
   statsHRV169.gnames = ['-3dpi'; '-2dpi'; '-1dpi'; '-0dpi'; '+1dpi'; '+2dpi'; '+3dpi'; '+4dpi'; '+5dpi'; '+6dpi'; '+7dpi'];
   figure;
   multcompare(statsHRV169);
   title('M169 HRV DPI Pairwise Comparisons')
```

BIBLIOGRAPHY

1. Bennett, J.E., R. Dolin, and M.J. Blaser, *Mandell, Douglas, and Bennett's principles and practice of infectious diseases*. 2014: Elsevier Health Sciences.
2. Markoff, L., *Alphaviruses*, in *Mandell, Douglas, and Bennett's Principles and Practice of Infectious Diseases*. 2010, Elsevier BV. p. 2117-2125.
3. Stollar, V., *Alphavirus*, in *The Springer Index of Viruses*, C.A. Tidona, G. Darai, and C. Büchen-Osmond, Editors. 2001, Springer Berlin Heidelberg: Berlin, Heidelberg. p. 1148-1155.
4. Griffin, D.E., *Alphavirus Pathogenesis and Immunity*, in *The Togaviridae and Flaviviridae*, S. Schlesinger and M.J. Schlesinger, Editors. 1986, Springer New York: Boston, MA. p. 209-249.
5. Schmaljohn, A.L. and D. McClain, *Alphaviruses (Togaviridae) and Flaviviruses (Flaviviridae)*, in *Medical Microbiology*, S. Baron, Editor. 1996: Galveston (TX).
6. Lwande, O.W., et al., *Global emergence of Alphaviruses that cause arthritis in humans.* Infect Ecol Epidemiol, 2015. **5**: p. 29853.
7. Weaver, S.C., et al., *Alphaviruses: population genetics and determinants of emergence.* Antiviral Res, 2012. **94**(3): p. 242-57.
8. Broeck, G.T. and M.H. Merrill, *A serological difference between eastern and western equine encephalomyelitis virus.* Proceedings of the Society for Experimental Biology and Medicine, 1933. **31**(2): p. 217-220.
9. Meyer, K., C. Haring, and B. Howitt, *The etiology of epizootic encephalomyelitis of horses in the San Joaquin Valley, 1930.* Science, 1931. **74**(1913): p. 227-228.
10. Findlay, G., *Variation in viruses*, in *Handbuch der Virusforschung*. 1938, Springer. p. 861-994.
11. Beck, C.E. and R.W.G. Wyckoff, *Venezuelan Equine Encephalomyelitis.* Science, 1938. **88**(2292): p. 530.
12. Kennedy, P.G., *Viral encephalitis: causes, differential diagnosis, and management.* J Neurol Neurosurg Psychiatry, 2004. **75 Suppl 1**: p. i10-5.
13. Arechiga-Ceballos, N. and A. Aguilar-Setien, *Alphaviral equine encephalomyelitis (Eastern, Western and Venezuelan).* Rev Sci Tech, 2015. **34**(2): p. 491-501.
14. Deresiewicz, R.L., et al., *Clinical and neuroradiographic manifestations of eastern equine encephalitis.* N Engl J Med, 1997. **336**(26): p. 1867-74.
15. Whitley, R.J., *Viral encephalitis.* N Engl J Med, 1990. **323**(4): p. 242-50.
16. Jain, S., B. Patel, and G.C. Bhatt, *Enteroviral encephalitis in children: clinical features, pathophysiology, and treatment advances.* Pathog Glob Health, 2014. **108**(5): p. 216-22.
17. Reddy, A.J., C.W. Woods, and K.E. Welty-Wolf, *Eastern equine encephalitis leading to multi-organ failure and sepsis.* Journal of Clinical Virology, 2008. **42**(4): p. 418-421.
18. Wang, E., et al., *Reverse Transcription-PCR-Enzyme-Linked Immunosorbent Assay for Rapid Detection and Differentiation of Alphavirus Infections.* Journal of Clinical Microbiology, 2006. **44**(11): p. 4000-4008.
19. Zacks, M.A. and S. Paessler, *Encephalitic alphaviruses.* Vet Microbiol, 2010. **140**(3-4): p. 281-6.

20. Reed, Douglas S., et al., *Severe Encephalitis in Cynomolgus Macaques Exposed to Aerosolized Eastern Equine Encephalitis Virus.* The Journal of Infectious Diseases, 2007. **196**(3): p. 441-450.
21. Molaei, G., et al., *Host-feeding patterns of potential mosquito vectors in Connecticut, U.S.A.: molecular analysis of bloodmeals from 23 species of Aedes, Anopheles, Culex, Coquillettidia, Psorophora, and Uranotaenia.* J Med Entomol, 2008. **45**(6): p. 1143-51.
22. Mitchell, C.J., et al., *Isolation of eastern equine encephalitis virus from Aedes albopictus in Florida.* Science, 1992. **257**(5069): p. 526-7.
23. Casals, J., *Antigenic Variants of Eastern Equine Encephalitis Virus.* J Exp Med, 1964. **119**: p. 547-65.
24. Weaver, S.C. and A.D. Barrett, *Transmission cycles, host range, evolution and emergence of arboviral disease.* Nat Rev Microbiol, 2004. **2**(10): p. 789-801.
25. Young, D.S., et al., *Molecular Epidemiology of Eastern Equine Encephalitis Virus, New York.* Emerging Infectious Diseases, 2008. **14**(03): p. 454-460.
26. Hollidge, B.S., F. Gonzalez-Scarano, and S.S. Soldan, *Arboviral encephalitides: transmission, emergence, and pathogenesis.* J Neuroimmune Pharmacol, 2010. **5**(3): p. 428-42.
27. Forrester, N.L., et al., *Western Equine Encephalitis submergence: lack of evidence for a decline in virus virulence.* Virology, 2008. **380**(2): p. 170-2.
28. Reed, Douglas S., et al., *Aerosol Infection of Cynomolgus Macaques with Enzootic Strains of Venezuelan Equine Encephalitis Viruses.* The Journal of Infectious Diseases, 2004. **189**(6): p. 1013-1017.
29. Yu, G.Y., et al., *Complete coding sequences of eastern equine encephalitis virus and venezuelan equine encephalitis virus strains isolated from human cases.* Genome Announc, 2015. **3**(2).
30. Rossi, S.L., et al., *IRES-Containing VEEV Vaccine Protects Cynomolgus Macaques from IE Venezuelan Equine Encephalitis Virus Aerosol Challenge.* PLOS Neglected Tropical Diseases, 2015. **9**(5): p. e0003797.
31. Ryzhikov, A.B., et al., *Spread of Venezuelan equine encephalitis virus in mice olfactory tract.* Arch Virol, 1995. **140**(12): p. 2243-54.
32. Liu, D., *Manual of security sensitive microbes and toxins*. 2014, Boca Raton: CRC Press, Taylor & Francis Group. xxi, 860 pages.
33. Greenlee, J.E., *The equine encephalitides.* Handb Clin Neurol, 2014. **123**: p. 417-32.
34. Honnold, S.P., et al., *Eastern equine encephalitis virus in mice I: clinical course and outcome are dependent on route of exposure.* Virol J, 2015. **12**: p. 152.
35. Couch, R.B., et al., *Effect of route of inoculation on experimental respiratory viral disease in volunteers and evidence for airborne transmission.* Bacteriological reviews, 1966. **30**(3): p. 517.
36. Charles, P.C., et al., *Mechanism of neuroinvasion of Venezuelan equine encephalitis virus in the mouse.* Virology, 1995. **208**(2): p. 662-71.
37. Bosch, A.A., et al., *Viral and bacterial interactions in the upper respiratory tract.* PLoS Pathog, 2013. **9**(1): p. e1003057.
38. Roy, C., D. Reed, and J. Hutt, *Aerobiology and inhalation exposure to biological select agents and toxins.* Veterinary Pathology Online, 2010. **47**(5): p. 779-789.

39. Danes, L., et al., *The role of the olfactory route on infection of the respiratory tract with Venezuelan equine encephalomyelitis virus in normal and operated Macaca rhesus monkeys. I. Results of virological examination.* Acta Virol, 1973. **17**(1): p. 50-6.
40. Oberdorster, G., et al., *Translocation of inhaled ultrafine particles to the brain.* Inhal Toxicol, 2004. **16**(6-7): p. 437-45.
41. van Riel, D., R. Verdijk, and T. Kuiken, *The olfactory nerve: a shortcut for influenza and other viral diseases into the central nervous system.* The Journal of Pathology, 2014. **235**(2): p. 277-287.
42. Sahin-Yilmaz, A. and R.M. Naclerio, *Anatomy and physiology of the upper airway*. Proc Am Thorac Soc, 2011. **8**(1): p. 31-9.
43. Gang Hu, W. and L.P. Nagata, *Opportunities and Challenges of Therapeutic Monoclonal Antibodies as Medical Countermeasures for Biodefense.* Journal of Bioterrorism & Biodefense, 2016. **7**(3).
44. Edelman, R., et al., *Evaluation in Humans of a New, Inactivated Vaccine for Venezuelan Equine Encephalitis Virus (C-84).* Journal of Infectious Diseases, 1979. **140**(5): p. 708-715.
45. Ericsson, A.C., M.J. Crim, and C.L. Franklin, *A brief history of animal modeling.* Missouri medicine, 2013. **110**(3): p. 201.
46. Adams, A.P., et al., *Common marmosets (Callithrix jacchus) as a nonhuman primate model to assess the virulence of eastern equine encephalitis virus strains.* J Virol, 2008. **82**(18): p. 9035-42.
47. Lewis, J., et al., *Alphavirus-induced apoptosis in mouse brains correlates with neurovirulence.* J Virol, 1996. **70**(3): p. 1828-35.
48. Roy, C.J., et al., *A chimeric Sindbis-based vaccine protects cynomolgus macaques against a lethal aerosol challenge of eastern equine encephalitis virus.* Vaccine, 2013. **31**(11): p. 1464-1470.
49. Mehendale, A.C., et al., *Unlock the information in your data: Software to find, classify, and report on data patterns and arrhythmias.* J Pharmacol Toxicol Methods, 2016. **81**: p. 99-106.
50. Saper, C.B., T.E. Scammell, and J. Lu, *Hypothalamic regulation of sleep and circadian rhythms.* Nature, 2005. **437**(7063): p. 1257-1263.
51. Saper, C.B. and B.B. Lowell, *The hypothalamus.* Current Biology, 2014. **24**(23): p. R1111-R1116.
52. Einthoven, W., G. Fahr, and A. De Waart, *On the direction and manifest size of the variations of potential in the human heart and on the influence of the position of the heart on the form of the electrocardiogram.* Am Heart J, 1950. **40**(2): p. 163-211.
53. Atkins, C.E. and B.C. Dickie, *Electrocardiogram of the clinically normal, ketamine-sedated Macaca fascicularis.* Am J Vet Res, 1986. **47**(2): p. 455-7.
54. Andrade, M.C.R., et al., *Biologic data of Macaca mulatta, Macaca fascicularis, and Saimiri sciureusused for research at the fiocruz primate center.* Memórias do Instituto Oswaldo Cruz, 2004. **99**(6): p. 584-589.
55. Sztajzel, J., *Heart rate variability: a noninvasive electrocardiographic method to measure the autonomic nervous system.* Swiss Med Wkly, 2004. **134**(35-36): p. 514-22.
56. Lackemeyer, M., et al., *ABSL-4 Aerobiology Biosafety and Technology at the NIH/NIAID Integrated Research Facility at Fort Detrick.* Viruses, 2014. **6**(1): p. 137-150.

57. Reed, D.S., et al., *Aerosol exposure to western equine encephalitis virus causes fever and encephalitis in cynomolgus macaques.* J Infect Dis, 2005. **192**(7): p. 1173-82.
58. Bhatia, A. *The Math Trick Behind MP3s, JPEGs, and Homer Simpson's Face*. Facts So Romantic On Numbers 2013 [cited 2017 01/11/2017]; Available from: http://nautil.us/blog/the-math-trick-behind-mp3s-jpegs-and-homer-simpsons-face.
59. Brennan, M., M. Palaniswami, and P. Kamen, *Poincare plot interpretation using a physiological model of HRV based on a network of oscillators.* Am J Physiol Heart Circ Physiol, 2002. **283**(5): p. H1873-86.
60. Chen, Y., et al., *ATP release guides neutrophil chemotaxis via P2Y2 and A3 receptors.* Science, 2006. **314**(5806): p. 1792-5.
61. Yang, J.N., et al., *Adenosine A(3) receptors regulate heart rate, motor activity and body temperature.* Acta Physiol (Oxf), 2010. **199**(2): p. 221-30.
62. Wolpert, C., et al., *Is a narrow and tall QRS complex an ECG marker for sudden death?* Heart Rhythm, 2008. **5**(9): p. 1339-45.
63. Chreiteh, S.S. and K.B. Fisker, *Morphological Changes of the QRS Complex as a Marker of Autonomic Modulation of the Heart Rate*, in *Department of Health Science and Technology*. 2009, Aalborg University: Denmark.
64. McKinley, P.S., et al., *The impact of menstrual cycle phase on cardiac autonomic regulation.* Psychophysiology, 2009. **46**(4): p. 904-11.
65. Berns, K.I., *Grand Challenges for Biosafety and Biosecurity.* Frontiers in Bioengineering and Biotechnology, 2014. **2**.
66. Koblentz, G.D. and B.M. Mazanec, *Viral Warfare: The Security Implications of Cyber and Biological Weapons.* Comparative Strategy, 2013. **32**(5): p. 418-434.
67. Yeh, J.-Y., et al., *Animal Biowarfare Research: Historical Perspective and Potential Future Attacks.* Zoonoses and Public Health, 2012. **59**(8): p. 536-544.
68. Leitenberg, M. and R.A. Zilinskas, *The Soviet Biological Weapons Program*. 2012: Harvard University Press.
69. Moran, G.J., *Threats in bioterrorism. II: CDC category B and C agents.* Emerg Med Clin North Am, 2002. **20**(2): p. 311-30.
70. Gottschalk, R. and W. Preiser, *Bioterrorism: is it a real threat?* Med Microbiol Immunol, 2005. **194**(3): p. 109-14.
71. Hart, B.L. and L. Ketai, *Armies of pestilence: CNS infections as potential weapons of mass destruction.* AJNR Am J Neuroradiol, 2015. **36**(6): p. 1018-25.